DESCRIPTION OF HOT COMPRESSED HADRONIC MATTER BASED ON AN EFFECTIVE CHIRAL LAGRANGIAN*

Wojciech Florkowski

H. Niewodniczański Institute of Nuclear Physics
Radzikowskiego 152, 31-342 Kraków, Poland

To Krysia and Kasia

A review of the recent results obtained in the Nambu–Jona-Lasinio model is given. In particular, the following topics are discussed in detail: the effects of screening of the meson fields at finite temperature and density, the temperature dependence of the quark condensate in the approach including meson loops, the formulation of a chirally invariant transport theory for quark matter and, finally, the critical scattering at the chiral phase transition. Our presentation of the new results follows the general introductions to the ultra-relativistic heavy-ion collisions and to the imaginary/real time formalism.

PACS numbers: 12.38. Mh, 12.39. Fe, 25.75. -q

CONTENTS

I OVERVIEW

II EQUILIBRIUM ENSEMBLES

III NON-EQUILIBRIUM PHENOMENA

IV SUMMARY

I OVERVIEW

1. Introduction

It is now commonly accepted that *quantum chromodynamics* (QCD) is the underlying theory of strong interactions [1]. Consequently, one tries to understand all hadronic phenomena in terms of quark-gluon processes. To large extent, the success of such a program has been already achieved in the *deep inelastic lepton-hadron collisions* [2]; due to the asymptotic freedom of QCD, in the high energy regime one can apply perturbation theory. On the other hand, description of low energetic processes in terms of QCD is very difficult, since in this case the theory exhibits a complicated nonperturbative structure, responsible for such important phenomena like, *e.g.*, confinement or spontaneous breaking of chiral symmetry. The most fundamental approach to low energetic QCD (energies smaller or comparable to the typical hadron mass, ~ 1 GeV) is based on the *lattice simulations* [3]. However, due to the problems with, *e.g.*, finite size effects or proper inclusion of fermions, such calculations are still not fully satisfactory. In this situation, the important role is played by various *effective theories* which maintain the basic features of QCD but, at the same time, they are much easier to deal with. One of such theories is the Nambu–Jona-Lasinio (NJL) model. The NJL model was introduced already in the early sixties as a theory of interacting nucleons [4]. Later it was reformulated in terms of quark degrees of freedom. Numerous calculations demonstrate the success of the model in describing hadronic data. In this report we are going to discuss the properties of hot compressed hadronic matter as described by this model.

The two very important characteristics of QCD are: the nonperturbative structure of its ground state, characterized by a nonvanishing value of the quark condensate, and the appearance of light pseudoscalar particles, which are identified with the (quasi) Goldstone bosons of the spontaneously broken chiral symmetry. There is another feature of QCD which concerns hot (dense) systems. Due to the asymptotic freedom, at high temperature (density) the quarks and gluons are not confined to hadrons anymore but form the so-called *quark-gluon plasma* (QGP). Moreover, one expects that during such a deconfinement phase transition the chiral symmetry is additionally restored [5]. The successful effective theory of QCD should incorporate these properties.

An essential feature of the NJL model is its chiral invariance, spontaneously broken in the true ground state of the theory. This phenomenon leads directly to the appearance of the Goldstone bosons. The relative simplicity of the model allows for explicit calculations in this case. The model includes also the chiral symmetry restoration phase transition. This fact re-

sembles us the case of QCD where an analogous phase transition is expected. In consequence, the NJL model seems to be a very interesting tool to study the temperature and density dependence of various physical quantities.

There are also other interesting properties of the NJL model, which deserve some comments. The addition of small (a few MeV) current quark masses to the NJL Lagrangian breaks explicitly chiral invariance. In this case, the latter becomes only an approximate symmetry. Moreover, the difference between various current quark masses leads to the mass splittings among the mesons (baryons) with different flavour content. We note that this type of behaviour is typical for QCD, where the small current quark masses play a similar role. The NJL model allows us also to understand the success of the constituent quark picture. Due to the strong four-fermion pointlike interaction, the light (current) quarks appearing in the NJL Lagrangian gain large (constituent) masses. In this way, we can find connections between the concepts of the spontaneous breaking of the chiral symmetry and the concepts of the nonrelativistic quark model.

The shortcomings of the NJL model are: *(i)* the pointlike character of the quark-antiquark interaction causes that the theory is not renormalized, *(ii)* the NJL type of the quark interaction does not explain the confinement, moreover *(iii)* there are no gluons in the model. The fact that the model is not renormalizable is not so important as long as we do not want to treat it as a fundamental theory. The lack of confinement is a more serious problem. This may lead to unphysical processes like, *e.g.*, decays of heavy mesons into quark-antiquark pairs. The treatment of such cases in the NJL model must be done with a special care. Similarly, the fact that there are no gluons as dynamic degrees of freedom may lead to problems, especially, if one tries to apply the model at relatively high energies. Because of these disadvantages the model can be easily criticized. Nevertheless, in our opinion, the NJL model is, in spite of its deficiencies, a very interesting tool for studying phenomena related to the chiral symmetry and the chiral phase transition.

Through the use of the NJL model one can evaluate the temperature (density) dependence of various physical quantities like, *e.g.*, the quark condensate (constituent quark mass) [6–8], the pion decay constant [7,9], the meson masses [6, 9–13], the meson-meson and quark-meson coupling constants [9, 11]. In the framework of the model, the calculations of the critical temperature and the critical baryon chemical potential have been performed [6, 7], and the order of the chiral symmetry restoration phase transition was studied [14]. Moreover, the thermodynamic properties of the quark-meson plasma were investigated [15, 16]. Many results obtained from the NJL model (*e.g.*, the temperature dependence of the quark-number susceptibility [17], or of the meson screening masses [18]) are in good qualitative agreement with the lattice simulations of QCD.

In contrast to the abundant studies of the equilibrium situations, the investigations of the non-equilibrium cases in the NJL model are relatively rare. Initially, a transport theory for the model has been derived in the framework of the Keldysh closed-time-path formalism combined with the effective action method [19]. Later, another derivation (in the mean-field approximation) has been presented [20], which leads to the kinetic equations whose form is explicitly chirally invariant and which include the spin dynamics. A certain class of solutions of the classical transport equations found in [19] has been studied in both [21] and [22]. The aim of a series of publications [23] was the evaluation of the in-medium cross sections. Such cross sections can be used in the phenomenological kinetic equations describing non-equilibrium phenomena in hadronic matter. In particular, the singular cross sections (giving the critical scattering at the chiral phase transition) were used in the rate equations describing the hadronization of the quark plasma [24].

In this report we give the review of the recent results obtained in the NJL model, describing the properties of hot compressed hadronic matter. The first large class of problems concerns the behaviour of static meson correlation functions. In particular, this includes the investigation of the *screening of meson fields* at finite temperature or density. Another wide range of problems presented in our report concerns the *formulation of the transport theory* for the NJL model and its applications to the description of high energy nuclear collisions. Recently, several reviews of the NJL model have been published [25]. The aim of the present article is not to give yet another wide and complete review, but rather to summarize a series of the new results. Our report is based on the original articles [8,18,20,22,24,52,57].

Let us now outline the organization of this paper. Since our studies within the NJL model have been motivated by the physics of the relativistic heavy-ion collisions, Chapter 2 serves as a brief survey of high-energy nuclear reactions. This gives us a general background for the discussion of the properties of hot and dense hadronic matter. Chapter 3 is the introduction to the NJL model, where the basic concepts are presented and the connections between different formulations of the model are clarified. In Chapters 4–9 [EQUILIBRIUM ENSEMBLES] we discuss the physical systems in thermodynamic equilibrium, whereas in Chapters 10–13 [NON-EQUILIBRIUM PHENOMENA] the cases out of equilibrium are described. In order to make our report more self-contained, Chapters 4 and 10 are the short introductions to the imaginary-time and real-time formalisms. (We note that the imaginary-time formalism is usually used to describe the equilibrium ensembles, whereas the real-time formalism is used to study the systems out of equilibrium. We follow this tendency here.) More details about the structure of this article can be found in the Table of Contents.

2. High energy nuclear collisions

2.1. Relativistic collisions

In the *relativistic heavy-ion collisions*, the energies of the colliding nuclei are of the order of a few GeV per nucleon. In this energy range, the basic properties of the nuclear equation of state can be tested, which has important astrophysical relevance to neutron stars and supernova explosions. Here one encounters many interesting and well established phenomena like, *e.g.*, collective flows or subthreshold production of particles. In general, during heavy-ion collisions, large systems of hot and dense hadronic matter are produced (central collisions of symmetric heavy ions at 1 GeV per nucleon are likely to yield about 3 times normal nuclear matter density). The particles inside such a fireball do not propagate completely freely: their Compton wavelength may be comparable with their mean free path. In this situation, we expect that some of the particle properties (*e.g.*, their masses, widths or coupling constants) can be changed. These *in-medium modifications* can lead to the experimentally observed phenomena. For example, the change of the ρ meson mass in dense matter can influence the measured dilepton spectrum [26]. Nowadays, one attempts to connect in-medium modifications of hadron properties with the partial restoration of chiral symmetry. If this idea turns out to be correct, we can treat the change of hadron properties as a signature of the rearrangement of the QCD vacuum.

The experiments with relativistic heavy-ions are intensely carried out in many places, for example, at the Gesellschaft für Schwerionenforschung in Darmstadt (GSI), at the Grand Accelerateur d'Ions Lourds in Caen (GANIL), at the Joint Institute for Nuclear Research in Dubna (JINR), and at the Lawrence Berkeley Laboratory in Berkeley (LBL).

2.2. Ultra-relativistic collisions

If the beam energies are larger (the energy per nucleon exceeds 10 GeV) we talk usually about the *ultra-relativistic heavy-ion collisions*. The ultimate goal of such collisions is the observation of the phase transition from hadronic matter to the quark-gluon plasma [27–30]. The search for signatures of this phase transition is one of the most challenging problems of high-energy nuclear physics, both from the experimental and theoretical points of view. Several plasma signatures have been proposed so far. They can be grouped into the following categories: photons and lepton pairs, strangeness and antibaryon enhancement, J/ψ suppression, transverse flow and thermodynamic variables measuring equation of state (for a complete review see [31]).

The first experiments with ultra-relativistic heavy-ion collisions took place at the Brookhaven National Laboratory (BNL) and CERN in 1986. The Alternating Gradient Synchrotron (AGS) accelerated beams up to ^{20}Si at 14.5 GeV per nucleon. At CERN, the Super Proton Synchrotron (SPS) accelerated ^{16}O at 60 and 200 GeV per nucleon in 1986 and ^{32}S at 200 GeV per nucleon in 1987. In 1990 a long-term project on heavy-ion physics was realized at CERN with several weeks of ^{32}S beams. Initially, no special heavy-ion machines were constructed for ultra-relativistic heavy ion collisions, but rather old existing accelerators had been upgraded. Only now, the completely new experiments take place at CERN with ^{208}Pb beams. These are for the first time really "heavy" ions, providing large volumes and lifetimes of the reaction zone. The future of the field is connected with the construction of the colliders: RHIC at BNL (Au on Au reactions at $\sqrt{s} =$ 200 GeV per nucleon), and LHC at CERN (Pb on Pb reactions at $\sqrt{s} = 6.3$ TeV per nucleon).

The present experimental evidence indicates that in ultra-relativistic heavy-ion collisions an extended and very dense system of hadronic matter is indeed formed. It differs in many aspects from the systems formed in elementary hadron-hadron reactions. However, it has also become clear that our search for QGP will not be an easy exercise. Although a number of "plasma signals" have been observed, at the same time the conventional theoretical models have been improved to such a level of the agreement with the data, that it does not require any radically new physics. Nevertheless, the physics of the ultra-relativistic heavy-ion collisions only now comes into its mature age. With Pb on Pb collisions at LHC, which offer the initial energy density 50 to 100 times larger than that of normal nuclear matter, the "new physics" of one kind or another should certainly appear.

2.3. Theoretical concepts

The physics of the (ultra)relativistic heavy-ion collisions is an interdisciplinary field which combines different methods and ideas from the particle and nuclear physics. Since we deal with macroscopic objects containing a large number of particles, the methods of *statistical physics* and *thermodynamics* are especially useful. In fact, many estimates are done on the basis of purely thermodynamic considerations. Nevertheless, the systems produced in these collisions are not static. The need for the dynamical description involves rich applications of *hydrodynamics*. Furthermore, since the matter produced in high energy nuclear collisions lives only for a short while, it is natural to expect that its space-time evolution proceeds far away from equilibrium. Consequently, there exists a growing interest in applying and developing *transport theories* which are suitable for the description

of non-equilibrium processes. For the relativistic heavy-ion collisions one uses transport equations of the BUU (Boltzmann–Uehling–Uhlenbeck) type, which evolve phase-space densities of nucleons, pions and other hadrons. With the ultra-relativistic collisions in mind, a quark-gluon kinetic theory based directly on QCD has been formulated [32,33]. However this approach, with a few exceptions [34], is still far from practical applications.

To a large extent the successful description of ultra-relativistic reactions has been obtained on the basis of the *microscopic Monte-Carlo simulations*. These models are in some sense an extrapolation of low energy hadron-hadron string models [35]. At energies of 200 GeV per nucleon or higher, the density of strings becomes high and they start to overlap. Consequently, the interaction and fusion of strings must be taken into account in most cases [36]. For extremely high energies, the concept of strings and flux tubes can be even abandoned and replaced by the picture of a parton cascade developing in the perturbative vacuum [37].

Last but not at least, the physics of the ultra-relativistic heavy-ion collisions has triggered the fast development of the *quantum theory of fields in and out of equilibrium*. Using the methods of field theory one can study the in-medium properties of particles. Moreover, this approach allows also for the formulation of the kinetic equations satisfied by the particle distribution functions.

A description of the whole complexity of high-energy nuclear collisions in terms of a simple model is impossible. In particular, effective chiral theories cannot explain the mechanism of all processes happening at different energy scales. However, many important problems discussed in the context of high-energy nuclear collisions can be successfully analyzed within the NJL model. Let us mention a few of them: rearrangement of the QCD vacuum under extreme conditions, modification of the properties of the particles propagating through a hot and dense hadronic medium, structure of the chiral phase transition, and non-equilibrium dynamics of hadronic matter. It is an attractive feature of the NJL model that these problems can be addressed in a unified manner.

3. Nambu–Jona-Lasinio model

This Chapter is the introduction to the NJL model. We define here our notation and conventions. The relationship between the model and QCD is claryfied. The presentation starts with the discussion of the simplest, one-flavour version. Later on, more realistic cases are considered.

3.1. One-flavour case

The simplest variant of the NJL model is its one-flavour version based on the following form of the Lagrange density

$$\mathcal{L} = \bar{\psi}\left(i\,\partial\!\!\!/ - m\right)\psi + G\left[(\bar{\psi}\psi)^2 + (\bar{\psi}i\gamma_5\psi)^2\right]. \tag{3.1}$$

Here ψ is the Dirac field describing quarks, m is the current quark mass, and G is the coupling constant [1]. The latter has a dimension $(\text{mass})^{-2}$ and is assumed to be positive (in this case the forces between quarks and antiquarks are attractive). The field ψ can carry additional colour degrees of freedom. In such a case, the notation in (3.1) assumes summation over colour indices, for example, $\bar{\psi}\psi = \sum_{a=1}^{N_c} \bar{\psi}^a\psi^a$, where N_c is the number of colours.

Expression (3.1) is an effective Lagrangian describing the local quark-antiquark interaction. The pointlike character of this coupling is usually explained by the assumption that the gluon degrees of freedom can be absorbed in the effective quark-antiquark coupling constant G. This type of reduction is considered to be a suitable approximation to QCD in the low-energy (long wavelength) limit.

In the case $m = 0$, Lagrangian (3.1) is invariant under $U_A(1)$ transformations

$$\psi \to \psi' = \exp\left(-i\gamma_5\frac{\chi}{2}\right)\psi. \tag{3.2}$$

Consequently, we find that the *axial* current is conserved

$$\partial_\mu A^\mu(x) = 0, \quad A^\mu(x) = \bar{\psi}(x)\gamma^\mu\gamma_5\psi(x). \tag{3.3}$$

If the current quark mass does not vanish, $m \neq 0$, the equality (3.3) is not fulfilled anymore. In this case we find

$$\partial_\mu A^\mu(x) = 2im\bar{\psi}(x)\gamma_5\psi(x). \tag{3.4}$$

Since m is small, Eq. (3.4) is usually called the *partial conservation* of the axial current (PCAC).

For arbitrary m Lagrangian (3.1) is invariant under $U_V(1)$ transformations,

$$\psi \to \psi' = \exp\left(-i\frac{\phi}{2}\right)\psi, \tag{3.5}$$

which leads to the conservation of the *baryon* current,

$$\partial_\mu V^\mu(x) = 0, \quad V^\mu(x) = \bar{\psi}(x)\gamma^\mu\psi(x). \tag{3.6}$$

---

[1] In our report we shall always work in 1+3 dimensions. The formulation of the theory in 1+1 dimensions has different aspects, since in this case the model is renormalizable. A 2-dimensional massless theory is commonly called the Gross–Neveu model [38].

3.2. Two-flavour symmetric case

A straightforward generalization of the one-flavour model leads to the following Lagrangian

$$\mathcal{L} = \bar{\psi}\left(i\,\slashed{\partial} - \hat{m}\right)\psi + \sum_{i=0}^{3} \frac{G_S}{2}\left[(\bar{\psi}\tau_i\psi)^2 + (\bar{\psi}i\gamma_5\tau_i\psi)^2\right]. \tag{3.7}$$

In this case, the field ψ has an extra flavour index and τ_i are the isospin Pauli matrices (with $\tau_0 = 1$). The quantity $\hat{m}$ is a two by two diagonal matrix containing the current quark masses, *i.e.*, $\hat{m} = \text{diag}(m_u, m_d)$.

In the chiral limit, $\hat{m} \to 0$, Lagrangian (3.7) is invariant under $U_A(1)$ transformations defined by the rule (3.2). This fact gives the conservation of the axial current, which we already know from the consideration of the one-flavour model, see Eq. (3.3). Moreover, also for $\hat{m} = 0$, Lagrangian (3.7) does not change if we make $SU_A(2)$ transformations

$$\psi \to \psi' = \exp\left(-i\gamma_5\frac{\boldsymbol{\tau}\cdot\boldsymbol{\chi}}{2}\right)\psi, \tag{3.8}$$

where $\boldsymbol{\tau} = (\tau_1, \tau_2, \tau_3)$. This symmetry leads us to the conservation of the *chiral* current

$$\partial_\mu \boldsymbol{A}^\mu(x) = 0, \quad \boldsymbol{A}^\mu(x) = \bar{\psi}(x)\gamma^\mu\gamma_5\boldsymbol{\tau}\psi(x). \tag{3.9}$$

Similarly to the one-flavour case, if $\hat{m} \neq 0$ instead of Eq. (3.9) one finds

$$\partial_\mu \boldsymbol{A}^\mu(x) = i\bar{\psi}(x)\left(\boldsymbol{\tau}\hat{m} + \hat{m}\boldsymbol{\tau}\right)\gamma_5\psi(x). \tag{3.10}$$

In the case $m_u = m_d = m$, one finds that Lagrangian (3.7) is invariant under $SU_V(2)$ transformations

$$\psi \to \psi' = \exp\left(-i\frac{\boldsymbol{\tau}\cdot\boldsymbol{\phi}}{2}\right)\psi, \tag{3.11}$$

which gives the conservation of the *isospin* current

$$\partial_\mu \boldsymbol{V}^\mu(x) = 0, \quad \boldsymbol{V}^\mu(x) = \bar{\psi}(x)\gamma^\mu\boldsymbol{\tau}\psi(x). \tag{3.12}$$

Finally, for any value of $\hat{m}$, one can check that the Lagrange density (3.7) is invariant under $U_V(1)$ transformations, such that the baryon current defined by Eq. (3.6) is conserved.

Let us now make a few comments about our terminology. Both $U_A(1)$ and $SU_A(2)$ symmetries will be later called axial or chiral ones. Similarly,

A^μ and $\boldsymbol{A}^\mu$ can be called axial or chiral currents. However, the name axial current will be usually reserved for A^μ, and the name chiral will refer to $\boldsymbol{A}^\mu$. In the analogous way, both baryon and isospin currents, V^μ and $\boldsymbol{V}^\mu$, can be shortly called the vector currents. Finally, since the theory based on Lagrangian (3.7) is for $\hat{m} = 0$ invariant under both $U_A(1)$ and $SU_A(2)$ symmetry groups, we shall call this version of the model symmetric.

Discussing the properties of our two Lagrangians, we have introduced four types of symmetries, and associated with them four conserved currents. It is well known that these symmetries characterize also the QCD Lagrangian. In this sense, the NJL model has symmetry features common with QCD. Symmetries connected with the unitary transformations $U_V(1)$ and $SU_V(2)$ have a simple manifestation in nature. The first one leads to the baryon number conservation, whereas the second one is responsible for the organization of hadrons into the isospin multiplets. On the other hand, the axial symmetries $U_A(1)$ and $SU_A(2)$ do not have any direct realization. In particular, they do not lead to any degeneracy of the particle spectra: If the $U_A(1)$ symmetry were naively realized in nature, each hadron would have an opposite parity partner. Similarly, a naive realization of the $SU_A(2)$ symmetry would require that each isospin multiplet has a partner multiplet which groups the particles with opposite parity. Such a situation, however, does not take place.

The problem with the $SU_A(2)$ symmetry is resolved by the assumption that this symmetry is realized in the Goldstone mode, *i.e.*, it is spontaneously broken. The phenomenon of the spontaneous symmetry breaking is always accompanied by the appearance of the so-called Goldstone bosons. Hence, in the case of $SU_A(2)$ we expect that there exist isovector pseudoscalar massless particles. Having in mind the smallness of the pion mass, we can state that such particles indeed exist. Speaking more precisely, pions should be regarded as quasi Goldstone bosons, *i.e.*, particles which appear after the breaking of an approximate symmetry.

The situation with the $U_A(1)$ symmetry looks different. Since we do not observe any Goldstone bosons which could be associated with $U_A(1)$, we conclude that this symmetry cannot be spontaneously broken. In fact, as it was shown by 't Hooft [39], the $U_A(1)$ symmetry is broken due to the instanton effects.

The two versions of the NJL model, which have been discussed so far, exhibit the spontaneous breaking of the $U_A(1)$ symmetry. In addition, the two-flavour symmetric model breaks spontaneously the $SU_A(2)$ invariance. Unfortunately, as we have just learnt, the $U_A(1)$ symmetry is not spontaneously broken in the real world. Consequently, these two models must be still improved, if we want to use them for the description of real particles. In fact, this can be easily done by the modification of Lagrangian (3.7).

One can add a term to expression (3.7), which simulates instanton effects and breaks explicitly the $U_A(1)$ invariance. At the same time, this term leaves the $SU_A(2)$ symmetry intact (including its spontaneous breaking). This procedure will be described in detail in the next Section.

Although the study of more realistic situations requires the elimination of the $U_A(1)$ symmetry, the two simplest forms of the NJL model can be still useful. The point is, that in the discussed versions of NJL model, the mechanism of the symmetry breaking is the same for both $U_A(1)$ and $SU_A(2)$ groups. Consequently, in many problems where the flavour structure is not so important, we can study simplified theories. In this report, we shall investigate the properties of particles in hot and dense medium. In such a case, the extra complexities resulting from the exact consideration of the flavour content of particles are very often not so important. Therefore, many of our investigations will be based on simplified models defined by Lagrangians (3.1) and (3.7).

3.3. Two-flavour standard case

The $U_A(1)$ breaking interaction, accounting for the axial anomaly in QCD, can be described by the following Lagrangian [39]

$$\mathcal{L}_A = G_A \Big\{ \det\big[\bar{\psi}_i(1+\gamma_5)\psi_j\big] + \det\big[\bar{\psi}_i(1-\gamma_5)\psi_j\big] \Big\}$$
$$= \frac{G_A}{2}\left[(\bar{\psi}\psi)^2 + (\bar{\psi}i\gamma_5\boldsymbol{\tau}\psi)^2 - (\bar{\psi}\boldsymbol{\tau}\psi)^2 - (\bar{\psi}i\gamma_5\psi)^2\right], \qquad (3.13)$$

Here det stands for the determinant with respect to the flavour indices, and G_A is the coupling constant describing the strength of this interaction. (The last equality in (3.13) is valid only for the two-flavour case.) One can check that expression (3.13) is invariant under $SU_A(2)$ transformations. The easiest way of proving this property is the consideration of an infinitesimal $SU_A(2)$ transformation. The formula (3.8) for very small χ (denoted later by $\delta\chi$) gives

$$\bar{\psi}'\psi' = \bar{\psi}\psi - \bar{\psi}i\gamma_5\boldsymbol{\tau}\psi\delta\chi, \qquad \bar{\psi}'i\gamma_5\psi' = \bar{\psi}i\gamma_5\psi + \bar{\psi}\boldsymbol{\tau}\psi\delta\chi, \qquad (3.14)$$

$$\bar{\psi}'\boldsymbol{\tau}\psi' = \bar{\psi}\boldsymbol{\tau}\psi - \bar{\psi}i\gamma_5\psi\delta\chi, \qquad \bar{\psi}'i\gamma_5\boldsymbol{\tau}\psi' = \bar{\psi}i\gamma_5\boldsymbol{\tau}\psi + \bar{\psi}\psi\delta\chi. \qquad (3.15)$$

One can notice that the first two terms on the right-hand side (RHS) of the second line in (3.13) and the last two terms (also in this line) are separately $SU_A(2)$ invariant. On the other hand, Lagrangian (3.13) is not $U_A(1)$ invariant. Thus, adding formula (3.13) to Lagrangian (3.7), we obtain a theory which is only $SU_A(2)$ invariant. In the case $G_A = G_S = G$ one finds

$$\mathcal{L} = \bar{\psi}\left(i\,\slashed{\partial} - \hat{m}\right)\psi + G\left[(\bar{\psi}\psi)^2 + (\bar{\psi}i\gamma_5\boldsymbol{\tau}\psi)^2\right]. \qquad (3.16)$$

The first Lagrangian having exactly the same form as expression (3.16) was written by Nambu and Jona-Lasinio (the second paper published in 1961 [4]). Since at that time quarks and gluons were not known, the field ψ was used to describe nucleons (protons and neutrons). However, shortly after its formulation, the model of Nambu and Jona-Lasinio was abandoned because its non-fundamental character (reflected mainly in the nonrenormalizability of the theory) became clear. Later on the model was reinterpreted in terms of the quark degrees of freedom.

3.4. Mean-field approximation

Let us now come back to the discussion of the one-flavour model. By introducing the fields $\hat{\sigma}$ and $\hat{\pi}$ defined as

$$\hat{\sigma} = -2G\,\bar{\psi}\psi, \quad \hat{\pi} = -2G\,\bar{\psi}i\gamma_5\psi, \tag{3.17}$$

we can recast Lagrangian (3.1) into the form

$$\mathcal{L} = \bar{\psi}(i\,\slashed{\partial} - m)\psi - \hat{\sigma}\,\bar{\psi}\psi - \hat{\pi}\,\bar{\psi}i\gamma_5\psi - \frac{\hat{\sigma}^2 + \hat{\pi}^2}{4G}. \tag{3.18}$$

The equivalence of (3.1) and (3.18) becomes clear if one checks that the variation of (3.1) with respect to $\bar{\psi}$ gives the same equation of motion for ψ as the variation of (3.18) with respect to $\bar{\psi}, \hat{\sigma}$ and $\hat{\pi}$, namely

$$[i\,\slashed{\partial} - m - \hat{\sigma}(x) - i\gamma_5\hat{\pi}(x)]\,\psi(x) = 0. \tag{3.19}$$

In the *mean-field approximation*, the operators $\hat{\sigma}$ and $\hat{\pi}$ are replaced by their mean values, namely

$$\hat{\sigma} \to \sigma = \langle\hat{\sigma}\rangle = \mathrm{Tr}(\hat{\rho}\hat{\sigma}), \quad \hat{\pi} \to \pi = \langle\hat{\pi}\rangle = \mathrm{Tr}(\hat{\rho}\hat{\pi}). \tag{3.20}$$

This leads to the self-consistent mean-field equations:

$$[i\,\slashed{\partial} - m - \sigma(x) - i\gamma_5\pi(x)]\,\psi(x) = 0, \tag{3.21}$$

$$-2G\,\mathrm{Tr}\left[\hat{\rho}\bar{\psi}(x)\psi(x)\right] = \sigma(x), \tag{3.22}$$

$$-2G\,\mathrm{Tr}\left[\hat{\rho}\bar{\psi}(x)i\gamma_5\psi(x)\right] = \pi(x). \tag{3.23}$$

In Eqs (3.20)–(3.23) $\hat{\rho}$ is the density operator and Tr denotes the trace over all physical states of the system. The particular form of $\hat{\rho}$ is not important for our considerations. We only note that in typical situations, $\hat{\rho}$ is either an operator projecting on the parity invariant ground state or it describes parity invariant statistical ensembles. In these two cases $\langle\hat{\pi}\rangle = 0$. In more

general situations (*e.g.*, when the system is out of equilibrium) we cannot exclude the case $\langle \hat{\pi} \rangle \neq 0$ [2].

The $U_A(1)$ transformation of the quark field ψ induces the change of the fields $\hat{\sigma}$ and $\hat{\pi}$. Altogether, the fields ψ, $\hat{\sigma}$ and $\hat{\pi}$ obey the following transformation rule

$$\psi \rightarrow \psi' = \exp(-i\gamma_5 \frac{\chi}{2})\psi, \tag{3.24}$$

$$\hat{\sigma} \rightarrow \hat{\sigma}' = \hat{\sigma}\cos\chi - \hat{\pi}\sin\chi, \tag{3.25}$$

$$\hat{\pi} \rightarrow \hat{\pi}' = \hat{\pi}\cos\chi + \hat{\sigma}\sin\chi. \tag{3.26}$$

In the vector space spanned by the fields $\hat{\sigma}$ and $\hat{\pi}$, the chiral symmetry manifests itself simply as a rotation.

It is also important to realize that in the mean-field approximation the conservation of the axial current holds only for the mean value. Speaking more precisely, in the limit $m = 0$ one finds

$$\partial_\mu A^\mu(x) = 2\sigma(x)\bar{\psi}(x)i\gamma_5\psi(x) - 2\pi(x)\bar{\psi}(x)\psi(x), \tag{3.27}$$

which after calculation of the trace gives

$$\partial_\mu \langle A^\mu(x) \rangle = \partial_\mu \operatorname{Tr}(\hat{\rho} A^\mu(x)) = 0. \tag{3.28}$$

II EQUILIBRIUM ENSEMBLES

4. Imaginary-time formalism

Chapters 5–9 of our report will be devoted to the study of systems in thermodynamic equilibrium. In order to calculate different physical quantities at finite temperature or at finite baryon chemical potential, we shall use the imaginary-time formalism [41–43]. In this Chapter, we give a short introduction to this formalism and discuss several computational rules used at finite T or μ.

---

[2] Generally speaking, in the space-time regions where $\langle \hat{\pi} \rangle \neq 0$ the quark condensate is chirally rotated from its usual orientation in the isospin space. Such a piece of wrongly oriented condensate is called the *disoriented chiral condensate* [40]. Its production may explain rare events with a deficit or excess of neutral pions observed in cosmic ray experiments.

4.1. Temperature Green's functions

While studying many particle systems, it is convenient to use the *grand canonical ensemble*. Introducing the operator $\hat{K} = \hat{H} - \mu\hat{N}$ ($\hat{H}$ is the Hamiltonian and $\hat{N}$ is the baryon number operator) we can define the partition function and the statistical density operator by the following expressions

$$Z = \mathrm{Tr}\; e^{-\beta\hat{K}} \equiv e^{-\beta\Omega} \tag{4.1}$$

and

$$\hat{\rho} = Z^{-1}\, e^{-\beta\hat{K}}, \tag{4.2}$$

where β is the inverse temperature and Ω is the thermodynamic potential ($k_B = 1$).

The operator $\hat{K}$ can be interpreted as the grand canonical Hamiltonian. Thus, for each operator in the Schrödinger picture, $\hat{O}_S(\boldsymbol{x})$, we can define its partner in the modified Heisenberg picture, namely

$$O_K(\tau, \boldsymbol{x}) = e^{\hat{K}\tau}\, \hat{O}_S(\boldsymbol{x})\, e^{-\hat{K}\tau}. \tag{4.3}$$

Using this prescription, we introduce the quark *temperature Green's* function

$$\mathcal{G}_{ab}(\tau, \boldsymbol{x}; \tau', \boldsymbol{x}') = -\,\mathrm{Tr}\left\{ \hat{\rho}\hat{T}_\tau \left[\psi_{K\,a}(\tau, \boldsymbol{x})\bar{\psi}_{K\,b}(\tau', \boldsymbol{x}') \right] \right\}. \tag{4.4}$$

Here $\psi_{K\,a}(\tau, \boldsymbol{x})$ is the quark field operator, a and b are the indices describing internal degrees of freedom (spinor, flavour and colour), and $\hat{T}_\tau$ is the τ-ordering operator. Of course, an analogous expression can be given for other types of fields. Therefore, from now on we shall continue our discussion treating simultaneously the case of fermions and bosons.

In the typical situations ($\hat{H} = $ const, the system is uniform) $\mathcal{G}_{ab}(\tau, \boldsymbol{x}; \tau', \boldsymbol{x}')$ is a function of the difference of its arguments, *i.e.*, we can write $\mathcal{G}_{ab}(\tau, \boldsymbol{x}; \tau', \boldsymbol{x}') = \mathcal{G}_{ab}(\tau - \tau', \boldsymbol{x} - \boldsymbol{x}')$. Using the fermion (boson) commutation relations and the cyclic property of the trace, we find that the Green's function is an anti-periodic (periodic) function of time

$$\mathcal{G}_{ab}(\tau - \tau', \boldsymbol{x} - \boldsymbol{x}') = \mp \mathcal{G}_{ab}(\tau - \tau' + \beta, \boldsymbol{x} - \boldsymbol{x}'). \tag{4.5}$$

Equation (4.5) allows us to write the following representation

$$\mathcal{G}_{ab}(\tau, \boldsymbol{x} - \boldsymbol{x}') = T\sum_n e^{-i\omega_n\tau}\, \mathcal{G}_{ab}(i\omega_n, \boldsymbol{x} - \boldsymbol{x}'), \tag{4.6}$$

where

$$\mathcal{G}_{ab}(i\omega_n, \boldsymbol{x} - \boldsymbol{x}') = \int_0^\beta d\tau\, e^{i\omega_n\tau}\, \mathcal{G}_{ab}(\tau, \boldsymbol{x} - \boldsymbol{x}'). \tag{4.7}$$

and ω_n are the so-called *Matsubara frequencies*:

$$\omega_n = (2n+1)\pi T \quad \text{(for fermions)}, \quad \omega_n = 2n\pi T \quad \text{(for bosons)}. \tag{4.8}$$

The temperature Green's functions are very useful for the quantitative calculation of the thermodynamic properties of the system. On the other hand, in order to study the frequencies and lifetimes of excited states at finite temperature, we should study the structure of the *real-time Green's functions*. They are defined by the expression

$$i\overline{G}_{ab}(t,\boldsymbol{x};t',\boldsymbol{x}') = \text{Tr}\left\{\hat{\rho}T\left[\psi_{K\,a}(t,\boldsymbol{x})\bar{\psi}_{K\,b}(t',\boldsymbol{x}')\right]\right\}, \tag{4.9}$$

which is a straightforward generalization of the $T = \mu = 0$ case

$$iG_{ab}(t,\boldsymbol{x};t',\boldsymbol{x}') = \langle 0|T\left[\psi_{K\,a}(t,\boldsymbol{x})\bar{\psi}_{K\,b}(t',\boldsymbol{x}')\right]|0\rangle. \tag{4.10}$$

In Eqs (4.9) and (4.10) $\hat{T}$ is the t-ordering operator and the field operators are written in the standard Heisenberg picture. *i.e.*, the following notation is used here

$$O_K(t,\boldsymbol{x}) = e^{i\hat{K}t}\,\hat{O}_S(\boldsymbol{x})\,e^{-i\hat{K}t}. \tag{4.11}$$

We note that the real-time Green's function (4.10) is defined as the expectation value of the operator product in the ground state $|0\rangle$, and that the grand canonical density operator $\hat{\rho}$ is reduced to the projection operator onto this state in the case $T = \mu = 0$.

Besides the formula (4.9), one employs also the *retarded* and *advanced* Green's functions

$$i\overline{G}^{R}_{ab}(t,\boldsymbol{x};t',\boldsymbol{x}') = \theta(t-t')\,\text{Tr}\left\{\hat{\rho}\left[\psi_{K\,a}(t,\boldsymbol{x}),\bar{\psi}_{K\,b}(t',\boldsymbol{x}')\right]_{\pm}\right\} \tag{4.12}$$

and

$$i\overline{G}^{A}_{ab}(t,\boldsymbol{x};t',\boldsymbol{x}') = -\theta(t'-t)\,\text{Tr}\left\{\hat{\rho}\left[\psi_{K\,a}(t,\boldsymbol{x}),\bar{\psi}_{K\,b}(t',\boldsymbol{x}')\right]_{\pm}\right\}, \tag{4.13}$$

where $[\,,\,]_{\pm}$ denotes the anticommutator for fermions and the commutator for bosons. These two functions have the following spectral representations

$$\overline{G}^{R}_{ab}(\omega,\boldsymbol{q}) = \int\limits_{-\infty}^{\infty}\frac{d\omega'}{2\pi}\frac{\rho_{ab}(\omega',\boldsymbol{q})}{\omega-\omega'+i\epsilon} \tag{4.14}$$

and

$$\overline{G}^{A}_{ab}(\omega,\boldsymbol{q}) = \int\limits_{-\infty}^{\infty}\frac{d\omega'}{2\pi}\frac{\rho_{ab}(\omega',\boldsymbol{q})}{\omega-\omega'-i\epsilon}. \tag{4.15}$$

In Eqs (4.14) and (4.15) the function $\rho_{ab}(\omega', \boldsymbol{q})$ is the spectral density (the same in the two cases) and ϵ is an infinitesimally positive constant.

The crucial point in the imaginary-time formalism is that the temperature Green's function has the same spectral representation, *i.e.*, we can write

$$\mathcal{G}_{ab}(i\omega_n, \boldsymbol{q}) = \int\limits_{-\infty}^{\infty} \frac{d\omega'}{2\pi} \frac{\rho_{ab}(\omega', \boldsymbol{q})}{i\omega_n - \omega'}, \qquad (4.16)$$

where again the same spectral function $\rho_{ab}(\omega', \boldsymbol{q})$ appears. Using Eqs (4.14)–(4.16) and the requirement of the correct asymptotics of the Green's function in infinity, one can show that the temperature Green's function (defined only at complex and discrete frequencies $i\omega_n$) has a unique analytic continuation to the whole complex plane, where it coincides either with $\overline{G}_{ab}^{R}(\omega, \boldsymbol{q})$ (for upper half-plane) or $\overline{G}_{ab}^{A}(\omega, \boldsymbol{q})$ (for lower half-plane) [44]. This allows us for the calculation of $\overline{G}_{ab}^{R}$ and $\overline{G}_{ab}^{A}$ from the knowledge of the temperature Green's function $\mathcal{G}_{ab}(i\omega_n, \boldsymbol{q})$. Furthermore, knowing $\overline{G}_{ab}^{R}$ and $\overline{G}_{ab}^{A}$ we find $\overline{G}_{ab}(\omega, \boldsymbol{q})$ through the relation [41]

$$\overline{G}_{ab}(\omega, \boldsymbol{q}) = [1 \pm e^{-\beta\omega}]^{-1} \overline{G}_{ab}^{R}(\omega, \boldsymbol{q}) + [1 \pm e^{\beta\omega}]^{-1} \overline{G}_{ab}^{A}(\omega, \boldsymbol{q}). \qquad (4.17)$$

The importance of the discussed connections between the temperature and real-time Green's functions is related to the fact that the Feynman perturbation theory applies only to the temperature Green's functions; at finite temperature the real-time Green's functions do not have such a diagrammatic expansion, unless one introduces an extended Hilbert space [42]. Thus, when studying excited states at finite temperature we first calculate the temperature Green's function (in this case we can use all known techniques for Feynman diagrams), and only afterwards we do the analytic continuation to real frequencies.

4.2. Sums over frequencies

The Feynman rules for the temperature Green's functions [45] coincide with the $T = \mu = 0$ rules with the replacement

$$\int \frac{d^4p}{(2\pi)^4} \longrightarrow iT \sum_n \int \frac{d^3p}{(2\pi)^3}, \qquad (4.18)$$

where the continuous variable p^0 should be replaced by discrete complex energies [3]:

---

[3] In this report we consider the case when the bosonic chemical potential is zero.

$$p^0 \longrightarrow i\omega_n + \mu = (2n+1)\pi iT + \mu \quad \text{(for fermions)} \tag{4.19}$$

and

$$p^0 \longrightarrow i\omega_n = 2n\pi iT \quad \text{(for bosons)}. \tag{4.20}$$

Very often, it is convenient to convert the frequency sums to contour integrals. In the case of fermions, one can write [41]

$$iT \sum_n f(i\omega_n + \mu) = -\frac{1}{2\pi} \oint_{\mathcal{C}_M} \frac{dp^0 f(p^0 + \mu)}{\exp(\beta p^0) + 1}, \tag{4.21}$$

where $\mathcal{C}_M$ denotes the integration contour in the complex p^0 space, see Fig. 4.1. Changing the integration variable, we obtain [45]

$$iT \sum_n f(i\omega_n + \mu) = -\frac{1}{2\pi} \int_{-i\infty+\mu+\epsilon}^{+i\infty+\mu+\epsilon} \frac{dp^0 f(p^0)}{\exp[\beta(p^0 - \mu)] + 1}$$

$$- \frac{1}{2\pi} \int_{-i\infty+\mu-\epsilon}^{+i\infty+\mu-\epsilon} \frac{dp^0 f(p^0)}{\exp[\beta(\mu - p^0)] + 1}$$

$$+ \frac{1}{2\pi} \oint_{\mathcal{C}} dp^0 f(p^0) + \frac{1}{2\pi} \int_{-i\infty}^{+i\infty} dp^0 f(p^0), \tag{4.22}$$

where $\mathcal{C}$ is another integration contour in the complex energy plane, shown in Fig. 4.2. The position of $\mathcal{C}$ is fixed by the value of the chemical potential μ.

There are two special cases which will be particularly interesting for us, *i.e.*, the case of vanishing chemical potential and the case when the temperature is zero. For $\mu = 0$ and $T \neq 0$, Eq. (4.22) can be simplified to the form

$$iT \sum_n f(i\omega_n) = \frac{1}{2\pi} \int_{-i\infty}^{+i\infty} dp^0 f(p^0) - \frac{1}{2\pi} \int_{-i\infty+\epsilon}^{+i\infty+\epsilon} \frac{dp^0 \left[f(p^0) + f(-p^0)\right]}{\exp(\beta p^0) + 1}, \tag{4.23}$$

whereas in the limit $T \to 0$ and $\mu \neq 0$, we can use the rule

$$iT \sum_n f(i\omega_n + \mu) \to \frac{1}{2\pi} \int_{-i\infty}^{+i\infty} dp^0 f(p^0) + \frac{1}{2\pi} \oint_{\mathcal{C}} dp^0 f(p^0). \tag{4.24}$$
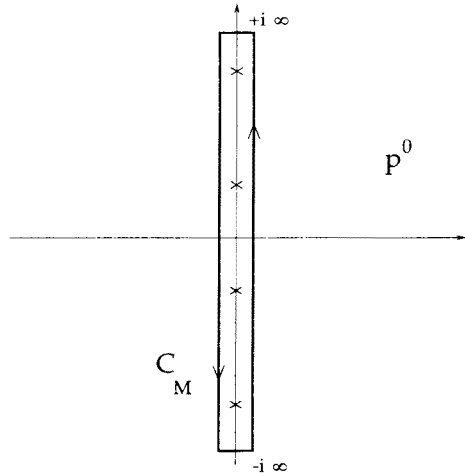
Fig. 4.1. The sum over the Matsubara frequencies can be calculated as a contour integral in the complex energy plane.
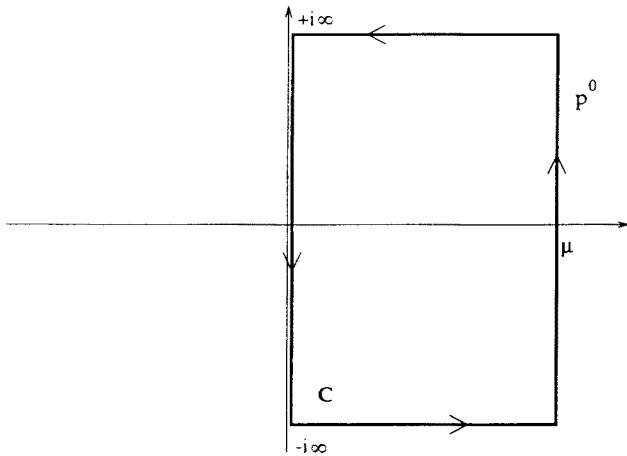
Fig. 4.2. Integration contour in the complex energy plane used for the evaluation of the matter parts.

In the case when the integrand depends additionally on the external frequency, $e.g.$, $f = f(p^0, \boldsymbol{p}, \omega)$, the integrals on the RHS of expressions (4.23) and (4.24) should be evaluated for purely imaginary values of ω and *subsequently* analytically continued to real frequencies. Similar prescriptions for the conversion of the frequency sum into the contour integrals can be given for bosons. We skip their presentation here since our later considerations will be restricted mainly to the fermionic sums.

The meaning of the decompositions (4.23) and (4.24) is that we can separate the so-called *vacuum part* from the *medium part*. The vacuum part of a physical quantity does not *explicitly* depend on the occupation of phase space and reduces at $T = \mu = 0$ to its vacuum expectation value. On the other hand, the medium part depends explicitly on the occupation of phase space and consequently vanishes in vacuum.

4.3. Meson correlation functions

Let us now consider again the special case when $\psi_{Ka}(t, \boldsymbol{x})$ is the quark field operator. In this situation, we define the meson correlation function by the expression

$$\chi_{ab}(t, \boldsymbol{x}) = i \operatorname{Tr} \left\{ \hat{\rho} \hat{T} \hat{O}_{Ka}(t, \boldsymbol{x}) \hat{O}_{Kb}(0, \boldsymbol{0}) \right\}, \qquad (4.25)$$

where

$$\hat{O}_{Ka}(t, \boldsymbol{x}) = \bar{\psi}_K(t, \boldsymbol{x}) M_a \psi_K(t, \boldsymbol{x}) - \operatorname{Tr} \left\{ \hat{\rho} \hat{T} \bar{\psi}_K(t, \boldsymbol{x}) M_a \psi_K(t, \boldsymbol{x}) \right\}. \quad (4.26)$$

The quantities M_a in Eq. (4.26) are products of the Dirac spinor matrices Γ_A and the Pauli isospin matrices τ_i (in the case of the SU(3) flavour group the Pauli matrices should be replaced by the Gell-Mann matrices λ_a). In writing Eq. (4.25) we have assumed that the Hamiltonian is independent of time and that the system is uniform (this allowed us to make a shift of one of the arguments to zero).

The meson correlation function (4.25) describes the real-time propagation of a meson which consists of a $q\bar{q}$ pair. Similarly to the case of one-particle Green's functions discussed before, in order to calculate the real-time correlation function (4.25) we initially calculate the temperature correlation function and subsequently do the analytic continuation. The temperature meson correlation function is defined as

$$\chi_{ab}(\tau, \boldsymbol{x}) = \operatorname{Tr} \left\{ \hat{\rho} \hat{T}_\tau \hat{O}_{Ka}(\tau, \boldsymbol{x}) \hat{O}_{Kb}(0, \boldsymbol{0}) \right\}, \qquad (4.27)$$

where the field operators are written in the modified Heisenberg picture (4.3) (we do not introduce the special notation for the temperature correlation function, it can be distinguished by its imaginary time argument τ).

5. Quark self-energy and the gap equation

In the NJL model, one calculates the quark self-energy from the self-consistent Schwinger–Dyson equation. This is usually done either in the

Hartree or *Hartree–Fock* approximation. Furthermore, different regularization schemes can be used to define divergent integrals. In order to illustrate these possibilities, we come back to the separate discussion of the one-flavour, two-flavour symmetric, and two-flavour standard models. The one-flavour case will be treated in the Hartree approximation and the 3-dimensional cutoff will be used as a regulator. The two-flavour symmetric case will be considered in the Hartree–Fock approximation and we shall regularize it using a version of the Pauli–Villars method. Finally, we shall discuss the standard version of the two-flavour model in the Hartree–Fock approximation, regularizing it with the help of the Schwinger proper-time method.

We analyze the differences in the formulation of the theory in more detail, since several problems of interest for us will be studied later in different versions of the model — it often happens that one version is more suitable for the analysis of a given problem than other versions. In particular, the in-medium dependence of the dynamic and screening masses of mesons (Chapters 6 and 7) as well as the oscillations of the static meson fields at finite baryon density (Chapter 8) are studied within the two-flavour symmetric model. The methods going beyond the Hartree–Fock approximation (Chapter 9) are introduced on the basis of the two-flavour standard model. On the other hand, the transport theory for the model (Chapter 11) is constructed for the one-flavour model.

Using the methods introduced in Chapter 4, we calculate the quark self-energy at finite temperature or density. In this way we can determine the in-medium dependence of the constituent quark mass. Illustrative calculations done in different versions of the model lead to the same qualitative conclusion: with increasing $T(\mu)$ the constituent mass decreases, and for sufficiently large temperature (density) it approaches the value of the current mass.

5.1. One-flavour case

In the one-flavour model, using the Hartree approximation we write the self-consistent Schwinger–Dyson equation in the following form

$$\Sigma = 2iG \int \frac{d^4p}{(2\pi)^4} \left\{ \text{tr}\left[G(p)\right] + i\gamma_5 \,\text{tr}\left[i\gamma_5 G(p)\right] \right\}, \tag{5.1}$$

where tr is the trace over spinor (and colour) indices and $G(p)$ is the quark propagator

$$G(p)^{-1} = \slashed{p} - \Sigma - m + i\epsilon. \tag{5.2}$$

The two terms on the RHS of Eq. (5.1) appear since Lagrangian (3.1) describes both scalar and pseudoscalar interactions, see Fig. 5.1. However, parity implies that the second term in (5.1) vanishes.

Hartree terms
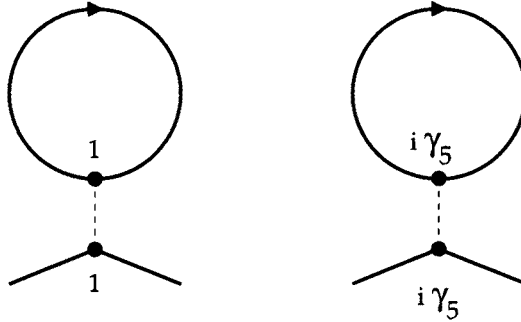
Fig. 5.1. Diagrams used for the calculation of the quark self-energy in the Hartree approximation (one-flavour model). The solid line describes the quark propagator, whereas the dashed line is introduced to describe the point-like quark-antiquark interaction. Only the first term gives a non-zero contribution to the self-energy.

Using the general formula for the quark propagator, Eq. (4.10), we define the *quark condensate* through equation

$$\langle \overline{q}q \rangle = -i \operatorname{tr} G(x = 0^-). \tag{5.3}$$

Rewriting Eq. (5.3) in the momentum space, we find that

$$\langle \overline{q}q \rangle = -4N_c\, i \int \frac{d^4p}{(2\pi)^4} \frac{\Sigma + m}{p^2 - (\Sigma + m)^2 + i\epsilon}. \tag{5.4}$$

The sum $\Sigma + m$ can be regarded as the *constituent* (effective or dynamic) quark mass M, whose origin are the quark-antiquark interactions. Eqs (5.1) and (5.4) lead to the simple relation

$$M = m - 2G\langle \overline{q}q \rangle, \tag{5.5}$$

which connects the constituent quark mass directly to the condensate. Eq. (5.5) is called the *gap equation* since it determines the energy gap in the energy spectrum of one-particle excitations.

In writing expressions (5.1)–(5.5) we have used the Feynman rules for $T = \mu = 0$. As it was pointed out in Chapter 4, the Feynman rules at finite T and μ have the same structure. Consequently, we can always start our discussion with the consideration of the standard Feynman diagrams. Later

on, the expressions valid at finite T and μ are obtained by employing the prescriptions: (4.18), (4.23) and (4.24). In particular, it turns out that the form of formula (5.5) is valid also at finite T and μ provided one writes $\langle \bar{q}q \rangle$ as a sum of two contributions

$$\langle \bar{q}q \rangle = \langle \bar{q}q \rangle_{\text{vac}} + \langle \bar{q}q \rangle_{\text{med}}. \tag{5.6}$$

For the moment, let us concentrate in more detail on the vacuum part of the condensate $\langle \bar{q}q \rangle_{\text{vac}}$. Of course, it can be evaluated directly from Eq. (5.4). For further use, it is convenient to introduce the function $I_{1,\text{vac}}(M^2)$ defined as

$$I_{1,\text{vac}}(M^2) = 8iN_c \int \frac{d^4p}{(2\pi)^4} \frac{1}{p^2 - M^2 + i\epsilon}. \tag{5.7}$$

Using Eqs (5.4) and (5.7) we write

$$\langle \bar{q}q \rangle_{\text{vac}} = -\frac{M}{2} I_{1,\text{vac}}(M^2). \tag{5.8}$$

Integration over energy in (5.7) leads to the following expression

$$I_{1,\text{vac}}(M^2) = 4N_c \int \frac{d^3p}{(2\pi)^3} \frac{1}{E_p}, \quad E_p = \sqrt{p^2 + M^2}. \tag{5.9}$$

The 3-dimensional integral appearing in Eq. (5.9) diverges. The simplest way of its regularization is the introduction of a cutoff Λ, confining the region of integration to the sphere $|p| < \Lambda$. In this case one finds

$$I_{1,\text{vac}}^{R,3D}(M^2) = \frac{N_c \Lambda^2}{\pi^2} \left[\sqrt{1 + \left(\frac{M}{\Lambda}\right)^2} - \left(\frac{M}{\Lambda}\right)^2 \ln \frac{\Lambda + \sqrt{\Lambda^2 + M^2}}{M} \right]. \tag{5.10}$$

Using now Eqs (5.5), (5.8) and (5.10) we obtain the following explicit form of the gap equation

$$M\left[1 - \frac{m}{M}\right] = M \frac{N_c G \Lambda^2}{\pi^2} \left[\sqrt{1 + \left(\frac{M}{\Lambda}\right)^2} - \left(\frac{M}{\Lambda}\right)^2 \ln \frac{\Lambda + \sqrt{\Lambda^2 + M^2}}{M} \right]. \tag{5.11}$$

It is interesting to look at some consequences of Eq. (5.11). At first, let us consider the case of the chiral limit $m = 0$. The expression in the square bracket on the RHS of formula (5.11) is positive and smaller than 1 for $M > 0$. Thus, the nontrivial solution exists only if $0 < \pi^2/(N_c G \Lambda^2) < 1$.

See Fig. 5.2, where Eq. (5.11) has been plotted for two different values of G. As $G\Lambda^2$ increases over the critical value π^2/N_c, M starts rising from zero. Consequently, the form of Eq. (5.11) indicates that the force between quarks and antiquarks must be positive $(G > 0)$ and strong enough to cause the formation of the condensate. In the analogy to the BCS theory of super-conductivity, one expects that the nontrivial solution of Eq. (5.11) corresponds to the true ground state of the model [4]. This is indeed so, and this fact can be verified by performing a variational calculation (for more details on this subject see the original paper by Nambu and Jona-Lasinio [4] or the last review listed in [25]). If the current quark mass m does not vanish, one can find out that there is always a nontrivial solution to Eq. (5.11). Moreover, it corresponds to the ground state of the theory, similarly as in the special case $m = 0$.
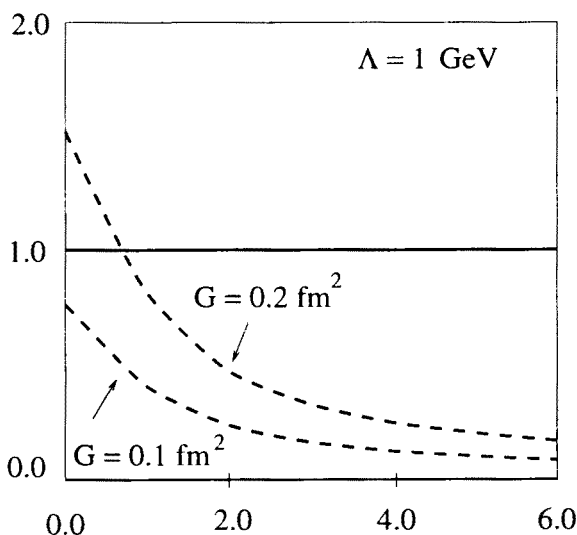
Fig. 5.2. Graphical representation of Eq. (5.11) in the limiting case $m = 0$ and for two different values of the coupling constant G. The common factor M, appearing on both sides of Eq. (5.11), has been omitted. The LHS is represented by the solid line, whereas the RHS is represented by the two dashed lines. Only if $G\Lambda^2$ is greater than the critical value π^2/N_c, there exists a nontrivial solution.

Of course, formula (5.11) is valid only for $T = \mu = 0$. If the system is in contact with a heat bath or with a reservoir of particles, Eq. (5.11) has to be

----

[4] In the Hartree approximation the true ground state of the theory can be described as consisting of the Dirac sea of the constituent quarks — *complicated* vacuum of strongly interacting *light* current quarks is approximated by a *simple* vacuum of the *heavy* constituent quarks.

generalized. To find the in-medium form of the gap equation we calculate the in-medium part of the condensate $\langle \bar{q}q \rangle_{\text{med}}$. Similarly to Eq. (5.8) we can write

$$\langle \bar{q}q \rangle_{\text{med}} = -\frac{M}{2} I_{1,\text{med}}(M^2). \qquad (5.12)$$

In the special cases (i.e., for $T > 0$ and $\mu = 0$ or for $T = 0$ and $\mu > 0$) we have:

$$
\begin{aligned}
I_{1,\text{tem}}(M^2) &= -16iN_c \int\limits_{-i\infty+\epsilon}^{i\infty+\epsilon} \frac{dp^0}{2\pi} \int \frac{d^3p}{(2\pi)^3} \frac{1}{p_0^2 - \boldsymbol{p}^2 - M^2} \frac{1}{e^{p^0/T} + 1} \\
&= -\frac{4N_c}{\pi^2} \int\limits_0^\infty \frac{dp\, p^2}{E_p} \frac{1}{e^{E_p/T} + 1}
\end{aligned}
\qquad (5.13)
$$

and

$$
\begin{aligned}
I_{1,\text{mat}}(M^2) &= 8iN_c \oint\limits_{\mathcal{C}} \frac{dp^0}{2\pi} \int \frac{d^3p}{(2\pi)^3} \frac{1}{p_0^2 - \boldsymbol{p}^2 - M^2} \\
&= -\frac{2N_c}{\pi^2} \int\limits_0^\infty \frac{dp\, p^2}{E_p} \theta(\mu - E_p) = -\frac{2N_c}{\pi^2} \int\limits_0^{\sqrt{\mu^2 - M^2}} \frac{dp\, p^2}{E_p}.
\end{aligned}
\qquad (5.14)
$$

The form of Eqs (5.13) and (5.14) follows from the application of the replacement rules (4.18), (4.23) and (4.24) in the expression on the RHS of Eq. (5.7).

It is important to realize that expressions (5.13) and (5.14) are well defined converging integrals, and they do not have to be regularized, which is in contrast to the calculation of the vacuum part (5.7). Note that the sum $I_{1,\text{vac}}(M^2) + I_{1,\text{med}}(M^2)$ should vanish in the limit $T \to \infty$ or $\mu \to \infty$. This condition follows from the general property of the fermionic Matsubara sums. Since we have introduced the finite cutoff in the calculation of $I_{1,\text{vac}}(M^2)$, the discussed condition may not be fulfilled. For instance, at finite temperature we find the expression

$$I_{1,\text{vac}}^{R,3D}(M^2) + I_{1,\text{tem}}(M^2) = \frac{2N_c}{\pi^2} \left[\int\limits_0^\Lambda \frac{dp\, p^2}{E_p} - \int\limits_0^\infty \frac{dp\, p^2}{E_p} \frac{2}{e^{E_p/T} + 1} \right], \qquad (5.15)$$

which does not vanish at $T \to \infty$. However, if the function $I_{1,\text{tem}}(M^2)$ is regularized in the same way as the function $I_{1,\text{vac}}(M^2)$, the sum $I_{1,\text{vac}}^{R,3D}(M^2) + I_{1,\text{tem}}^{R,3D}(M^2)$ has the desired high temperature limit. This example leads us to the simple conclusion: *if the cutoffs used for the regularization of the vacuum parts are finite, the temperature (matter) parts must be additionally regularized.* This ensures the correct high temperature (density) behaviour of the complete expression.

With these conditions in mind, we write the finite temperature gap equation in the form

$$M \left[1 - \frac{m}{M} \right] = M \frac{2 N_c G}{\pi^2} \int_0^\Lambda \frac{dp\, p^2}{E_p} \left[1 - \frac{2}{e^{E_p/T} + 1} \right]. \tag{5.16}$$

Since the RHS of Eq. (5.16) vanishes in the limit $T \to \infty$, the constituent quark mass M drops to the current one m (with increasing T). In the special case $m = 0$, there exists a critical temperature T_c such that for $T > T_c$ formula (5.16) has only a trivial solution $M = 0$. This fact implies the restoration of chiral symmetry at high temperature. See Fig. 5.3, where the temperature dependence of the constituent quark mass has been plotted.
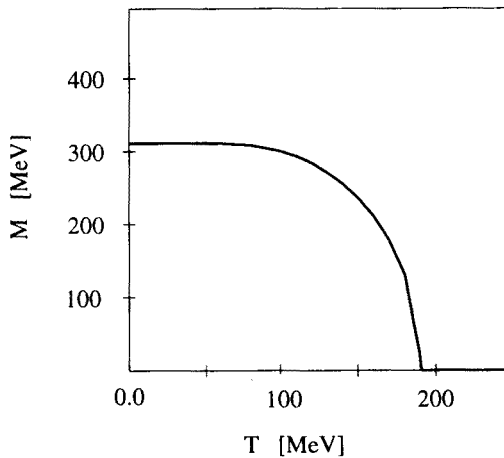
Fig. 5.3. Temperature dependence of the constituent quark mass M in the limiting case $m = 0$. If temperature is greater than the critical one (in this case T_c turns out to be 190 MeV) there exists only a trivial solution to the gap equation (5.16), *i.e.*, $M = 0$ for $T > T_c$. This fact indicates the restoration of chiral symmetry. In the present calculation the 3-dimensional cutoff regularization was adopted and we used the following parameters: $\Lambda = 0.65$ GeV, $G = 0.4$ fm^2 and $N_c = 3$ (this gives $M = M_0 = 313$ MeV at $T = 0$).

In the analogous way, for finite densities but $T = 0$, one finds

$$M \left[1 - \frac{m}{M} \right] = M \frac{2N_c G}{\pi^2} \int\limits_{p_F}^{\Lambda} \frac{dp \, p^2}{E_p}, \tag{5.17}$$

where p_F is the Fermi momentum of quarks, *i.e.*, $p_F = \sqrt{\mu^2 - M^2}$. Calculating explicitly the integral on the RHS of expression (5.17) one finds

$$M \left[1 - \frac{m}{M} \right] = M \frac{N_c G \Lambda^2}{\pi^2} \left\{ \sqrt{1 + \left(\frac{M}{\Lambda} \right)^2} - \left(\frac{M}{\Lambda} \right)^2 \ln \frac{\Lambda + \sqrt{\Lambda^2 + M^2}}{M} \right.$$

$$\left. - \sqrt{1 + \left(\frac{M}{p_F} \right)^2} + \left(\frac{M}{p_F} \right)^2 \ln \frac{p_F + \sqrt{p_F^2 + M^2}}{M} \right\}. \tag{5.18}$$

Equation (5.17), or equivalently Eq. (5.18), leads again to the chiral restoration. See Fig. 5.4, where the constituent quark mass (being the solution of Eq. (5.17) for the case $m = 0$) has been plotted as a function of p_F. Now the phase transition takes place at finite baryon density. Similarly to the finite-temperature case, there is a critical value p_F^c, such that for $p_F > p_F^c$ there is only a trivial solution to the gap equation.
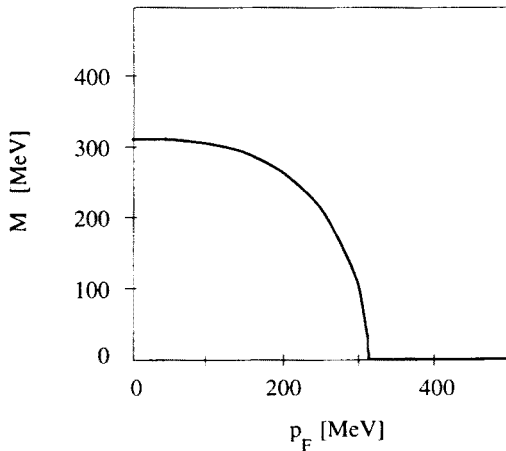

Fig. 5.4.   Density dependence of the constituent quark mass M (for the 3-dimensional cutoff regularization and in the chiral limit $m = 0$). The mass is plotted as a function of the quark Fermi momentum p_F. In this case, there is also a chiral restoration phase transition happening at $p_F^c = 314$ MeV. The numerical values of the parameters are the same as in the previous figure.

To our knowledge, the first evaluation of the in-medium dependence of the constituent quark mass in the NJL model was given by Hatsudo and Kunihiro [6]. Afterwards, many authors repeated this kind of calculation. The results shown in Figs 5.3 and 5.4 are obtained for the set of parameters equivalent to that used in [16]. The decrease of M with increasing temperature, see Fig. 5.3, implies the decrease of the quark condensate (strictly speaking of the absolute value of $\langle \overline{q}q \rangle$). We note that, a similar tendency in the behaviour of $\langle \overline{q}q \rangle$ has been observed in the lattice simulations of QCD as well as in the calculations based on the chiral perturbation theory. A more quantitative comparison of the NJL results with other estimates will be given in Chapter 9.

5.2. Two-flavour symmetric case

We shall consider the two-flavour symmetric model in the Hartree–Fock approximation. The appropriate form of the Schwinger-Dyson equation, see Fig. 5.5, is now

$$
\Sigma = G_S i \sum_{i=0}^{3} \int \frac{d^4 p}{(2\pi)^4} \left\{ \tau_i \text{tr} \left[\tau_i G(p) \right] - \tau_i G(p) \tau_i \right.
$$
$$
\left. + i\tau_i \gamma_5 \text{tr} \left[i\tau_i \gamma_5 G(p) \right] - i\tau_i \gamma_5 G(p) i\tau_i \gamma_5 \right\}. \tag{5.19}
$$

Because the second term with the trace in Eq. (5.19) vanishes and the terms without the trace cancel each other, expression (5.19) can be rewritten in a simpler form, namely

$$
\Sigma = G_S i \sum_{i=0}^{3} \int \frac{d^4 p}{(2\pi)^4} \tau_i \text{tr} \left[\tau_i G(p) \right]. \tag{5.20}
$$

We note that the quark propagator has now extra isospin indices (in comparison to the one-flavour model discussed before) and tr includes now the trace over the isospin space. Consequently, in the present case we have $2\langle \overline{q}q \rangle = -i \text{tr} G(x = 0^-)$. This is due to our convention that $\langle \overline{q}q \rangle$ describes the contribution to the quark condensate from one flavour only, see Eq. (5.4). Nevertheless, one can check that the form of Eq. (5.5) remains unchanged in the present case — the replacements $\langle \overline{q}q \rangle \to 2\langle \overline{q}q \rangle$ and $G \to G_S/2$ in (5.5) compensate each other giving $M = m - 2G_S \langle \overline{q}q \rangle$.

The 3-dimensional regularization scheme (introduced in the previous Section) has several drawbacks, *e.g.*, it is not Lorentz invariant. Therefore, we

Hartree (direct) terms

Fock (exchange) terms
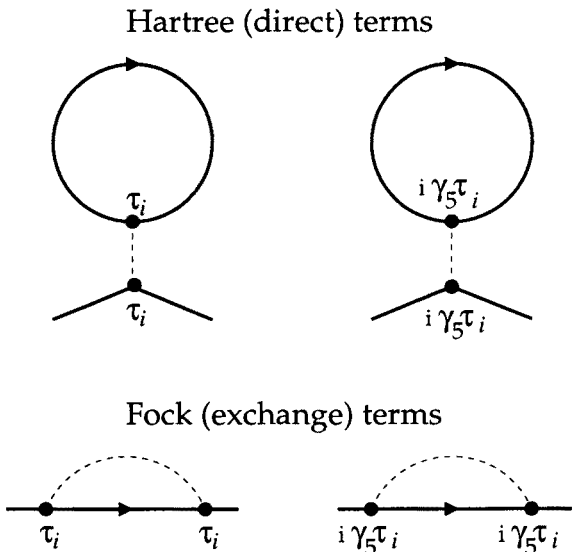
Fig. 5.5 Diagrams contributing to the quark self-energy in the Hartree–Fock approximation (two-flavour symmetric model). We note that the introduction of the dashed lines, describing the point-like quark-antiquark interaction, allows us to distinguish graphically the Hartree and the Fock terms.

shall now discuss another method of regularization. As we shall later see, it can be regarded as a version of the Pauli-Villars subtraction scheme. At first, let us consider the function $I_{1,\text{vac}}(M^2)$ defined by Eq. (5.7). By making the Wick rotation to the variable $p_4 = -ip^0$ we can write

$$I_{1,\text{vac}}(M^2) = 8N_c \int \frac{d^4 p_E}{(2\pi)^4} \frac{1}{p_E^2 + M^2}, \qquad (5.21)$$

where $d^4 p_E = dp_4 d^3 p$ and $p_E^2 = p_4^2 + \boldsymbol{p}^2$. We replace now $I_{1,\text{vac}}(M^2)$ by the series

$$I_{1,\text{vac}}(M^2) \to I_{1,\text{vac}}^{R,PV}(M^2) = \sum_{i=0}^{N} A_i I_{1,\text{vac}}(\Lambda_i^2). \qquad (5.22)$$

Here $A_0 = 1$, $\Lambda_0 = M$ and N is the number of the so-called subtractions. The regulating masses Λ_i and the coefficients A_i $(i > 0)$ should be chosen in such a way as to provide the finite result for $I_{1,\text{vac}}^{R,PV}(M^2)$. This requirement leads to the following set of constraints

$$\sum_{i=0}^{N} A_i = 0, \quad \sum_{i=0}^{N} A_i \Lambda_i^2 = 0, \quad \ldots \quad , \sum_{i=0}^{N} A_i \Lambda_i^{2(N-1)} = 0. \tag{5.23}$$

Using Eq. (5.23) we find

$$I_{1,\text{vac}}^{R,PV}(M^2) = \frac{N_c}{2\pi^2} \sum_{i=0}^{N} A_i \, \Lambda_i^2 \ln \Lambda_i^2. \tag{5.24}$$

As it was discussed above, the temperature (matter) parts should be regularized as well. We do it again by making the replacement

$$I_{1,\text{med}}(M^2) \to I_{1,\text{med}}^{R,PV}(M^2) = \sum_{i=0}^{N} A_i I_{1,\text{med}}(\Lambda_i^2), \tag{5.25}$$

where $I_{1,\text{med}}(\Lambda_i^2)$ is defined by Eqs (5.13) and (5.14).

In Figs 5.6 and 5.7 we show the in-medium dependence of M obtained from the two-flavour symmetric model regularized with the help of the Pauli-Villars method described above. Of course, these two figures are analogs of Figs 5.4 and 5.5 from the previous Section. In the present case we do not limit ourselves to the limit $m = 0$. As the result we find that M does not drop suddenly to zero, but it goes smoothly to the value $M = m$ for $T \to \infty$ or $\mu \to \infty$. Moreover, the method of subtractions "switches off" large momenta more gradually than the 3-dimensional cutoff procedure. Thus, the temperature and density dependence of M shown in Figs 5.6 and 5.7 looks weaker than that shown in Figs 5.4 and 5.5. Nevertheless, the qualitative behaviour of M in the two versions of the model is the same. In particular, vanishing of the condensate at large T or μ in both cases indicates the chiral symmetry restoration phase transition.

We note that at $T = 0$ all values of the chemical potential in the range $0 < \mu < M$ are equivalent and correspond to the physical vacuum. The reason is that the chemical potential μ is the energy needed to add a quark to the system. Clearly μ must exceed the minimal energy, the vacuum rest mass of a quark M, before the Fermi sea of quarks begins to be populated.
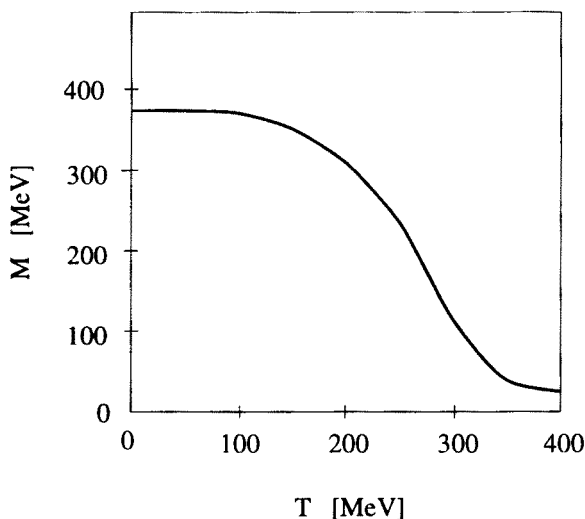
Fig. 5.6. Temperature dependence of the constituent quark mass. Pauli–Villars regularization scheme (as described in the text) was employed here with three regulating masses: $\Lambda_1 = 0.68$ GeV, $\Lambda_2 = 2.1\Lambda_1$ and $\Lambda_3 = 2.1\Lambda_2$. The coupling constant $G_S = 0.75$ fm^2, and the current quark mass $m = 8.56$ MeV.
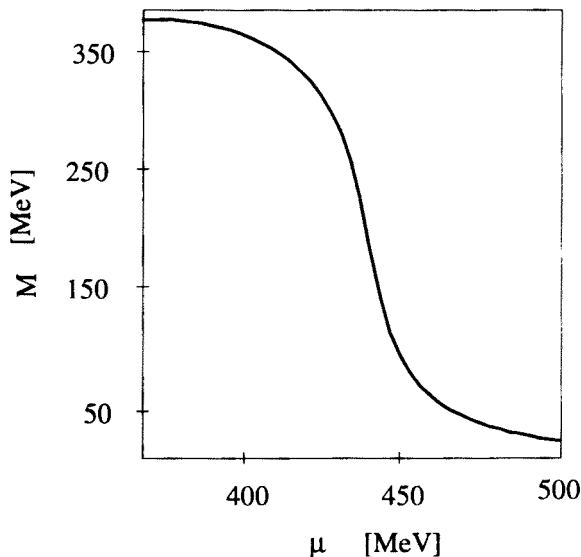
Fig. 5.7. Constituent quark mass as a function of the quark chemical potential μ. Pauli-Villars regularization procedure was used here with the same parameters as in Fig. 5.6.

5.3. Two-flavour standard case

Let us turn to the discussion of the two-flavour standard model. Calculating the quark self-energy in the Hartree–Fock approximation one finds

$$\Sigma = 2G\,i \int \frac{d^4p}{(2\pi)^4} \left\{ \mathrm{tr}[G(p)] - G(p) + i\tau\gamma_5 \mathrm{tr}\left[i\tau\gamma_5 G(p)\right] - i\tau\gamma_5 G(p) i\tau\gamma_5 \right\}, \tag{5.26}$$

which after calculation of the trace over spinor indices gives

$$M = m + 4iMG\left(2N_c N_f + 1\right) \int \frac{d^4p}{(2\pi)^4} \frac{1}{p^2 - M^2 + i\epsilon}. \tag{5.27}$$

In contrast to the symmetric version of the model, in this case the Fock terms (see Fig. 5.8) do not cancel each other. The extra "1" in (5.27) comes just from the inclusion of the exchange terms. Nevertheless, for $N_c = 3$ and $N_f = 2$ the contribution from the Fock terms can be regarded as a small correction to the result obtained only with the Hartree approximation. Consequently, one typically neglects the Fock terms arguing that this is allowed in the leading order of the $1/N_c$ expansion. A more rigorous treatment of the model in the $1/N_c$ expansion, which generalizes the results of this Section, will be presented in Chapter 9.

Neglecting the Fock terms, we find the gap equation in the form

$$M = m - 4G\langle \bar{q}q \rangle = m + 2MG I_{1,\mathrm{vac}}(M^2). \tag{5.28}$$

In this case, we can again use our definitions (5.4) and (5.8). We note that there is a factor $4G$ in the gap equation (5.28), which is in contrast to our two previous cases where a factor $2G$ appeared.

Discussing the standard version of the model, we shall introduce yet another regularization procedure. This is so-called Schwinger proper-time method based on the following replacement

$$I_{1,\mathrm{vac}}(M^2) = 8N_c \int \frac{d^4p_E}{(2\pi)^4} \frac{1}{p_E^2 + M^2}$$

$$\longrightarrow 8N_c \int \frac{d^4p_E}{(2\pi)^4} \int_{\Lambda^{-2}}^{\infty} ds \, \exp\left\{ -s[p_E^2 + M^2] \right\}. \tag{5.29}$$

Introducing the exponential integral function defined as

$$E_n(x) \equiv \int_{1}^{\infty} dt \, t^{-n} \exp(-xt), \tag{5.30}$$

we can write

$$I_{1,\text{vac}}^{R,\text{SPT}}(M^2) = \frac{N_c \Lambda^2}{2\pi^2} E_2 \left[\frac{M^2}{\Lambda^2}\right]. \tag{5.31}$$

Using the Schwinger proper-time regularization at finite temperature, it is not convenient to separate the vacuum and temperature parts. We only replace the integral over energy by the sum over the Matsubara frequencies. According to formula (4.18), we can generalize Eq. (5.31) to the finite temperature case writing

$$I_1^{R,\text{SPT}}(M^2, T)$$

$$= 8N_c T \sum_j \int \frac{d^3p}{(2\pi)^3} \int_{\Lambda^{-2}}^{\infty} ds \, \exp\left\{-s\left[(2j+1)^2\pi^2T^2 + \boldsymbol{p}^2 + M^2\right]\right\}$$

$$= N_c \frac{T\Lambda}{\pi^{\frac{3}{2}}} \sum_j E_{\frac{3}{2}} \left[\frac{M^2 + (2j+1)^2\pi^2T^2}{\Lambda^2}\right]. \tag{5.32}$$

Solving the gap equation (5.28) with $I_{1,\text{vac}}(M^2)$ replaced by $I_1^{R,SPT}(M^2, T)$ we find again the characteristic T-dependence of M, similar to that shown in Fig. 5.3 or 5.6.

Hartree (direct) terms
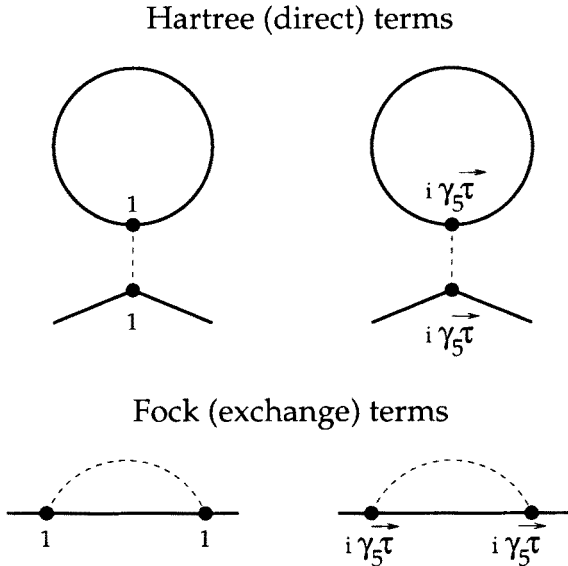

Fock (exchange) terms

Fig. 5.8. Diagrams used for the calculation of the quark self-energy in the case of the standard two-flavour model.

At this place we close our considerations of the Schwinger-Dyson equation in the different formulations of the model. The results derived by us in Sections 5.1–5.3 will be frequently used in the next Chapters. In particular, we shall return to the discussion of the two-flavour standard model and the Schwinger proper-time method in Chapter 9, where the calculations extending the HF approach will be presented.

6. Mesonic excitations

Mesons are quark-antiquark excitations of the true ground state of the theory. Their quantitative description requires introduction of the meson correlation functions, as we did it in the end of Chapter 4. In the NJL model, the overall scheme used to describe mesons is similar to the standard HF (Hartree–Fock) + RPA (random phase approximation) approach known from nuclear physics. The Hartree–Fock ground state (vacuum) contains the quark condensate. It is determined through a nontrivial solution of the gap equation. Mesons, being quark-antiquark excitations of the vacuum, behave very much like particle-hole states in a strongly interacting manybody system.

In the first Section of this Chapter we present details of the calculation of the zeroth-order correlation functions at finite T and μ. The second Section contains further discussion concerning the regularization of the model. In the third Section we define the full correlation function in the RPA approximation and discuss the difference between the dynamic and screening masses. Finally, we show that at sufficiently large T or μ, the dynamic masses of chiral partners become equal. Such degeneracy is a characteristic feature of the chiral symmetry restoration phase transition.

6.1. Zeroth-order correlation functions

Our investigation of the meson properties in the NJL model starts with the calculation of the meson correlation functions. At first, using Eqs (4.25) and (4.26), we construct the zeroth-order correlation functions. They correspond to the following quark loop diagram [5]

$$\chi_{AB}^{(0)\,ij}(Q) = i \operatorname{tr} \int \frac{d^4 p}{(2\pi)^4} [\Gamma_A \tau^i G(p+Q) \Gamma_B \tau^j G(p)]. \tag{6.1}$$

---

[5] Conventions introduced in this Chapter are suitable for the two-flavour symmetric model defined in Sections 3.2 and 5.2. Nevertheless, as we have seen in Chapter 5, changing N_f and/or G_S one can easily obtain expressions whose form is valid for other versions of the model.

Here $Q^\mu = (\omega, \boldsymbol{q})$ is the external (meson) momentum. The indices A and B take on the values P or S and Γ_P, Γ_S are the Dirac matrices in the spinor space: $\Gamma_P = i\gamma_5$ and $\Gamma_S = 1$. We note that the indices a and b in Eq. (4.26) correspond to two pairs of indices in Eq. (6.1), namely $a = (A, i)$ and $b = (B, j)$, see also Fig. 6.1.
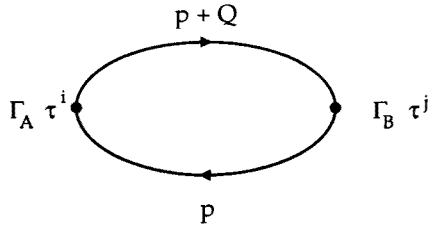
Fig. 6.1. Quark loop diagram corresponding to the zeroth-order meson correlation function.

In the isospin symmetric case the matrix $\chi_{AB}^{(0)\,ij}$ is diagonal in flavour indices and its all diagonal elements are the same. Consequently, we can write $\chi_{AB}^{(0)\,ij} = \delta^{ij} \chi_{AB}^{(0)}$, where

$$\chi_{AB}^{(0)}(Q) = 2iN_c \, \mathrm{Sp} \int \frac{d^4p}{(2\pi)^4} \left[\Gamma_A G(p+Q) \Gamma_B G(p) \right]. \tag{6.2}$$

Calculation of the trace over the Dirac indices, denoted here by Sp, shows that the nondiagonal terms $(A \neq B)$ vanish. Therefore, we are left with two non-vanishing functions

$$\chi_{PP}^{(0)}(Q) = 8iN_c \int \frac{d^4p}{(2\pi)^4} \frac{p^2 - M^2 + p \cdot Q}{[(p+Q)^2 - M^2 + i\epsilon][p^2 - M^2 + i\epsilon]} \tag{6.3}$$

and

$$\chi_{SS}^{(0)}(Q) = 8iN_c \int \frac{d^4p}{(2\pi)^4} \frac{p^2 + M^2 + p \cdot Q}{[(p+Q)^2 - M^2 + i\epsilon][p^2 - M^2 + i\epsilon]}. \tag{6.4}$$

6.1.1. Vacuum parts

Using the imaginary-time formalism, discussed in detail in Chapter 4, we generalize expressions (6.3) and (6.4) to the case of finite temperature (density). To do it, we replace the integration over energy in Eqs (6.3) and (6.4) by the Matsubara sums (4.18), and convert these sums to the contour integrals using expressions (4.23) and (4.24). In this case, the vacuum parts of the correlation functions can be represented in a compact form

$$\chi_{PP,\mathrm{vac}}^{(0)}(Q) = I_{1,\mathrm{vac}}(M^2) - Q^2 I_{2,\mathrm{vac}}(M^2, Q^2) \tag{6.5}$$

and

$$\chi_{SS,\text{vac}}^{(0)}(Q) = I_{1,\text{vac}}(M^2) - (Q^2 - 4M^2)I_{2,\text{vac}}(M^2, Q^2). \qquad (6.6)$$

The function $I_{1,\text{vac}}(M^2)$, appearing in Eqs (6.5) and (6.6), has been already defined by formula (5.7). The new function $I_{2,\text{vac}}(M^2, Q^2)$ is defined by the integral

$$I_{2,\text{vac}}(M^2, -q_E^2) = -4N_c \int \frac{d^4 p_E}{(2\pi)^4} \frac{1}{[(p_E + \frac{q_E}{2})^2 + M^2][(p_E - \frac{q_E}{2})^2 + M^2]}, \qquad (6.7)$$

where $p_4 = -ip^0$, $q_4 = -i\omega$ and $d^4 p_E = dp_4 d^3 p$. We note that frequency Q^0 is purely imaginary now ($Q^0 = \omega \to iq_4$), thus the "Euclidean" form of expression (6.7) is natural here.

6.1.2. Temperature parts

The form of the temperature part of $\chi_{PP}^{(0)}(Q)$ follows from Eqs (6.3) and (4.23)

$$\chi_{PP,\text{tem}}^{(0)}(Q)$$

$$= -8iN_c \int_{-i\infty+\epsilon}^{i\infty+\epsilon} \frac{dp^0}{2\pi} \int \frac{d^3 p}{(2\pi)^3} \left[\frac{1}{(p+Q)^2 - M^2} + \frac{1}{(p-Q)^2 - M^2} \right] \frac{1}{e^{p^0/T} + 1}$$

$$- 8iN_c \int_{-i\infty+\epsilon}^{i\infty+\epsilon} \frac{dp^0}{2\pi} \int \frac{d^3 p}{(2\pi)^3} \left[\frac{p \cdot Q}{[(p+Q)^2 - M^2][p^2 - M^2]} \right.$$

$$\left. - \frac{p \cdot Q}{[(p-Q)^2 - M^2][p^2 - M^2]} \right] \frac{1}{e^{p^0/T} + 1}. \qquad (6.8)$$

Using again the fact that Q^0 is the bosonic Matsubara frequency ($Q^0 = \omega \to i\omega_m = 2m\pi iT$), we make the shifts of the integration variable p^0, and simplify expression (6.8) to the form [6]

$$\chi_{PP,\text{tem}}^{(0)}(Q) = -16iN_c \int_{-i\infty+\epsilon}^{i\infty+\epsilon} \frac{dp^0}{2\pi} \int \frac{d^3 p}{(2\pi)^3} \frac{1}{p^2 - M^2} \frac{1}{e^{p^0/T} + 1}$$

$$+ 8iN_c Q^2 \int_{-i\infty+\epsilon}^{i\infty+\epsilon} \frac{dp^0}{2\pi} \int \frac{d^3 p}{(2\pi)^3} \frac{1}{\left[\left(p + \frac{Q}{2}\right)^2 - M^2\right]\left[\left(p - \frac{Q}{2}\right)^2 - M^2\right]}$$

$$\times \frac{1}{e^{(p^0 + i\omega_m/2)/T} + 1}. \qquad (6.9)$$

---

[6] At this place we write $\omega = i\omega_m$ rather than $\omega = iq_4$ in order to point out the discrete character of the complex variable ω. This fact allows us to make the shifts of the argument of the exponent.

The last result indicates that the analogous decomposition to that find in vacuum, see Eq. (6.5), holds also at finite temperature, namely

$$
\chi_{PP,\text{tem}}^{(0)}(Q) = I_{1,\text{tem}}(M^2) - Q^2 I_{2,\text{tem}}(M^2, Q), \tag{6.10}
$$

where $I_{1,\text{tem}}(M^2)$ is defined by Eq. (5.13) and the function $I_{2,\text{tem}}(M^2, Q)$ has the form

$$
I_{2,\text{tem}}(M^2, Q) = - \; 8iN_c \int_{-i\infty+\epsilon}^{i\infty+\epsilon} \frac{dp^0}{2\pi} \int \frac{d^3p}{(2\pi)^3} \frac{1}{\left[\left(p+\frac{Q}{2}\right)^2 - M^2\right]\left[\left(p-\frac{Q}{2}\right)^2 - M^2\right]}
$$

$$
\times \; \frac{1}{e^{(p^0+i\omega_m/2)/T}+1}. \tag{6.11}
$$

Since $I_{2,\text{tem}}(M^2, Q)$ is a function of ω^2 and q^2, we shall also use the notation $I_{2,\text{tem}}(M^2, \omega^2, q^2)$. In the special cases (*i.e.*, either for $q = 0$ or $\omega = 0$) one finds

$$
I_{2,\text{tem}}(M^2, \omega^2, 0) = \frac{N_c}{\pi^2} \int_0^\infty \frac{dp\, p^2}{E_p} \frac{1}{e^{E_p/T}+1} \frac{1}{E_p^2 - \frac{1}{4}\omega^2} \tag{6.12}
$$

and

$$
I_{2,\text{tem}}(M^2, 0, q^2) = -\frac{N_c}{q\pi^2} \int_0^\infty \frac{dp\, p}{E_p} \frac{1}{e^{E_p/T}+1} \ln\left|\frac{2p - q}{2p + q}\right|. \tag{6.13}
$$

We note that Eq. (6.12) has been obtained for a purely imaginary frequency $\omega = i\omega_m$. Thus, the expression on the RHS of (6.12) is a well defined quantity. Furthermore, according to the rules discussed by us in Chapter 4, the result (6.12) can be analytically continued to real frequencies. This can be achieved by making the substitution $i\omega_m \to \omega \pm i\epsilon$, where ω is *real*.

In the similar way one does the calculations in the scalar channel finding the following decomposition

$$
\chi_{SS,\text{tem}}^{(0)}(Q) = I_{1,\text{tem}}(M^2) - (Q^2 - 4M^2) I_{2,\text{tem}}(M^2, Q), \tag{6.14}
$$

which is the analog of Eq. (6.6).

6.1.3. Matter parts

In order to calculate the matter part of the correlation function $\chi_{PP}^{(0)}(Q)$, we use Eqs (6.3) and (4.24), which yield

$$
\chi_{PP,\text{mat}}^{(0)}(Q) = 8iN_c \int_C \frac{dp^0}{2\pi} \int \frac{d^3p}{(2\pi)^3} \left[\frac{1}{(p+Q)^2 - M^2} \right.
$$
$$
\left. + \frac{p \cdot Q}{[(p+Q)^2 - M^2][p^2 - M^2]} \right]. \tag{6.15}
$$

Making the shifts of the integration variable p^0, one can check that the decomposition of the form (6.5) or (6.10) is valid at finite density. Indeed, after a few manipulations we obtain

$$
\chi_{PP,\text{mat}}^{(0)}(Q) = I_{1,\text{mat}}(M^2) - Q^2 I_{2,\text{mat}}(M^2, Q), \tag{6.16}
$$

where $I_{1,\text{mat}}(M^2)$ is defined by Eq. (5.14) and the function $I_{2,\text{mat}}(M^2, Q)$ is given by expression

$$
I_{2,\text{mat}}(M^2, Q) = 4iN_c \int_C \frac{dp^0}{2\pi} \int \frac{d^3p}{(2\pi)^3} \frac{1}{\left[\left(p+\frac{Q}{2}\right)^2 - M^2\right]\left[\left(p-\frac{Q}{2}\right)^2 - M^2\right]}. \tag{6.17}
$$

The calculation of $I_{2,\text{mat}}(M^2, \omega^2, q^2)$ proceeds in the same way as the calculation of the function $I_{1,\text{mat}}(M^2)$. Now, as remarked above, the integral over p^0 is evaluated for imaginary ω and subsequently analytically continued to real frequencies. The final results (for $\omega > 0$) are

$$
I_{2,\text{mat}}(M^2, \omega^2 \pm i\epsilon, 0) = \frac{N_c}{2\pi^2} \int_0^{p_F} \frac{dp\, p^2}{E_p} \frac{1}{E_p^2 - \frac{1}{4}(\omega \pm i\epsilon)^2}
$$
$$
= \frac{N_c}{2\pi^2} \left[\log\left(\frac{p_F + E_F}{M}\right) + \mathcal{F}(M^2, \omega^2 \pm i\epsilon) \right] \tag{6.18}
$$

and

$$
I_{2,\text{mat}}(M^2, 0, q^2) = -\frac{N_c}{2q\pi^2} \int_0^{p_F} \frac{dp\, p}{E_p} \cdot \ln\left|\frac{2p-q}{2p+q}\right|
$$
$$
= -\frac{N_c}{2q\pi^2} \mathcal{G}(M^2, q^2), \tag{6.19}
$$

where $E_F = \sqrt{p_F^2 + M^2}$,

$$
\begin{aligned}
\mathcal{F}(M^2, \omega^2 \pm i\epsilon) &= -\frac{1}{\omega}\left[\sqrt{4M^2 - \omega^2}\,\arctan\left(\frac{p_F\omega}{E_F\sqrt{4M^2 - \omega^2}}\right)\right] \quad (\omega < 2M) \\
&= -\frac{1}{\omega}\sqrt{\omega^2 - 4M^2}\,\ln\left[\frac{E_F\sqrt{\omega^2 - 4M^2} + p_F\omega}{E_F\sqrt{\omega^2 - 4M^2} - p_F\omega}\right] \\
&\quad \pm i\frac{\pi}{2\omega}\theta\left(\omega - 2M\right)\theta\left(2E_F - \omega\right)\sqrt{\omega^2 - 4M^2} \qquad (\omega > 2M)
\end{aligned}
\tag{6.20}
$$

and

$$
\begin{aligned}
\mathcal{G}(M^2, q^2) &= \left(\frac{\sqrt{q^2 + 4M^2}}{2} - E_F\right)\ln\left|\frac{2p_F + q}{2p_F - q}\right| \\
&\quad + \frac{\sqrt{q^2 + 4M^2}}{2}\ln\left[\frac{2M^2 + qp_F + E_F\sqrt{q^2 + 4M^2}}{2M^2 - qp_F + E_F\sqrt{q^2 + 4M^2}}\right] \\
&\quad - q\ln\left[\frac{p_F + E_F}{M}\right].
\end{aligned}
\tag{6.21}
$$

It becomes clear now, that for the scalar channel we find the analog of Eq. (6.14), namely

$$
\chi_{SS,\mathrm{mat}}^{(0)}(Q) = I_{1,\mathrm{mat}}(M^2) - (Q^2 - 4M^2)I_{2,\mathrm{mat}}(M^2, Q).
\tag{6.22}
$$

6.2. Regularization of the zeroth-order correlation functions

In the last Section, we have reduced the problem of the evaluation of zeroth order correlation functions to the calculation of the functions $I_1 \equiv I_{1,\mathrm{vac}} + I_{1,\mathrm{med}}$ and $I_2 \equiv I_{2,\mathrm{vac}} + I_{2,\mathrm{med}}$. Nevertheless, one can easily notice that the function $I_{2,\mathrm{vac}}(M^2, -q_E^2)$ is defined by the divergent integral (6.7). Moreover, although the functions $I_{2,\mathrm{med}}(M^2, \omega^2, q^2)$ are finite, they should be regularized in the same way as the vacuum functions. In this way, see discussion in Section 5.1 following Eq. (5.15), we ensure the correct high temperature (density) behaviour of the complete expression $I_2 = I_{2,\mathrm{vac}} + I_{2,\mathrm{med}}$. Thus, in the next three Sections, we shall present three different ways of the regularization of the function $I_2(M^2, \omega^2, q^2)$. We shall use the methods introduced in Chapter 5.

6.2.1. 3-dimensional regularization

At first, let us discuss the simplest method, which is based on the introduction of a 3-dimensional cutoff. Similarly as it was done in Section 5.1, we perform integration over energy in Eq. (6.7). Setting $q=0$ and collecting the contributions from the poles one finds

$$I_{2,\text{vac}}(M^2, -q_4^2) = -\frac{N_c}{2\pi^2} \int \frac{dp\, p^2}{E_p} \frac{1}{E_p^2 + \frac{1}{4} q_4^2}. \tag{6.23}$$

Doing analytic continuation of expression (6.23), $q_4 \rightarrow -i(\omega \pm i\epsilon)$, and introducing the cutoff for p-integration we find $(\omega > 0)$

$$I_{2,\text{vac}}^{R,3D}(M^2, \omega^2 \pm i\epsilon) = -\frac{N_c}{2\pi^2} \int_0^\Lambda \frac{dp\, p^2}{E_p} \frac{1}{E_p^2 - \frac{1}{4}(\omega \pm i\epsilon)^2}. \tag{6.24}$$

This integral can be calculated in the same way as expression (6.18) — there is only an overall difference in sign between these two integrals and p_F in (6.18) corresponds to Λ in (6.24).

The final formula for the regularized function $I_2(M^2, \omega^2 \pm i\epsilon, 0)$ is

$$I_2^{R,3D}(M^2, \omega^2 \pm i\epsilon, 0) = -\frac{N_c}{2\pi^2} \int_0^\Lambda \frac{dp\, p^2}{E_p} \left[1 - \frac{2}{e^{E_p/T} + 1}\right] \frac{1}{E_p^2 - \frac{1}{4}(\omega \pm i\epsilon)^2} \tag{6.25}$$

for finite temperature $(\mu = 0)$, and

$$I_2^{R,3D}(M^2, \omega^2 \pm i\epsilon, 0) = -\frac{N_c}{2\pi^2} \int_{p_F}^\Lambda \frac{dp\, p^2}{E_p} \frac{1}{E_p^2 - \frac{1}{4}(\omega \pm i\epsilon)^2} \tag{6.26}$$

for finite density $(T = 0)$. We note that integral (6.26) also can be done analytically, similarly as Eqs (6.18) or (6.24).

Doing calculations for $q_4 = 0$ and $q \neq 0$ one finds the analogs of (6.25) and (6.26), namely

$$I_2^{R,3D}(M^2, 0, q^2) = \frac{N_c}{2\pi^2 q} \int_0^\Lambda \frac{dp\, p}{E_p} \left[1 - \frac{2}{e^{E_p/T} + 1}\right] \ln \left|\frac{2p - q}{2p + q}\right| \tag{6.27}$$

and

$$I_2^{R,3D}(M^2, 0, q^2) = \frac{N_c}{2\pi^2 q} \int_{p_F}^\Lambda \frac{dp\, p}{E_p} \ln \left|\frac{2p - q}{2p + q}\right|. \tag{6.28}$$

Although the 3-dimensional cutoff regularization is frequently used, for many purposes it is not satisfactory since it explicitly breaks the Lorentz invariance. We have collected the results based on this regularization in order to facilitate the comparison of different formulations of the model. Nevertheless, the major part of our further calculations will employ the covariant Pauli-Villars method.

6.2.2. Pauli–Villars subtraction scheme

In this Section we shall calculate the function

$$I_2(M^2, Q) = I_{2,\text{vac}}(M^2, Q^2) + I_{2,\text{med}}(M^2, Q)$$

using the Pauli-Villars regularization scheme. This calculation proceeds in the similar way as the evaluation of the function $I_1^{R,PV}(M^2)$ in Section 5.2. The regularized form of (6.7) is obtained by making the substitution

$$I_{2,\text{vac}}(M^2, -q_E^2) \to I_{2,\text{vac}}^{R,PV}(M^2, -q_E^2) = \sum_{i=0}^{N} A_i I_{2,\text{vac}}(\Lambda_i^2, -q_E^2), \qquad (6.29)$$

where the coefficients A_i are defined by formula (5.23). To calculate $I_{2,\text{vac}}^{R,PV}(M^2, -q_E^2)$ one has to use first the identity

$$\frac{1}{AB} = 2 \int\limits_{-1}^{1} du \frac{1}{[A(1+u) + B(1-u)]^2}, \qquad (6.30)$$

which allows us to simplify the form of the denominator in the integral on the RHS of Eq. (6.7). Afterwards exchanging the order of integration over p_E and u and introducing the new variable $p_E' = p_E + uq_E/2$ one obtains the expressions which can be easily integrated. The final result is

$$I_{2,\text{vac}}^{R,PV}(M^2, -q_E^2)$$
$$= \frac{N_c}{2\pi^2} \sum_{i=0}^{N} A_i \left[\frac{2\Lambda_i}{q_E} \sqrt{1 + \left(\frac{q_E}{2\Lambda_i}\right)^2} \ln \left(\sqrt{1 + \left(\frac{q_E}{2\Lambda_i}\right)^2} + \frac{q_E}{2\Lambda_i} \right) + \ln \Lambda_i \right].$$
$$(6.31)$$

The function $I_{2,\text{vac}}^{R,PV}(M^2, \omega^2)$ can be obtained by performing the analytic continuation of the expression given on the RHS of Eq. (6.31). The substitution $q \to -i(\omega \pm i\epsilon)$ leads to the following formula ($\omega > 0$)

$$I_{2,\text{vac}}^{R,PV}(M^2, \omega^2 \pm i\epsilon)$$

$$= \frac{N_c}{2\pi^2} \sum_{i=0}^{N} A_i \Big\{ \Theta(2\Lambda_i - \omega) \Big[\frac{2\Lambda_i}{\omega} \sqrt{1 - \left(\frac{\omega}{2\Lambda_i}\right)^2} \arcsin\left(\frac{\omega}{2\Lambda_i}\right) + \ln \Lambda_i \Big]$$

$$+ \Theta(\omega - 2\Lambda_i) \Big[\frac{2\Lambda_i}{\omega} \sqrt{\left(\frac{\omega}{2\Lambda_i}\right)^2 - 1} \left(\operatorname{arcosh}\left(\frac{\omega}{2\Lambda_i}\right) \mp \frac{i\pi}{2} \right) + \ln \Lambda_i \Big] \Big\}. \quad (6.32)$$

The functions $I_{2,\text{med}}(M^2, Q)$ should be calculated in the same way as the function $I_{1,\text{med}}(M^2)$, namely we make the replacement

$$I_{2,\text{med}}(M^2, Q) \to I_{2,\text{med}}^{R,PV}(M^2, Q) = \sum_{i=0}^{N} A_i I_{2,\text{med}}(\Lambda_i^2, Q), \quad (6.33)$$

where the function $I_{2,\text{med}}(\Lambda_i^2, Q)$ is defined by Eqs (6.11) or (6.17).

6.2.3. Schwinger proper-time regularization

Using the Schwinger proper-time method of regularization, we rewrite Eq. (6.7) in the following form

$$I_{2,\text{vac}}^{R,SPT}(M^2, -q_E^2)$$

$$= -4N_c \int \frac{d^4 p_E}{(2\pi)^4} \int_{\Lambda^{-2}}^{\infty} ds\, s \int_0^1 du \exp\left\{ -s[p_E^2 + M^2 + u(1-u)q_E^2] \right\}$$

$$= -\frac{N_c}{4\pi^2} \int_0^1 du\, E_1\left[\frac{M^2}{\Lambda^2} + u(1-u)\frac{q_E^2}{\Lambda^2} \right]. \quad (6.34)$$

Replacing the integral over energy, p_4, by the sum over Matsubara frequencies we can generalize Eq. (6.34) to the case of finite temperatures

$$I_2^{R,SPT}(M^2, n, q, T)$$

$$= -4N_c T \sum_j \int \frac{d^3 p}{(2\pi)^3} \int_{\Lambda^{-2}}^{\infty} ds\, s \int_0^1 du \exp\Big\{ -s\Big[M^2 + u(1-u)((E_n^b)^2 + \boldsymbol{q}^2) $$

$$+ [\boldsymbol{p} - \boldsymbol{q}(1-u)]^2 + \Big[E_j^f - E_n^b(1-u) \Big]^2 \Big] \Big\}$$

$$= -\frac{N_c T}{2\pi^{\frac{3}{2}} \Lambda} \sum_j \int_0^1 du\, E_{\frac{1}{2}}\left[\frac{M^2}{\Lambda^2} + u(1-u)\frac{(E_n^b)^2 + \boldsymbol{q}^2}{\Lambda^2} + \frac{[E_j^f - E_n^b(1-u)]^2}{\Lambda^2} \right].$$

$$(6.35)$$

where $E_n^b = 2\pi n T$ and $E_j^f = (2j+1)\pi T$.

6.3. Meson masses

6.3.1. Definitions

In the random phase approximation (RPA) the full correlation function has the form

$$\chi_{AA}(Q) = \frac{\chi_{AA}^{(0)}(Q)}{1 - G_S \chi_{AA}^{(0)}(Q)}. \qquad (6.36)$$

This is a nonperturbative expression, which follows from the infinite summation of a certain class of diagrams, see Fig. 6.2.
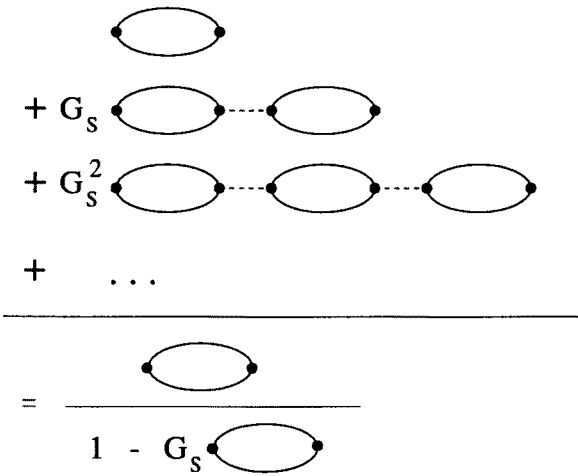
Fig. 6.2. The class of diagrams used to evaluate the full correlation function in the RPA approximation.

The correlation function $\chi_{AA}(Q)$ depends on Q through the variables ω^2 and q^2. Therefore, in the following we shall use the notation $\chi_{AA}(\omega^2, q^2)$ rather than $\chi_{AA}(Q)$. The *dynamic mass* is defined by the position of the nearest to zero pole of the function $\chi_{AA}(\omega^2, 0)$. In the NJL model it can be easily found by solving the equation

$$1 - G_S \chi_{AA}^{(0)}(m_{\text{dyn}}^2, 0) = 0. \qquad (6.37)$$

This comes directly from Eq. (6.36). On the other hand, the *screening mass* is defined by the asymptotic behaviour of the static correlation function in space, namely

$$m_{\text{scr}} = -\lim_{r \to \infty} \frac{d \ln \chi_{AA}(r)}{dr}, \qquad (6.38)$$

where

$$\chi_{AA}(r) = \int \frac{d^3q}{(2\pi)^3} \, \chi_{AA}(0, q^2) \, e^{iq \cdot r} = \frac{1}{4\pi^2 ir} \int\limits_{-\infty}^{+\infty} dq \, q \, \chi_{AA}(0, q^2) \, e^{iqr} .$$

(6.39)

To get the last term in Eq. (6.39) we first performed the integration over the angles, and then extended the region of integration over $q = |\boldsymbol{q}|$ to the interval from minus to plus infinity.

Let us now consider an arbitrary correlation function $\chi_{AA}(\omega^2, q^2)$, not necessarily obtained from the NJL model. One can ask the question when the dynamic mass is equal to the screening mass. At $T = 0$ the system is explicitly Lorentz invariant and $\chi_{AA}(\omega^2, 0) = \chi_{AA}(0, -\omega^2)$. Therefore, if the function $\chi_{AA}(\omega^2, 0)$ has a pole for $\omega = m_{\text{dyn}}$, the function $\chi_{AA}(0, q^2)$ has a pole for $q = im_{\text{dyn}}$. The latter gives the contribution to the integral (6.39), which has the form $\sim \exp(-m_{\text{dyn}}r)$. For very large r this contribution is the dominant one, since im_{dyn} is the nearest pole. Consequently, we find that $m_{\text{dyn}} = m_{\text{scr}}$. Of course one has to be careful because the analytic structure of the correlation function can be complicated and there might be some other contributions to the integral (6.39). Nevertheless at $T = 0$ we expect that $m_{\text{dyn}} = m_{\text{scr}}$. A different situation takes place when $T > 0$. In this case it is difficult to find a simple relation between the functions $\chi_{AA}(\omega^2, 0)$ and $\chi_{AA}(0, q^2)$. The Lorentz invariance is implicitly broken by the existence of the preferable reference frame connected with the heat bath. The fact that $\chi_{AA}(\omega^2, 0)$ has a pole for $\omega = m_{\text{dyn}}$ does not imply that $\chi_{AA}(0, q^2)$ has a pole for $q = im_{\text{dyn}}$. Furthermore, at $T > 0$ the contribution to Eq. (6.39) from the cuts of the correlation function may be important and it can substantially change the space asymptotics of the function $\chi_{AA}(r)$. In consequence, at $T > 0$, because of these at least two reasons, the dynamic mass and the screening one are different. Of course, the same arguments hold for the case of finite density.

6.3.2. In-medium meson dynamic masses

The dynamic masses of the pion and the sigma are obtained from Eq. (6.37), which has the form

$$1 - G_S \left[I_1(M^2) - m_{\text{dyn},\pi}^2 I_2(M^2, m_{\text{dyn},\pi}^2, 0) \right]$$
$$= \frac{m}{M} + m_{\text{dyn},\pi}^2 \, G_S \, I_2(M^2, m_{\text{dyn},\pi}^2, 0) = 0$$

(6.40)

for the pseudoscalar (pion) channel, and

$$1 - G_S \left[I_1(M^2) - (m_{\text{dyn},\sigma}^2 - 4M^2) I_2(M^2, m_{\text{dyn},\sigma}^2, 0) \right]$$
$$= \frac{m}{M} + (m_{\text{dyn},\sigma}^2 - 4M^2) G_S I_2(M^2, m_{\text{dyn},\sigma}^2, 0) = 0 \qquad (6.41)$$

for the scalar (sigma) channel. In Eqs (6.40) and (6.41), we have assumed that the parameters are such that the gap equation has a non-trivial solution, i.e., $M = m + G_S M I_1(M^2)$.

Formula (6.40) is the cornerstone of the NJL model. It explicitly shows, that the spontaneous symmetry breaking leads to the appearance of the Goldstone bosons. If the current quark mass is zero, $m = 0$, the pion dynamic mass turns out to be zero. Moreover, at the Hartree level the mass of the sigma is simply $2M$. We also note that the structure of Eqs (6.40) and (6.41) is independent of the regularization scheme (as long as our regularization procedure modifies the functions I_1 and I_2 only.)

We note that Eqs (6.40) and (6.41) are correct not only in vacuum but also at finite temperature or density. As follows from Eqs (6.32), (6.12) and (6.18), the correlation functions have cuts for arguments larger than $2M$. At high temperatures (densities) the meson poles merge with the quark-antiquark cuts, which means that in this model the mesons can decay into $q\bar{q}$ pairs. Thus, at these temperatures (densities) there are no isolated poles which can be identified with the mass of the pion or the sigma. We circumvent this difficulty by defining the mass as the zero of the real part of Eq. (6.37), *i.e.*,

$$1 - G_S \operatorname{Re} \chi_{AA}^{(0)}(m_{\text{dyn}}^2, 0) = 0. \qquad (6.42)$$

We note that by using Eq. (6.42) we implicitly neglect the $q\bar{q}$ widths of the mesons [7]. This seems reasonable, since these widths are non-zero only because the NJL model lacks confinement.

Our result concerning the temperature dependence of the dynamic masses of mesons is shown in Fig. 6.3. The calculations are based on the two-flavour symmetric model. We use now the same computational scheme as that used to calculate the temperature dependence of M in Section 5.2, *i.e.*, we make three subtractions with the regulating masses: $\Lambda_1 = 680$ MeV, $\Lambda_2 = 2.1\Lambda_1$ and $\Lambda_3 = 2.1\Lambda_2$. The coupling constant $G_S = 0.75\,\text{fm}^2$ and the current

---

[7] In a general situation, the mass and the width of a meson are determined by the shape of its spectral function. In our case the latter has the form $(2\operatorname{Im}\chi^{(0)})/(1 - G_S\chi^{(0)}) = (2G_S\operatorname{Im}\chi^{(0)})/([1 - G_S\operatorname{Re}\chi^{(0)}]^2 + [G_S\operatorname{Im}\chi^{(0)}]^2)$. If the imaginary part of $\chi^{(0)}$ (describing the width of a meson) is small, the spectral function is strongly peaked for the four-momenta satisfying the condition (6.42).
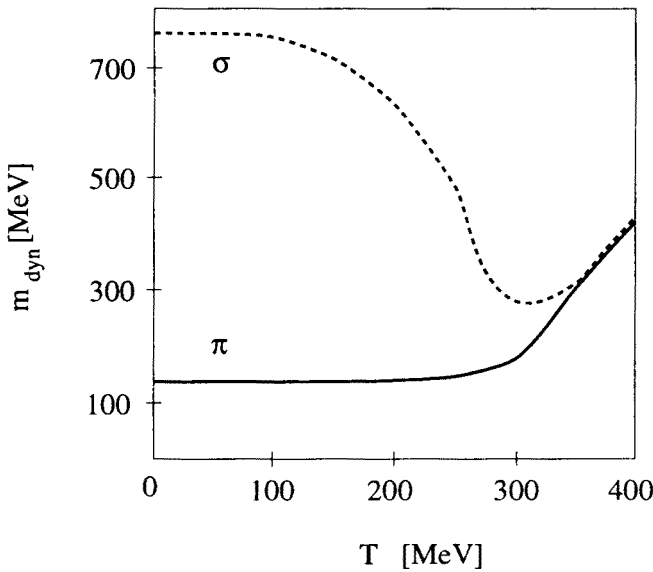
Fig. 6.3. Temperature dependence of the dynamic masses of pion (solid line) and sigma (dashed line).

quark mass $m = 8.56$ MeV. Using these values of the parameters we find that at zero temperature the constituent quark mass $M = M_0 = 376$ MeV, the pion mass $m_{\mathrm{dyn},\pi} = 138$ MeV and the sigma mass $m_{\mathrm{dyn},\sigma} = 760$ MeV. The pion and sigma masses are connected by relation

$$m_{\mathrm{dyn},\sigma}^2 \approx 4M^2 + m_{\mathrm{dyn},\pi}^2. \tag{6.43}$$

In Fig. 6.3 one can see that the pion mass remains constant as long as the temperature is smaller than 250 MeV. Afterwards it increases suddenly. The temperature dependence of the sigma mass is rather complicated. In the interval $0 < T < 250$ MeV it behaves in the similar way as the constituent quark mass, see Fig. 5.6. Moreover, in this region relation (6.43) is still fulfilled. When the temperature reaches 300 MeV, the sigma mass stops decreasing, remains for a while constant and later increases. At very high temperature the sigma mass and the pion mass are with a good approximation the same. *This fact signifies the chiral restoration.*

In Fig. 6.4 we show the density dependence of the dynamic masses of mesons. We use here the same values of the parameters as in the finite temperature calculations discussed above. Thus, our results for $\mu = 0$ and $T = 0$ coincide with each other. One can see that with the increasing value of the chemical potential the dynamic masses of pion and sigma become degenerate. This fact indicates restoration of the chiral symmetry at

high density. The overall μ-dependence shown in Fig. 6.4 is similar to the T-dependence shown in Fig. 6.3.

The first calculation of the in-medium dynamic masses of the pion and the sigma in the NJL model was done by Hatsuda and Kunihiro [6]. Their calculation employed the 3-dimensional regularization scheme. The results presented in Figs 6.3 and 6.4 follow from the calculation based on the Pauli–Villars method [18]. They qualitatively agree with those obtained in [6]. The advantage of using the Pauli–Villars method in our case is that it will allow us to compare directly the temperature dependence of the dynamic and screening masses. As follows from the discussion in the next Chapters, the 3-dimensional regularization scheme introduces unphysical contributions to the Fourier transform defining the static correlation function. Thus, this way of regularization spoils the expected relations between the screening and dynamic masses.
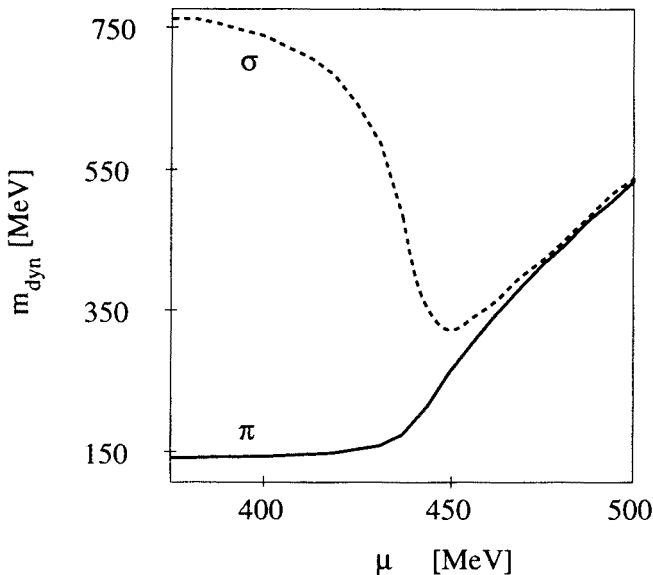
Fig. 6.4. Pion (solid line) and sigma (dashed line) dynamic masses plotted as functions of the quark chemical potential μ.

7. Static meson fields at finite temperature

In this Chapter we study the damping of static meson correlation functions at finite temperature. Our interest in these investigations has been triggered by the results of the lattice simulations of QCD. They indicate that high-temperature hadronic correlation functions describe a system of

(almost) non-interacting quarks. In the first Section of this Chapter we do the analytic calculations based on the perturbative QCD. This allows us to understand the high temperature behaviour of the correlation functions. In the second Section we come back to the study of the NJL model. We find that the screening masses obtained within the model have the desired temperature dependence. In particular, for stable mesons the screening masses at $T = 0$ are equal to the dynamic ones, whereas for extremely high temperatures they approach the values expected from the perturbative QCD calculation.

7.1. Screening of meson fields in hot QCD

Lattice "measurements" of hadronic correlation functions in QCD show exponential behaviour at large distances [46–49]. At high temperatures, $T > T_c$, the hadronic screening masses of chiral partners are equal, but non-vanishing. This is consistent with the restoration of chiral symmetry. Eletskii and Ioffe [50] pointed out that the meson screening masses approached the value $2\pi T$, whereas those of baryons were close to $3\pi T$ and argued that such a behaviour is typical for a gas of non-interacting massless quarks. Their reasoning was the following: In the considered case the space-time correlation function is the product of two (mesons) or three (baryons) quark propagators. The space asymptotics of each propagator is determined by the lowest lying pole in the complex $q = |q|$ plane. In the imaginary-time formalism this pole corresponds to the lowest fermionic Matsubara frequency πT and, therefore, the screening masses are multiples of πT. Shuryak has presented alternative arguments, based on the large-distance behaviour of the free quark propagator at finite temperatures, which lead to the same result [51].

We should emphasize that the screening masses obtained from the lattice calculations are not exactly the multiples of πT. For baryons and (axial)vector mesons the relation of Eletskii and Ioffe is indeed very well fulfilled. However, for (pseudo)scalar mesons one can see a deviation from $2\pi T$. This discrepancy indicates that there is a non-negligible interaction in this channel, present even at very high temperature. Nevertheless, in the limit $T \to \infty$ we expect that in all meson channels the screening masses would go to $2\pi T$.

The arguments of Eletskii and Ioffe allow us to understand intuitively how the screening masses turn out to be $2\pi T$ and $3\pi T$. We are of the opinion, however, that it is instructive to obtain this result from a more rigorous calculation. Actually, the aim of this Section is to show that starting from the regularized momentum representation of the static meson correlation function we can analytically derive its full spatial dependence [52]. Knowing

the asymptotic behaviour of the correlation function, we can find the values
of the screening masses which are in agreement with the result of Eletskii
and Ioffe.

The spatial dependence of the correlation function will be calculated by
us in two ways, namely

$$\tilde{\chi}(z) \equiv \int\limits_{-\infty}^{\infty} \frac{dq_z}{2\pi}\, \tilde{\chi}(0, q_z^2)\, e^{iq_z z} \tag{7.1}$$

or

$$\tilde{\chi}(r) \equiv \int \frac{d^3q}{(2\pi)^3}\, \tilde{\chi}(0, q^2)\, e^{i\boldsymbol{q}\cdot\boldsymbol{r}} = \frac{1}{4\pi^2 i r} \int\limits_{-\infty}^{\infty} dq\, q\, \tilde{\chi}(0, q^2)\, e^{iqr}\, . \tag{7.2}$$

The quantity $\tilde{\chi}(0, q^2)$ denotes the static meson correlation function obtained
in the framework of the perturbative QCD. We shall restrict our considera-
tions to the special case of the pseudoscalar channel. Eq. (7.1) describes the
situation in which the correlation function is used to find the response of the
system to the *static plane-like perturbation*. Here z is the distance from the
plane in the transverse direction and q_z is identified with the momentum in
this direction. Such a case is considered in the lattice simulations. Eq. (7.2),
equivalent to the definition (6.39), describes the situation when the pertur-
bation is the *static point*. We note that the functions $\tilde{\chi}(z)$ and $\tilde{\chi}(r)$ depend
differently on their arguments, however, for simplicity of notation we use for
them the same symbol.

In the perturbative QCD, the leading contribution to the meson correla-
tion function is given by the quark loop diagram, see Fig. 6.1 (the diagrams
with gluon lines contribute only in higher order terms). Thus, we can use our
results from the previous Chapters. In particular, if we employ the Pauli-
Villars regularization procedure, we can use expressions (6.5) and (6.10) with
the functions $I_{1,\text{vac}}(M^2)$, $I_{1,\text{tem}}(M^2)$, $I_{2,\text{vac}}(M^2, -q^2)$ and $I_{2,\text{tem}}(M^2, 0, q^2)$
given by expressions (5.24), (5.13), (6.31) and (6.13), respectively.

In practice, we do not use Eqs (7.1) and (7.2) directly in the form as
they have been written down. To evaluate the Fourier transform, in both
cases, we analytically continue $\tilde{\chi}(0, q^2)$ on the whole complex q plane. Later
we deform the contour of the integration, and represent the result as the
integral around the singularities appearing in the upper half-plane. The
Fourier integral (7.1) or (7.2) becomes in this case the sum of two terms
(the first one represents the integral over the vacuum part and the second
one is the integral over the temperature part).

7.1.1. Vacuum part

The vacuum part of the correlation functions $\tilde{\chi}_{\text{vac}}(0, q^2)$ is given by expression

$$
\tilde{\chi}_{\text{vac}}(0, q^2) = \frac{N_c}{2\pi^2} \sum_{i=0}^{N} A_i \left\{ A_i^2 \ln A_i^2 \right.
$$
$$
\left. + q^2 \left[\frac{2A_i}{q} \sqrt{1 + \left(\frac{q}{2A_i}\right)^2} \ln \left(\sqrt{1 + \left(\frac{q}{2A_i}\right)^2} + \frac{q}{2A_i} \right) + \ln A_i \right] \right\},
$$

(7.3)

which follows from Eqs (6.5), (5.24) and (6.31). The analytic continuation of (7.3) has cuts for purely imaginary $q = ik$, starting at $k = \pm 2M$, see Fig. 7.1. Consequently, the Fourier integral can be replaced by the integral around the cut stretching along the imaginary axis. In this way we obtain

$$
\tilde{\chi}_{\text{vac}}(z) = \frac{i}{2\pi} \int_{2M}^{\infty} dk \left[\tilde{\chi}_{\text{vac}}(0, -k^2 + i\epsilon) - \tilde{\chi}_{\text{vac}}(0, -k^2 - i\epsilon) \right] e^{-kz} . \quad (7.4)
$$

The real parts of $\tilde{\chi}_{\text{vac}}(0, -k^2 \pm i\epsilon)$ are the same on both sides of the cut, and the imaginary parts have opposite signs. Thus, the expression in the square brackets on the RHS of (7.4) equals $2i \, \text{Im} \, \tilde{\chi}_{\text{vac}}(0, -k^2 + i\epsilon)$. As the final result one gets

$$
\tilde{\chi}_{\text{vac}}(z) = \frac{N_c}{4\pi^2} \sum_{i=0}^{N} A_i \int_{2A_i}^{\infty} dk \, k \sqrt{k^2 - 4A_i^2} \, e^{-kz} = \frac{N_c}{\pi^2 z} \sum_{i=0}^{N} A_i \, A_i^2 \, K_2(2A_i z),
$$

(7.5)

where K_2 is the modified Bessel function [53]. The vacuum part of the correlation function $\tilde{\chi}_{\text{vac}}(0, q^2)$ is divergent and must be regularized. Nevertheless, the Fourier transform remains finite for $z > 0$ also when one sends the cutoff masses to infinity. For $A_i \to \infty$ $(i > 0)$, only the first term in the above series is non-negligible and we find

$$
\tilde{\chi}_{\text{vac}}(z) = \frac{N_c}{\pi^2 z} M^2 K_2(2Mz). \quad (7.6)
$$

Similar calculations starting from Eq. (7.2) lead to the result

$$
\tilde{\chi}_{\text{vac}}(r) = \frac{N_c}{2\pi^3 r^3} M^2 \left[3K_2(2Mr) + 2Mr K_1(2Mr) \right]. \quad (7.7)
$$

7.1.2. Temperature part

The temperature part of the correlation function is given by expression

$$\tilde{\chi}_{\text{tem}}(0, q^2) = -\frac{N_c}{\pi^2} \int\limits_0^\infty \frac{dp\, p^2}{E_p} \frac{1}{e^{E_p/T} + 1} \left[4 + \frac{q}{p} \ln \left| \frac{2p - q}{2p + q} \right| \right], \qquad (7.8)$$

which follows from Eqs (6.10), (5.13) and (6.13). In the following we shall make the substitution

$$\ln \left| \frac{2p - q}{2p + q} \right| = \frac{1}{2} \ln \frac{(2p - q)^2 + \epsilon^2}{(2p + q)^2 + \epsilon^2}. \qquad (7.9)$$

In this way $\tilde{\chi}_{\text{tem}}(0, q^2)$ becomes an analytic function of q. Of course, at the final stage of the calculations we have to consider the limiting case $\epsilon \to 0$.

The spatial dependence of the temperature part of the correlation function is obtained from Eqs (7.1) and (7.2). Exchanging the order of the
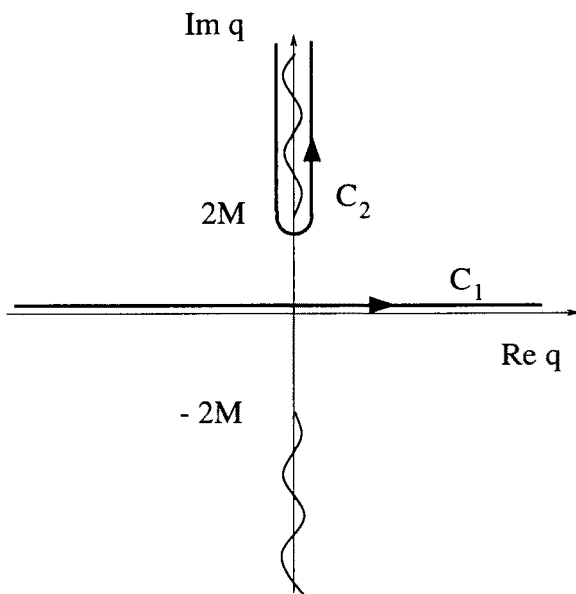

Fig. 7.1. The cuts of the vacuum part of the correlation function. They start at $\text{Im}\, q = \pm 2M$ and go along the imaginary axis to $\pm\infty$. The integrations along the curves $\mathcal{C}_1$ and $\mathcal{C}_2$ are equivalent.

integration over q and p we get

$$\tilde{\chi}_{\text{tem}}(z) = -\frac{N_c}{2\pi^3} \int\limits_0^\infty \frac{dp\, p^2}{E_p} \frac{F(p, z)}{e^{E_p/T} + 1}, \qquad (7.10)$$

where the function $F(p, z)$ is defined through the integral

$$
\begin{aligned}
F(p, z) &\equiv \int\limits_{-\infty}^\infty dq \left[4 + \frac{q}{2p} \ln \frac{(2p - q)^2 + \epsilon^2}{(2p + q)^2 + \epsilon^2} \right] e^{iqz} \\
&= \frac{\pi}{pz^2} \left[e^{-2ipz}\, (i - 2pz) - e^{2ipz}\, (i + 2pz) \right].
\end{aligned}
\qquad (7.11)
$$

The calculation of $F(p, z)$ proceeds as follows. First we analytically continue the integrand on the upper half-plane of complex q. Such a function has two cuts starting at $q = \pm 2p + i\epsilon$ and going upward, parallel the imaginary axis (see Fig. 7.2). Consequently, the initial integral can be replaced by the two integrals around the cuts. The values of the integrated function on both sides of the cuts are different only because the logarithm has a different phase there. However the difference of the phase, the quantity which enters our integrals, is constant. This simplifies our expressions and leads, in the limit $\epsilon \to 0$, to the result shown in the second line of Eq. (7.11).

Substitution of Eq. (7.11) into Eq. (7.10) leads to the following result

$$\tilde{\chi}_{\text{tem}}(z) = \frac{N_c}{2\pi^2} \left(\frac{1}{z^2} - \frac{1}{z} \frac{\partial}{\partial z} \right) \frac{\partial}{\partial z} \int\limits_0^\infty \frac{dp}{E_p} \frac{1}{e^{E_p/T} + 1} \cos(2pz). \qquad (7.12)$$

Now, using the series representation of the Fermi–Dirac distribution

$$\frac{1}{e^x + 1} = \frac{1}{2} - \sum_{l=-\infty}^{+\infty} \frac{x}{(2l + 1)^2 \pi^2 + x^2}, \qquad (7.13)$$

we can write the temperature part in the form

$$\tilde{\chi}_{\text{tem}}(z) = \frac{N_c}{2\pi^2} \left(\frac{1}{z^2} - \frac{1}{z} \frac{\partial}{\partial z} \right) \left[\tilde{G}_1^{\text{tem}}(z) + \tilde{G}_2^{\text{tem}}(z) \right] \qquad (7.14)$$

where

$$\tilde{G}_1^{\text{tem}}(z) \equiv \frac{\partial}{\partial z} \int\limits_0^\infty \frac{dp}{2E_p} \cos(2pz) = \frac{1}{2} \frac{\partial}{\partial z} K_0(2Mz) = -MK_1(2Mz), \quad (7.15)$$
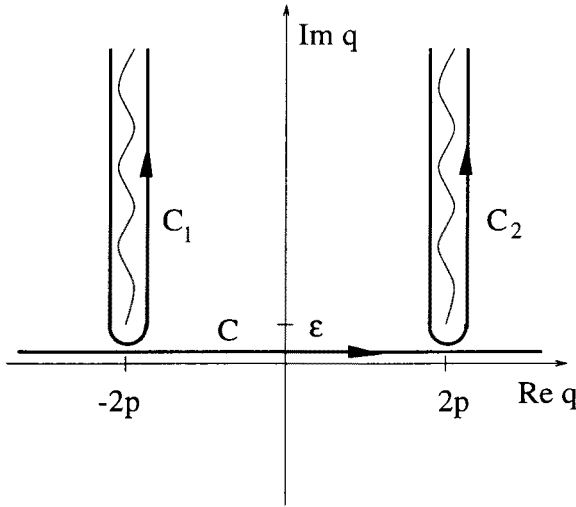
Fig. 7.2. The analytic structure of the function being the integrand in Eq. (7.11). The integration along the real axis (contour $\mathcal{C}$) can be replaced by the two integrals around the cuts (contours $\mathcal{C}_1$ and $\mathcal{C}_2$).

and

$$
\begin{aligned}
\tilde{G}_2^{\text{tem}}(z) &\equiv -T \frac{\partial}{\partial z} \sum_{l=-\infty}^{+\infty} \int_0^\infty \frac{dp \, \cos(2pz)}{(2l+1)^2 \pi^2 T^2 + E_p^2} \\
&= -iT \sum_{l=-\infty}^{+\infty} \int_{-\infty}^\infty \frac{dp \, p \, e^{2ipz}}{(2l+1)^2 \pi^2 T^2 + E_p^2} \\
&= \pi T \sum_{l=-\infty}^{+\infty} \exp(-2z\sqrt{(2l+1)^2 \pi^2 T^2 + M^2}).
\end{aligned}
\tag{7.16}
$$

In the 3-dimensional case one can derive an analogous expression

$$
\tilde{\chi}_{\text{tem}}(r) = \frac{N_c}{4\pi^3 r} \left(\frac{2}{r^3} - \frac{2}{r^2} \frac{\partial}{\partial r} + \frac{1}{r} \frac{\partial^2}{\partial r^2} \right) \left[\tilde{G}_1^{\text{tem}}(r) + \tilde{G}_2^{\text{tem}}(r) \right].
\tag{7.17}
$$

7.1.3. Asymptotics

Using Eqs (7.6) and (7.14), and also employing the recursion relations for the Bessel functions [54] we can check that in the full correlation function the vacuum part and the first piece of the temperature part (coming from

the differentiation of the function $\tilde{G}_1^{\text{tem}}$) cancel each other [8]. We are left only with the term coming from the differentiation of the function $\tilde{G}_2^{\text{tem}}$. Moreover, for large distances, it is enough to consider only the leading terms in the series which defines $\tilde{G}_2^{\text{tem}}$ ($l = 0$ and $l = -1$). Consequently, we find for large z and finite M that

$$\tilde{\chi}(z) \sim \frac{2N_c T}{\pi z} \sqrt{\pi^2 T^2 + M^2} \exp(-2z\sqrt{\pi^2 T^2 + M^2}). \qquad (7.18)$$

From Eq. (7.18) we read off the screening mass $m_{\text{scr}} = 2\sqrt{\pi^2 T^2 + M^2}$. The same screening mass is obtained if we use Eqs (7.7) and (7.17).

Let us also discuss in more detail the case of massless quarks. The expression for $\tilde{\chi}_{\text{tem}}(z)$ or $\tilde{\chi}_{\text{tem}}(r)$ can be then given in a compact form because the series appearing in the definition of $\tilde{G}_2^{\text{tem}}$ becomes a geometric one and can be easily summed up. Using Eq. (7.14) we obtain

$$\tilde{\chi}_{\text{tem}}(z) \xrightarrow{M \to 0} -\frac{N_c}{2\pi^2 z^3} + \frac{N_c T}{2\pi z^2 \sinh(2\pi T z)} [1 + 2\pi T z \coth(2\pi T z)], \quad (7.19)$$

and similarly from Eq. (7.17) we get

$$\tilde{\chi}_{\text{tem}}(r) \xrightarrow{M \to 0} -\frac{3N_c}{4\pi^3 r^5} + \frac{N_c T}{2\pi^2 r^4 \sinh(2\pi T r)} \left[1 + 2\pi T r \coth(2\pi T r) \right.$$
$$\left. + 2\pi^2 T^2 r^2 \left(\frac{2}{\sinh^2(2\pi T r)} + 1 \right) \right]. \qquad (7.20)$$

Eqs (7.6) and (7.7) in the limiting case $M = 0$ have the form

$$\tilde{\chi}_{\text{vac}}(z) \xrightarrow{M \to 0} \frac{N_c}{2\pi^2 z^3} \qquad (7.21)$$

and

$$\tilde{\chi}_{\text{vac}}(r) \xrightarrow{M \to 0} \frac{3N_c}{4\pi^3 r^5}. \qquad (7.22)$$

In this case we can easily see that the temperature parts of the correlation functions vanish if $T = 0$. On the other hand, in the expression for the complete correlation function, for each finite value of T, the temperature independent piece of the temperature part cancels exactly the vacuum part.

---

[8] Such cancellation takes place only because the vacuum part was calculated in the limit $\Lambda_i \to \infty$ ($i > 0$). If we kept Λ_i's finite, we would have to regularize the temperature part as well. Otherwise, we could not get the correct result for the screening masses.

7.1.4. Remarks on the temporal function

Finally, let us briefly discuss the screening in the temporal direction. In this case we need to evaluate the correlation function in the imaginary time direction

$$\tilde{\chi}^{(4)}(\tau) = T \sum_n e^{-i\omega_n \tau}\, \tilde{\chi}^R(i\omega_n, 0), \qquad (7.23)$$

where

$$\tilde{\chi}^R(\omega, 0) = \frac{8N_c}{\pi^2} \int\limits_0^\infty dp\, p^2 \tanh\left(\frac{E_p}{2T}\right) \frac{E_p}{4E_p^2 - \omega^2} + (\text{reg.}) \qquad (7.24)$$

is the regularized correlation function ("reg." denotes the regularization terms).

Using standard techniques we find

$$\tilde{\chi}^{(4)}(\tau) = \frac{N_c}{\pi^2} \int\limits_0^\infty dp\, p^2\, \frac{\cosh\left[2E_p(\tau - \beta/2)\right]}{\cosh^2(E_p\beta/2)} + (\text{reg.}), \qquad (7.25)$$

where $\beta = 1/T$. Since the integral converges for $0 < \tau < \beta$ we can again drop the regulating terms by letting $\Lambda_i \to \infty$. For massless quarks, the integral can be done analytically

$$\tilde{\chi}^{(4)}(\tau) = \frac{N_c T^3}{2\pi^2} \frac{\partial^2}{\partial(\tau/\beta)^2} \left(1 - \frac{2\tau}{\beta}\right) \frac{\pi}{\sin(2\pi\tau/\beta)}. \qquad (7.26)$$

The real time correlation function is obtained by analytically continuing to real times; for large t we find $\tilde{\chi}^{(4)}(t) \sim \exp(-2\pi T t)$. Thus, for massless non-interacting quarks, the mesonic screening mass in the time direction is the same as in the spatial direction, $m_{\text{scr}} = 2\pi T$. Consequently, we expect the temporal correlation function in mesonic channels to behave qualitatively in the following manner: For a uniform source at zero temperature, where mesonic modes exist, $\tilde{\chi}^{(4)}(t)$ oscillates in time with frequency m, the meson mass. On the other hand, at high temperatures, where the system consists of weakly interacting almost massless quarks, the correlation function is screened, with the screening mass $2\pi T$.

7.2. Screening in the NJL model

In this Section we analyze the spatial dependence of static meson correlation functions calculated within the NJL model. We use again the two-flavour symmetric model defined in Sections 3.2 and 5.2. Thus, our considerations are restricted to the scalar and pseudoscalar channels. We find

that the screening masses (obtained from the asymptotic behaviour of the correlation functions) differ from the dynamic masses (defined by a pole of the meson propagator in the energy plane, see discussions in Section 6.3). In the high temperature limit, the screening masses approach $2\pi T$, which corresponds to a gas of non-interacting quarks. Nevertheless, the interaction effects remain well beyond the chiral transition temperature. The overall temperature dependence of the screening masses is in the agreement with lattice results.

7.2.1. Analytic structure in complex momentum space

Similarly to the QCD case considered in the previous Section, the Fourier transform (6.39) can be rewritten as a sum of a few contributions, which appear due to the singularities of the correlation function in the complex q-plane. Thus, at first we are going to study the analytic structure of the correlation functions.

The results of Section 6.1 indicate that $\chi_{AA,\text{vac}}^{(0)}(0, q^2)$ has cuts (in the following we refer to these as the *vacuum cuts*) along the imaginary axis starting at $q = \pm 2iM$ and going to $\pm i\infty$. In order to find the analytic structure of the function $\chi_{AA,\text{tem}}^{(0)}(0, q^2)$ we study the function $I_{2,\text{tem}}(M^2, 0, q^2)$ in the whole complex $q = |q|$ plane. To this end we represent $I_{2,\text{tem}}(M^2, 0, q^2)$ as a sum of two functions, namely

$$I_{2,\text{tem}}(M^2, 0, q^2) = I_{2,\text{tem}}^{(+)}(q) + I_{2,\text{tem}}^{(-)}(q), \tag{7.27}$$

where

$$I_{2,\text{tem}}^{(\pm)}(z) = -\frac{N_c}{2z\pi^2} \int\limits_0^\infty \frac{dp\, p}{E_p} \frac{1}{e^{E_p/T}+1} \ln \frac{2p - z \pm i\epsilon}{-2p - z \pm i\epsilon}. \tag{7.28}$$

At the end of the calculations we let the infinitesimal ϵ go to zero. The functions $I_{2,\text{tem}}^{(\pm)}(z)$ have logarithmic cuts parallel to the real axis and stretching from minus to plus infinity. At the respective cut the imaginary part of the function $I_{2,\text{tem}}^{(\pm)}(z)$ is discontinuous. On the physical Riemann sheet, this amounts to a change in sign:

$$\text{Im}\, I_{2,\text{tem}}^{(+)}(q_R + i\delta_\pm) = \mp \frac{N_c T}{2q_R\pi} \ln\left[1 + \exp\left(-\frac{\sqrt{M^2 + q_R^2/4}}{T}\right)\right]. \tag{7.29}$$

Here q_R is real, $\delta_+ = 2\epsilon$ and $\delta_- = 0$. Thus, for the upper sign one is above the cut of $I_{2,\text{tem}}^{(+)}$ and for the lower sign below. Obviously the imaginary part of $I_{2,\text{tem}}^{(-)}$ above and below its cut is equal to that of $I_{2,\text{tem}}^{(+)}$ above and below

its cut. This can be summarized by the following equations

$$\text{Im } I_{2,\text{tem}}^{(-)}(z = q_R - i\delta_{\mp}) = \text{Im } I_{2,\text{tem}}^{(+)}(z = q_R + i\delta_{\pm}),$$

$$\text{Im } I_{2,\text{tem}}^{(-)}(z = q_R - i\delta_{\pm}) = -\text{Im } I_{2,\text{tem}}^{(+)}(z = q_R + i\delta_{\pm}). \qquad (7.30)$$

The cuts are arranged in such a way that for z on the real axis, the imaginary part of $I_{2,\text{tem}}^{(+)}(z)$ cancels that of $I_{2,\text{tem}}^{(-)}(z)$ and $I_{2,\text{tem}}(M^2, 0, q^2)$ is real for real q as it should be. Concluding, we state that the function $\chi_{AA,\text{tem}}^{(0)}(0, q^2)$ has cuts (in the following we refer to these as the *temperature cuts*) which are parallel to the real axis [9]. Thus, the full correlation function $\chi_{AA}(0, q^2)$ defined by Eq. (6.36) has at least these two cuts. Moreover, it can have poles for imaginary arguments in between the cuts. The general structure of the singularities of the correlation function is shown in Fig. 7.3.
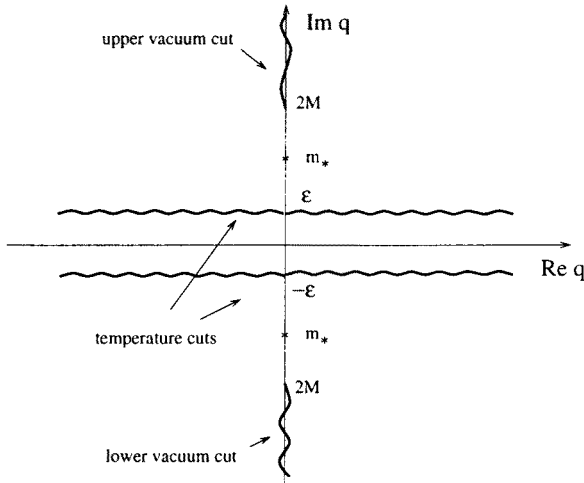
Fig. 7.3. A general analytic structure of the static correlation function in the complex three-momentum space $q = |\mathbf{q}|$ (finite temperature).

The position of the pole is given by the equation whose form is analogous to that of Eq. (6.37), namely,

$$1 - G_S \chi_{AA}^{(0)}(0, -m_*^2) = 0. \qquad (7.31)$$

---

[9] We note that the Pauli-Villars regularization of the function $I_{2,\text{tem}}(M^2, 0, q^2)$ does not change its analytic properties. On the other hand, the 3-dimensional cutoff procedure makes the temperature cuts finite, which leads to unphysical oscillations rather than to screening. This fact is the main reason why we have decided to use the Pauli-Villars method in the present investigations.

The pole can appear only in the interval $0 < m_* < 2M$ because for $m_* = 2M$ the cut starts. At zero temperature, due to the Lorentz invariance, we have $m_* = m_{\mathrm{dyn}}$. On the other hand, for $T > 0$ one finds that $m_* \neq m_{\mathrm{dyn}}$. Formally, the last property follows from the difference between the functions $I_{2,\mathrm{tem}}(M^2, k^2, 0)$ and $I_{2,\mathrm{tem}}(M^2, 0, -k^2)$. The latter is the analytic continuation of $I_{2,\mathrm{tem}}(M^2, 0, q^2)$ and has the form

$$I_{2,\mathrm{mat}}(M^2, 0, -k^2) = -\frac{N_c}{k\pi^2} \int\limits_0^\infty \frac{dp\, p}{E_p} \frac{1}{\mathrm{e}^{E_p/T} + 1} \left[\pi - 2\arctan\left(\frac{k}{2p}\right)\right]. \quad (7.32)$$

The contribution to the Fourier transform from the pole has, of course, the form $\sim \exp(-m_* r)$.

The integral around the vacuum cut can be written as follows

$$\chi_{AA}^{\mathrm{VC}}(r) = -\frac{1}{4\pi^2 ir} \int\limits_{2M}^\infty dk\, k \left[\chi_{AA}(0, -k^2 + i\epsilon) - \chi_{AA}(0, -k^2 - i\epsilon)\right] \mathrm{e}^{-kr}. \quad (7.33)$$

For large values of r, the exponential factor in (7.33) cuts down the integrand very quickly as a function of k. Thus, the remaining factors, which are slowly varying, can be approximated by their value at $k \approx 2M$. *Consequently, in the limit $r \to \infty$ the contribution of the vacuum cut is also of the exponential form,* $\sim \exp(-2Mr)$. The contribution of the temperature cut is

$$\chi_{AA}^{\mathrm{TC}}(r) = \frac{1}{4\pi^2 ir} \int\limits_{-\infty}^{+\infty} dq\, q \left[\chi_{AA}(0, [q + i\delta_-]^2) - \chi_{AA}(0, [q + i\delta_+]^2)\right] \mathrm{e}^{iqr}. \quad (7.34)$$

where $\delta_\pm$ is defined below Eq. (7.29). The imaginary shift of the argument, $i\delta_\pm$, denotes that the function should be calculated just above/below the temperature cut. We shall now discuss separately three different cases. The first two concern our analytic results for $T = 0$ and $T \to \infty$. The third one concerns intermediate temperatures for which we do numerical calculations.

7.2.2. Results for $T = 0$

At zero temperature the temperature cut vanishes so we are left only with one or two contributions. In the case of the pseudoscalar channel we have an isolated pole and a cut. This pole, because of the Lorentz invariance, coincides with that determining the dynamic mass. For large values of r the contribution from the pole, $\sim \exp(-m_{\mathrm{dyn},\pi} r)$, is larger than that from the vacuum cut, $\sim \exp(-2Mr)$. Thus, the pion screening mass at $T = 0$ is equal to the dynamic one: $m_{\mathrm{scr},\pi} = m_{\mathrm{dyn},\pi} = 138$ MeV. In the case of the scalar

channel we do not have an isolated pole and the only contribution to the Fourier transform comes from the vacuum cut. In consequence the sigma screening mass equals $2M$ and it is smaller than the dynamic one: $m_{\text{scr},\sigma} = 752$ MeV and $m_{\text{dyn},\sigma} = 760$ MeV.

We note that the result $m_{\text{scr},\sigma} = 2M$ is of course an artifact of the NJL model, which lacks confinement and of the approximation, which lacks the coupling of the sigma to the two-pion continuum. With this effect included, the screening mass in the sigma channel would equal $2m_{\text{dyn},\pi}$.

7.2.3. The case of extremely high temperature

In the limit $T \to \infty$ the zeroth-order correlation functions vanish. It means that at sufficiently high temperature they are very small and, at the same time, they are a good approximation for the full correlation functions. In this case the expression $G_S \chi_{AA}^{(0)}(0, q^2)$, appearing in the definition (6.36), can be neglected when compared to unity. Using this fact we define the high temperature correlation function in space by equation [10]

$$\chi_{AA}^{(0)}(r) = \frac{1}{4\pi^2 i r} \int\limits_{-\infty}^{\infty} dq\, q\, \chi_{AA}^{(0)}(0, q^2)\, e^{iqr} . \qquad (7.35)$$

Here the integration of the vacuum part $\chi_{AA,\text{vac}}^{(0)}(0, q^2)$ and the temperature part $\chi_{AA,\text{mat}}^{(0)}(0, q^2)$ defines the functions $\chi_{AA,\text{vac}}^{(0)}(r)$ and $\chi_{AA,\text{mat}}^{(0)}(r)$, respectively. Of course we have

$$\chi_{AA}^{(0)}(r) = \chi_{AA,\text{vac}}^{(0)}(r) + \chi_{AA,\text{tem}}^{(0)}(r). \qquad (7.36)$$

The Fourier transform (7.35) can be calculated analytically. Using the same method as that developed by us in Section 7.1, we find that

$$\chi_{PP,\text{vac}}^{(0)}(r) = \frac{N_c}{2\pi^3 r^3} \sum_{i=0}^{N} A_i \Lambda_i^2 \left[3 K_2(2\Lambda_i r) + 2\Lambda_i r K_1(2\Lambda_i r) \right]. \qquad (7.37)$$

On the other hand the temperature piece has the form

$$\chi_{PP,\text{mat}}^{(0)}(r) = \frac{N_c}{4\pi^3 r} \left(\frac{2}{r^3} - \frac{2}{r^2} \frac{\partial}{\partial r} + \frac{1}{r} \frac{\partial^2}{\partial r^2} \right) \left[G_1^{\text{tem}}(r) + G_2^{\text{tem}}(r) \right], \qquad (7.38)$$

where

$$G_1^{\text{tem}}(r) = - \sum_{i=0}^{N} A_i \Lambda_i K_1(2\Lambda_i r) \qquad (7.39)$$

---

[10] The situation described in this Section resembles the case of the perturbative QCD calculation discussed thoroughly in Section 7.1. The basic difference is that now the cutoffs are finite and fixed by fitting physical observables at $T = 0$.

and

$$G_2^{\text{tem}}(r) = \pi T \sum_{i=0}^{N} A_i \sum_{l=-\infty}^{+\infty} \exp(-2r\sqrt{(2l+1)^2\pi^2 T^2 + \Lambda_i^2}). \qquad (7.40)$$

Using the properties of the modified Bessel functions [54] we can check that in expression (7.36) the vacuum part (7.37) is exactly canceled by the first term of the temperature part (7.38), *i.e.*, by the term coming from differentiation of the function $G_1^{\text{tem}}(r)$. We want to emphasize that this cancellation is independent of the number of subtractions N and of the values of the regulating masses Λ_i.

The function $G_2^{\text{tem}}(r)$ has a simple asymptotic behaviour. For $r \to \infty$ it is enough to consider only the leading terms in the series, *i.e.*, these corresponding to $l = 0, -1$ and $i = 0$. The terms for $i > 0$ are suppressed since $\Lambda_i > \Lambda_0 = M$ (additionally we can neglect M with respect to T). Finally, we obtain the following asymptotic expressions

$$G_2^{\text{tem}}(r) \sim 2\pi T \, e^{-2\pi Tr} \qquad (7.41)$$

and

$$\chi_{PP}^{(0)}(r) \sim \frac{2T^3 N_c}{r^2} \, e^{-2\pi Tr} \, . \qquad (7.42)$$

From Eq. (7.42) we read off the screening mass in the pseudoscalar channel to be $2\pi T$. The calculations in the scalar channel look similarly. We can even immediately guess that the result will be the same: At very high temperature the constituent quark mass drops down and is equal to the current one. The latter is very small and the difference between the pseudoscalar and scalar channel practically disappears.

Our present considerations showed again how important is the regularization of the temperature part. It leads to cancellations between the vacuum and temperature parts and, finally, to the asymptotic behaviour of the form $\sim \exp(-2\pi Tr)$. If the temperature part were not regularized, the asymptotic behaviour of the correlation function would be governed by the lowest regulating mass, *i.e.*, by Λ_1. Such a case could not be accepted from the physical point of view.

7.2.4. Intermediate temperatures

For the temperature range $0 \leq T \leq 400$ MeV we did numerical calculations and read off the values of the screening masses from the logarithmic plots representing the correlation functions in space. We did the calculations in two ways checking whether the results were the same. The first method was to calculate the Fourier transform directly from Eq. (6.39). The second method was to calculate the contributions from the singularities separately

and later to sum them up. In the latter case we used Eqs (7.33) and (7.34). Moreover, we numerically calculated the residue corresponding to the pole (7.31). Both methods encounter numerical difficulties. The direct calculation of the Fourier transform requires an integration of a slowly converging and oscillating function. On the other hand, the contributions from the cuts show large cancellations. Therefore, each contribution should be evaluated with a very high accuracy. Let us also note here that the parameters used to calculate the screening masses were the same as those used in the case of the dynamic masses, see Section 6.3.2.

We had to restrict ourselves to rather small values of r, since the correlation functions decrease very rapidly and for large r their numerical evaluation is difficult. In fact, they decrease exponentially which suggests that the screening masses can be read off already for small r's. This exponential behaviour is shown in Figs 7.4 and 7.5, where we plotted the functions $r \chi_{PP}(r)$ and $r \chi_{SS}(r)$.
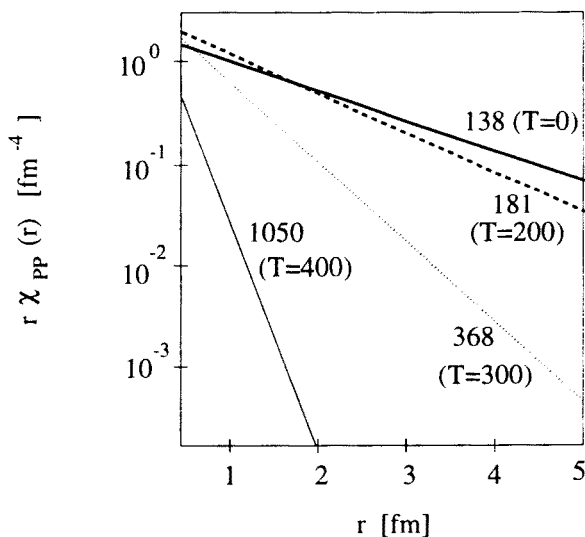
Fig. 7.4. The spatial dependence of the static correlation function in the pion channel. The numbers at the lines are the values of the screening masses at the corresponding temperatures (given in MeV).

At zero temperature our numerical procedure gives the results which are in good agreement with our estimates based on the analytic considerations, see Section 7.2.2. The numerically calculated pion screening mass agrees exactly with the analytic result, whereas in the sigma channel we find a small discrepancy. This difference is caused by the fact that we do not consider asymptotic distances in the numerical calculations.

Fig. 7.5. Same as Fig. 7.4. for the sigma channel.

The temperature dependence of the screening and dynamic masses is shown in Fig. 7.6. For $0 \leq T \leq 200$ MeV we observe that the screening masses are close to the dynamic ones. Such situation is expected, since for small temperatures the Lorentz invariance is only slightly broken. Interesting things can be observed for larger temperatures. *Both screening and dynamic masses exhibit the restoration of chiral symmetry although they substantially differ from each other.* In the full interval, $0 \leq T \leq 400$ MeV, the qualitative behaviour of the screening masses and of the dynamic ones is similar and resembles the results of the lattice simulations of QCD.

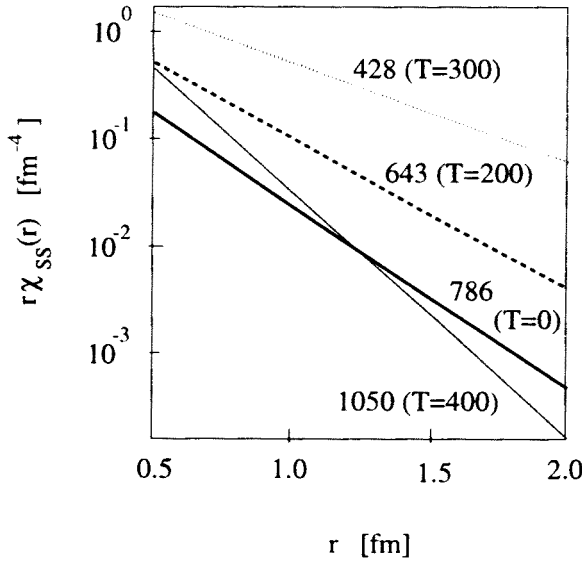Our observation that the dynamic masses are different from the screening masses contradicts the results of Ref. [13] where it was argued that they are the same even at finite T. In Ref. [13] the chiral limit, $m = 0$, is considered. Afterwards, the gap equation is used to find that the two masses are equal. The point is, however, that in Ref. [13] the non-trivial solution to the gap equation is used. It exists only if $T < T_c$ (in the chiral limit T_c is well defined) and for $T > T_c$ we have to take into account just the trivial solution $M = m = 0$. The trivial solution does not allow us to simplify the denominator of the correlation function, what is essential for the proof of the equality of two masses in [13]. Consequently, the arguments of Ref. [13] do not apply at $T > T_c$ and in this case we do not expect that $m_{\rm scr} = m_{\rm dyn}$. The problem remains what happens at $T < T_c$. The structure of the poles suggests that $m_{\rm scr} = m_{\rm dyn}$, but there exists a temperature
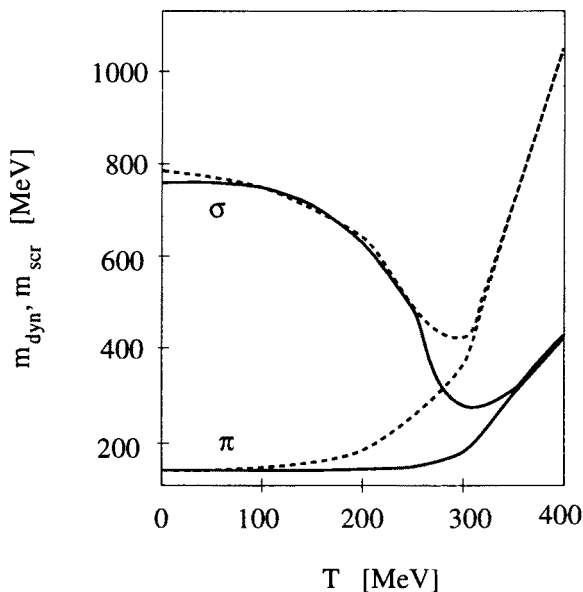
Fig. 7.6. The temperature dependence of the screening (dashed lines) and the
dynamic (solid lines) masses.

cut whose contribution might be not negligible. This situation deserves a
separate study.

Another interesting point is to check whether the screening masses ap-
proach the Eletskii–Ioffe limit, i.e., if they are equal to $2\pi T$ for large T.
Our numerical results for the pseudoscalar channel are shown in Fig. 7.7.
One can see that the ratio $m_{scr,\pi}/T$ grows with the temperature for $T > T_c$
but even at $T = 450$ MeV it is still smaller than 2π. (In the scalar channel
the high temperature behaviour is the same as in the pseudoscalar one.) As
we have already mentioned this type of behaviour is observed in the lattice
simulations. In the (pseudo)scalar channel the screening masses are smaller
than $2\pi T$, which is in contrast to the (axial)vector channel where they are
equal to $2\pi T$ already for the temperatures slightly exceeding T_c. Our result
suggests that the NJL model can explain the existence of the non-negligible
(residual) interaction in the (pseudo)scalar channel. Nevertheless, for draw-
ing more definite conclusions the calculations in the (axial)vector channel
are required. If the difference between the behaviour of the screening masses
in the (pseudo)scalar channel and the (axial)vector channel were found, this
would act in favor of the model.
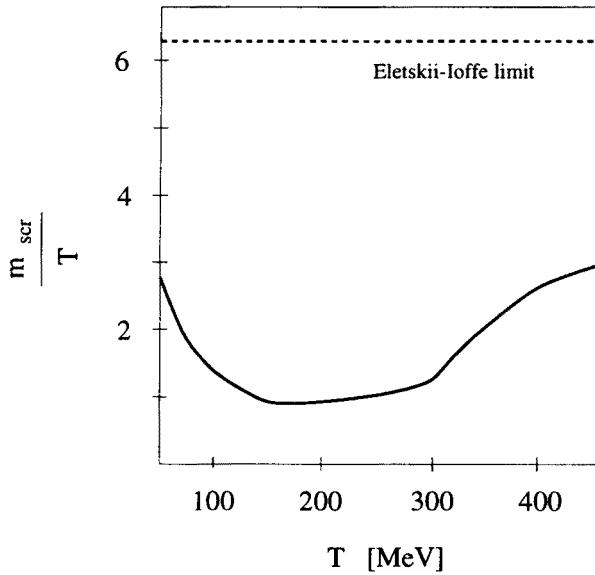
Fig. 7.7. The ratio m_{scr}/T plotted as a function of the temperature. The dashed line corresponds to the Eletskii–Ioffe limit: $m_{scr} = 2\pi T$.

8. Static meson fields at finite baryon density

In this Chapter we investigate the in-medium static meson correlation functions at finite baryon density. In contrast to the behaviour known from the high temperature calculations, studied by us in the previous Chapter, we find that the correlation functions at finite baryon density are not screened but oscillate in space [57]. This behaviour is analogous to the Friedel oscillations in a degenerate electron gas [41]; in both cases the oscillations are caused by the existence of the sharp Fermi surface.

In spite of the fact that it lacks confinement, the NJL model successfully describes many aspects of hadron structure [55, 56]. However, a realistic description of nuclear matter at low densities as a collection of composite nucleons would be very complicated and outside the scope of our approach. Hence, we work again in the HF + RPA scheme, where the correlations that bind quarks in nucleons are neglected and consequently nuclear matter is described as a Fermi gas of quarks. Although our model for nuclear matter at low densities is not realistic, we believe that our results on the correlation functions at finite baryon density are generic and should be qualitatively the same in more realistic models. This conjecture is supported by studies of the effective nucleon-nucleon interaction in nuclear matter, which also indicates the presence of the Friedel oscillations [58–60].

Already at moderate densities we find new singularities in the correlation function, which probably are artifacts of the NJL model in the HF + RPA approximation. This indicates that this approach to the correlation functions breaks down already at moderate densities. Hence, to complete the picture we compute the meson correlation function at higher densities in perturbative QCD. Keeping only the leading term, we find oscillations with a period $\delta r = \pi/p_F$, where p_F is the Fermi momentum of the quark sea.

8.1. Low density theorem

Before we analyze the properties of the correlation functions, let us discuss shortly the behaviour of the quark condensate at finite baryon density. In this way we shall supplement our discussion from Section 5.2. The calculation of the decrease of the condensate with increasing baryon density in the framework of the NJL model is instructive, since there are model independent estimates of this quantity, which impose constraints on the in-medium behaviour of the condensate.

At $T = \mu = 0$ the NJL model yields the Gell-Mann–Oakes–Renner (GOR) relation

$$F_\pi^2 m_{\text{dyn},\pi}^2 = -\tfrac{1}{2}(m_u + m_d)\langle \overline{u}u + \overline{d}d \rangle = -2m\langle \overline{q}q \rangle, \qquad (8.1)$$

where F_π is the pion decay constant. This relation is independent of the regularization scheme. One can use it to find the value of F_π provided the values of m, m_π and $\langle \overline{q}q \rangle$ are known. For the two-flavour symmetric model, with the values of the parameters the same as in Section 5.2, one finds $F_\pi = 94$ MeV.

Using the Hellmann–Feynman theorem and the GOR relation, one finds [61,62] to leading order in the density

$$\frac{\langle \overline{q}q \rangle}{\langle \overline{q}q \rangle_0} = 1 - \frac{\Sigma_{\pi N}}{m_\pi^2 F_\pi^2}\,\rho, \qquad (8.2)$$

where $\Sigma_{\pi N}$ is the pion nucleon sigma commutator, $\langle \overline{q}q \rangle_0$ is the vacuum value of the quark condensate, and ρ is the baryon density. The baryon density is for two flavours given by $\rho = 2p_F^3/3\pi^2$, where p_F, as usual, is the quark Fermi momentum. We compute the pion nucleon sigma term by using the relation [62]

$$\frac{1}{3}\Sigma_{\pi N} = \Sigma_{\pi q} = m\frac{dM_0}{dm}, \qquad (8.3)$$

where we assume that the πN sigma term is simply the sum of the πq sigma terms, like in the naive quark model. For our set of the parameters one gets
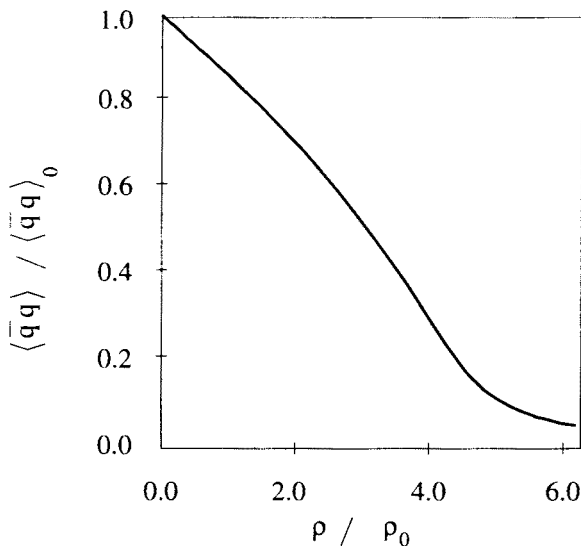
Fig. 8.1. Ratio of the in-medium quark condensate to the vacuum value, plotted as a function of baryon density.

$\Sigma_{\pi N} = 18$ MeV, which, using Eq. (8.2), implies that the condensate is reduced by 15 % at the saturation density of nuclear matter, $\rho_0 = 0.17$ fm^{-3}. In Fig. 8.1 we show the numerical results for the quark condensate (normalized to its vacuum value) as a function of the baryon density (normalized to the saturation density) [11]. One can see that our calculation agrees with the low-density theorem (8.2), when we use the sigma commutator obtained within the model. Since the sigma term is much smaller than the empirical value of 45 MeV, the density dependence of the quark condensate is too weak. Nevertheless, the fact that Eq. (8.2) is satisfied, shows that the calculation is consistent.

8.2. Friedel oscillations in the NJL model

Let us come back to the discussion of the correlation functions. Our analysis of the static meson correlation functions at finite baryon density is based on the two-flavour symmetric model. Moreover, we use again the same values of the parameters as in Sections 5.2, 6.3 and 7.2. Thus our results for zero baryon density agree with the results of Section 7.2 for the case $T = 0$. Our starting point are Eqs (6.39) and (6.36), where the zeroth-order correlation functions are given by formulae (6.5), (6.6), (6.16) and (6.22). Thus, the full correlation function (6.36) can be expressed in terms of the

[11] We note that Fig. 8.1 corresponds exactly to Fig. 5.7 showing dependence of M on μ.

functions $I_{1,\text{vac}}(M^2)$, $I_{1,\text{mat}}(M^2)$, $I_{2,\text{vac}}(-q^2)$ and $I_{2,\text{mat}}(0,q^2)$. We note that these four functions have been already calculated. In the case of the Pauli-Villars regularization scheme, which is adopted here, we can use Eqs (5.24), (5.25), (6.31) and (6.33), respectively.
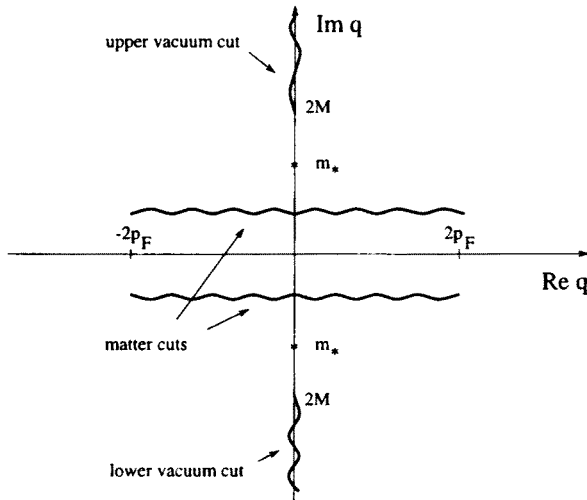
Fig. 8.2. A general analytic structure of the static correlation function in the complex three-momentum space $q = |\mathbf{q}|$ (finite baryon density).

The Fourier transform (6.39), defining the static correlation function in space, can be again written as a sum of a few contributions connected with the appearance of the singularities in the complex momentum plane. At finite baryon density, the structure of the singularities is very similar to that at finite temperature. It is shown in Fig. 8.2.

The basic difference between the finite temperature and finite density cases is that the matter cut has a finite range in q (the temperature cut, shown in Fig. 7.3, is infinite). To understand this behaviour, we can analyze the function $I_{2,\text{mat}}(M^2, 0, q^2)$ in the same way as the function $I_{2,\text{tem}}(M^2, 0, q^2)$ was analyzed in Section 7.2.1. First, we write

$$I_{2,\text{mat}}(M^2, 0, q^2) = I_{2,\text{mat}}^{(+)}(q) + I_{2,\text{mat}}^{(-)}(q), \qquad (8.4)$$

where

$$I_{2,\text{mat}}^{(\pm)}(z) = -\frac{N_c}{4z\pi^2} \int_0^{p_F} \frac{dp\,p}{E_p} \ln \frac{2p - z \pm i\epsilon}{-2p - z \pm i\epsilon}. \qquad (8.5)$$

The form of expression on the RHS of Eq. (8.5) shows that the functions $I_{2,\text{mat}}^{(\pm)}(z)$ have logarithmic cuts parallel to the real axis and stretching from

$-2p_F \pm i\epsilon$ to $+2p_F \pm i\epsilon$. The finite range of the cuts is caused by the finite range of momenta available in the integral (8.5).

Let us now discuss the results of the finite density calculations. In the case of the pseudoscalar channel, we did the numerical calculations in the energy range $M_0 = 376$ MeV $\leq \mu \leq 415$ MeV. In Fig. 8.3 we show the corresponding correlation for $\mu = 376, 400$ and 410 MeV. In contrast to the exponential decay found in vacuum (solid line), the correlation function at finite density (dashed and dotted lines) oscillates, with a power-law decay of the amplitude. Its period decreases with the increasing value of the chemical potential. From the physical point of view, such oscillations are caused by the existence of a sharp Fermi surface.
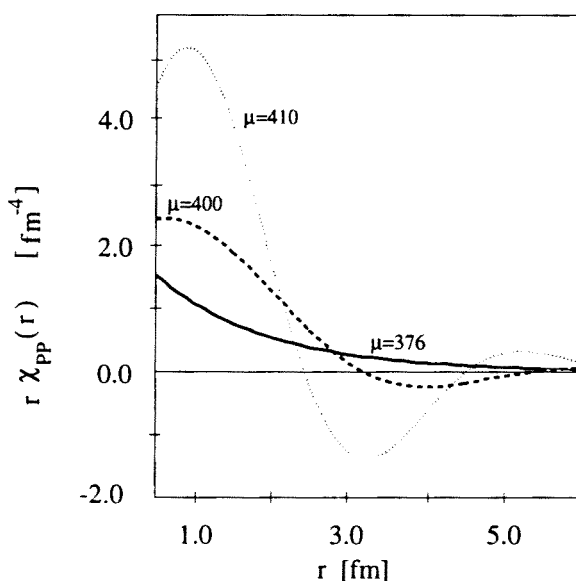
Fig. 8.3. Correlation function in the pseudoscalar channel plotted for three different values of the chemical potential: $\mu = 376$ MeV (solid line), $\mu = 400$ MeV (dashed line), and $\mu = 410$ MeV (dotted line).

The oscillatory behaviour of the correlation functions at finite density is well known for the non-relativistic degenerate electron gas, where the phenomenon is called the Friedel oscillations [41]. These long range oscillations lead to many interesting phenomena like, *e.g.*, broadening of the nuclear magnetic resonance lines. A characteristic feature of the Friedel oscillations (at very large distances) is their period $\delta r = \pi/p_F$. In our case the situation is similar; for very large values of r, the contribution from the matter cut dominates over the other contributions. Since the cut extends over a finite range in q ($|q| < 2p_F$) the correlation function oscillates with the pe-

riod π/p_F (at $r \to \infty$). The numerical study of the correlation functions at very large distances is difficult because the amplitudes decrease with r. Consequently, we restrict the numerical calculations to the interval 0.5 fm $< r <$ 6 fm.

So far we have discussed the results for $\mu < 415$ MeV. For larger values of the chemical potential (corresponding roughly to $\rho > \frac{1}{2}\rho_0$) the pseudoscalar correlation function acquires additional singularity on the real axis for $q \approx 2p_F$. In the scalar channel, a similar singularity appears at even smaller densities ($\rho > \frac{1}{3}\rho_0$). These singularities indicate instabilities of the ground state, which lead the system to states of lower energy. However, most likely the singularities are artifacts due to regularization procedure and do not correspond to physical instabilities. In order to check this point we have redone the calculation using a different regularization scheme with a 3-dimensional cutoff. Using the parameters obtained in Ref. [15], we find no singularities on the real axis. This shows that these singularities are unphysical, since their presence depends on details in the formulation of the model. Thus, our regularization scheme can be used only at low densities.

On the other hand, the 3-dimensional cutoff regularization is unsatisfactory because it explicitly breaks Lorentz invariance. This obscures the relation between the correlation functions in time-like and space-like regions. Moreover, in the 3-dimensional cutoff scheme, one does not recover the well known screening of the correlation function at finite temperatures. Instead, the correlation function oscillates, much like the Friedel oscillations at $T = 0$, with a period π/Λ, where Λ is the momentum cutoff. We stress that this behaviour is an artifact, due to the finite range of momenta ($|q| < \Lambda$) available in the Fourier transform.

Consequently, we stick to the covariant Pauli–Villars method, in spite of its shortcomings. However, since the results are inconclusive at densities $\rho \sim \rho_0$ and higher, we restrict the calculations to small densities $\rho < \frac{1}{3}\rho_0$. The physics at very large densities will be addressed in the following Section.

8.3. Oscillations in perturbative QCD

In a straightforward way, the formalism developed so far can be used to study finite-density correlations functions in perturbative QCD. Similarly to the high temperature case discussed in Section 7.1, the leading term in the meson correlation function is the lowest order quark loop diagram (as in Fig. 6.1). Thus, for the pseudoscalar channel we can write

$$\tilde{\chi}(r) = \tilde{\chi}_{\text{vac}}(r) + \tilde{\chi}_{\text{mat}}(r), \tag{8.6}$$

where $\tilde{\chi}_{\text{vac}}(r)$ is given by Eq. (7.7), and the matter piece has the form

$$\tilde{\chi}_{\text{mat}}(r) = \frac{N_c}{4\pi^3 r} \left(\frac{2}{r^3} - \frac{2}{r^2}\frac{\partial}{\partial r} + \frac{1}{r}\frac{\partial^2}{\partial r^2} \right) \left[\tilde{G}_1^{\text{mat}}(r) + \tilde{G}_2^{\text{mat}}(r) \right]. \tag{8.7}$$

Eq. (8.7) is the analog of Eq. (7.17) for the case of finite density. One can check that $\tilde{G}_1^{\text{mat}}(r) = \tilde{G}_1^{\text{tem}}(r)$. Similar cancellations to those described in Section 7.1 take place. Thus, finally only the function $\tilde{G}_2^{\text{mat}}(r)$ gives a non-vanishing contribution to the correlation function. A simple calculation yields

$$\tilde{G}_2^{\text{mat}}(r) = -\frac{\partial}{\partial r} \int\limits_{p_F}^{\infty} \frac{dp}{2\sqrt{p^2 + M^2}} \cos(2pr). \tag{8.8}$$

In the limit $M \to 0$ we find $\tilde{G}_2^{\text{mat}}(r) = \cos(2p_F r)/2r$, which implies that the correlation function $\tilde{\chi}(r)$ is not screened but oscillates in space with a period $\delta r = \pi/p_F$. For massless quarks the behaviour in the scalar channel is identical.

9. Beyond the Hartree–Fock approximation

Calculations based on the NJL model show that the value of the quark condensate is strongly modified by the in-medium effects. It eventually goes to zero for $T, \mu \to \infty$. The interesting question is whether the changes of the condensate (as described by the model) exhibit some universal features. At low density, we have seen (Section 8.1) that the NJL calculations agree with the model independent estimates. On the other hand, it turns out that the change of the condensate at small temperature is not compatible with the general requirements of the chiral perturbation theory: In the standard approach to the model (HF + RPA), the condensate remains completely flat at small T, whereas the chiral perturbation theory indicates that the absolute value of the condensate should decrease linearly with T^2.

As we shall see in this Chapter, the discrepancy between the NJL model and the chiral perturbation theory is an effect caused by the HF approximation. The standard approach is not sufficient to describe properly the thermodynamic properties of hadronic matter at small temperatures, which should be dominated by the lightest hadrons, *i.e.*, pions. In order to describe properly the low temperature change of the condensate in the NJL model, one has to go beyond the HF approximation, including the so-called meson loops. In this Chapter, we outline the characteristic features of this approach.

9.1. Effective action

Our present considerations will be based on the two-flavour standard model with scalar-isoscalar and pseudoscalar-isovector interactions. The corresponding Lagrangian is given by Eq. (3.16). In this Section, we shall apply the formalism of the effective action [63] to this Lagrangian. Details of this procedure have been given in [64]. In the following, we shall describe only the basic ingredients of this method.

At first we introduce the meson mean fields $\Phi = (\Phi_0, \boldsymbol{\Phi})$, where Φ_0 and $\boldsymbol{\Phi}$ correspond to the pion and the sigma, respectively. At the quark-loop level the effective action is

$$I(\Phi) = \int d^4x \left(\tfrac{1}{2}a^2\Phi^2 - a^2m\Phi_0 + \tfrac{1}{2}a^2m^2 \right) - \tfrac{1}{2}\mathrm{Tr}\,\ln(D^\dagger D), \qquad (9.1)$$

where $1/a^2 = 2G$ and D is the Dirac operator, i.e., $D = \partial_\tau - i\boldsymbol{\alpha} \cdot \boldsymbol{\nabla} + \beta\Phi_0 + i\beta\gamma_5\boldsymbol{\tau} \cdot \boldsymbol{\Phi}$. For the moment, we consider the case $T = 0$ and work in Euclidean space-time $(\tau, \boldsymbol{x})$. The generalization of our considerations to the case $T > 0$ will be described in the next Section. In Eq. (9.1) we have replaced the usual $\mathrm{Tr}\,\ln D$ term with $\tfrac{1}{2}\mathrm{Tr}\,\ln(D^\dagger D)$, which is exact for SU(2).

Meson loops bring an additional term to the effective action [63,64]

$$\Gamma(\Phi) = I(\Phi) + \tfrac{1}{2}\mathrm{Tr}\,\ln(K^{-1}), \qquad (9.2)$$

where K is the inverse *meson propagator* matrix defined as

$$K_{ab}^{-1}(x,y) = \frac{\delta^2 I(\Phi)}{\delta\Phi_a(x)\delta\Phi_b(y)}. \qquad (9.3)$$

In Eqs (9.1) and (9.2) Tr denotes the full trace, including functional space, isospin, and in addition colour and spinor trace for quarks. In the N_c-counting scheme, the quark loop term $I(\Phi)$ is the leading contribution of order $\mathcal{O}(N_c)$, and the meson loop term $\tfrac{1}{2}\mathrm{Tr}\,\ln(K^{-1})$ is of order $\mathcal{O}(1)$. Thus the one-meson-loop contributions give the first correction to the leading-N_c results.

Using standard methods, Green's functions can be obtained from Eq. (9.2) via differentiation with respect to mean meson fields. Of particular importance is the one-point function, which gives the expectation value of the sigma field. The condition

$$\frac{\delta\Gamma(\Phi)}{\delta\Phi_0(x)}\Big|_{\Phi_0(x)=S} = a^2(S-m) - \tfrac{1}{2}\mathrm{Tr}\left((D^\dagger D)^{-1}\frac{\delta(D^\dagger D)}{\delta\Phi_0(x)} \right)_{\Phi_0(x)=S}$$

$$+ \tfrac{1}{2}\mathrm{Tr}\left(K\frac{\delta K^{-1}}{\delta\Phi_0(x)} \right)_{\Phi_0(x)=S} = 0 \qquad (9.4)$$

yields the equation for the vacuum expectation value of Φ_0, which we denote by S. As shown in Ref. [64], introducing

$$K_\sigma(S, q_E^2) = \left[-I_{2,\text{vac}}(S^2, -q_E^2)\,(q_E^2 + 4S^2) + \frac{a^2 m}{S} \right]^{-1},$$

$$K_\pi(S, q_E^2) = \left[-I_{2,\text{vac}}(S^2, -q_E^2)\, q_E^2 + \frac{a^2 m}{S} \right]^{-1}, \qquad (9.5)$$

and retaining terms up to order $\mathcal{O}(N_c^0)$, Eq. (9.4) can be written in the form

$$a^2\,(S - m) - S\,I_{1,\text{vac}}(S^2) - \frac{S}{16\pi^4} \int d^4 q_E \Big\{ \Big[2\,I_{2,\text{vac}}(S^2, 0)$$

$$+ \frac{d}{dS^2}\Big(I_{2,\text{vac}}(S^2, -q_E^2)[q_E^2 + 4S^2] \Big) \Big] K_\sigma(S, q_E^2)$$

$$+ 3\Big[2\,I_{2,\text{vac}}(S^2, 0) + \frac{d}{dS^2} I_{2,\text{vac}}(S^2, -q_E^2)\, q_E^2 \Big] K_\pi(S, q_E^2) \Big\} = 0. \quad (9.6)$$

The functions $I_{1,\text{vac}}(S^2)$ and $I_{2,\text{vac}}(S^2, -q_E^2)$ have been defined by expressions (5.21) and (6.7). One can easily check that the leading-N_c term in (9.6) coincides with the gap equation (5.28).

It is important to observe that the one-meson-loop gap equation (9.6) requires introduction of an extra regulator for meson momenta. The regularization of the quark loop only is not sufficient to make meson loops finite, since at large q_E^2 one has $I_{2,\text{vac}}(S^2, -q_E^2) \sim 1/q_E^2$. Consequently, the structure of divergences is the same as, *e.g.*, in the linear σ model, in particular Eq. (9.6) is quadratically divergent without a cutoff in the q_E integration. The need for an additional cutoff is not surprising, since a non-renormalizable theory requires new cutoffs at next levels of a perturbative expansions. Therefore we have to regularize the divergent integral over $d^4 q_E$. In Ref. [64] this was achieved by the substitution

$$\int d^4 q_E \longrightarrow \pi^2 \int_0^{\Lambda_b^2} dq_E^2\, q_E^2, \qquad (9.7)$$

where Λ_b was the four-dimensional Euclidean meson momentum cutoff. At the same time, the quark loops were regularized with the Schwinger proper-time method. In the present study we employ the 3-dimensional cutoff procedure for the meson loops, *i.e.*, we make the replacement

$$\int d^4 q_E \longrightarrow 4\pi \int dq_4 \int_0^{\Lambda_b} dq\, q^2, \qquad (9.8)$$

where $q_E = (q_4, \boldsymbol{q})$ and $q = |\boldsymbol{q}|$. The form (9.8) is convenient for the implementation of the boundary conditions satisfied by temperature Green's functions. Similarly to Ref. [64], we regularize the quark loops (*i.e.*, the functions $I_{1,\text{vac}}(S^2)$ and $I_{2,\text{vac}}(S^2, -q_E^2)$) using the Schwinger proper-time method.

If chiral symmetry is broken, then Eq. (9.6) has a nontrivial solution for S. The quark condensate and S are related by the formula

$$\langle \bar{q}q \rangle = -a^2 (S - m) , \tag{9.9}$$

which follows immediately from the fact that $\langle \bar{q}q \rangle = \delta\Gamma(\Phi)/\delta m$ and Eq. (9.2).

9.2. Finite temperature

For calculations at $T > 0$ we shall again adopt the imaginary time formalism. In this situation, the finite-temperature analog of Eq. (9.6) can be written in the following form

$$a^2 (S - m) - SI_1^{R,SPT}(S^2, T) - \frac{ST}{2\pi^2} \sum_n \int_0^{\Lambda_b} dq q^2 \times \left\{ \left[2I_2^{R,SPT}(S^2, 0, 0, T) \right. \right.$$

$$+ \frac{d}{dS^2} \left(I_2^{R,SPT}(S^2, n, q, T) \left[(E_n^b)^2 + \boldsymbol{q}^2 + 4S^2 \right] \right) \right] K_\sigma(S, n, q, T)$$

$$+ 3 \left[2I_2^{R,SPT}(S^2, 0, 0, T) + \frac{d}{dS^2} I_2^{R,SPT}(S^2, n, q, T) \left[(E_n^b)^2 + \boldsymbol{q}^2 \right] \right]$$

$$\times K_\pi(S, n, q, T) \right\} = 0 . \tag{9.10}$$

where $K_\sigma(S, n, q, T)$ and $K_\pi(S, n, q, T)$ are the generalized expression for the inverse meson propagators

$$K_\sigma(S, n, q, T) = \left\{ -I_2^{R,SPT}(S^2, n, q, T) \left[(E_n^b)^2 + \boldsymbol{q}^2 + 4S^2 \right] + a^2 m/S \right\}^{-1} ,$$

$$K_\pi(S, n, q, T) = \left\{ -I_2^{R,SPT}(S^2, n, q, T) \left[(E_n^b)^2 + \boldsymbol{q}^2 \right] + a^2 m/S \right\}^{-1} . \tag{9.11}$$

In Eqs (9.10) and (9.11) $E_n^b = 2\pi nT$, and the functions $I_1^{R,SPT}(S^2, T)$ and $I_2^{R,SPT}(S^2, n, q, T)$ are given by expressions (5.32) and (6.35) — since in this Chapter the Schwinger proper-time method is used to make the quark loops finite, we make the reference to the expressions giving the regularized form of $I_1(S^2, T)$ and $I_2(S^2, n, q, T)$.

9.3. Low-temperature expansion in the chiral limit

Before presenting our numerical results for $\langle \overline{q}q \rangle_T$ let us consider the low-temperature expansion. As shown by Gasser and Leutwyler [66], *in the exact chiral limit* the low-temperature expansion of the quark condensate has the form

$$\langle \overline{q}q \rangle_T = \langle \overline{q}q \rangle_0 \left(1 - \frac{T^2}{8F_\pi^2} - \frac{T^4}{384F_\pi^4} + \ldots \right). \tag{9.12}$$

First, let us do the N_c counting in this formula. Since $F_\pi \sim \mathcal{O}(\sqrt{N_c})$, subsequent terms in the expansion are suppressed by $1/N_c$. Since our one-meson-loop calculation accounts for first sub-leading effects in the $1/N_c$ expansion, we can hope for reproducing only the T^2 term in Eq. (9.12). Further terms would require more loops.

Using techniques described in Chapter 4, the sum over the bosonic Matsubara frequencies in Eq. (9.10) can be converted to a contour integral in the complex energy plane. By deforming this contour we collect all contributions from the singularities of the integrand, weighted with the thermal Bose distribution. At low temperatures, the dominant contribution comes from the lowest lying pion pole, and other singularities are negligible. Thus, the third term in (9.10) becomes

$$\frac{3T}{\pi^2} \sum_n \int_0^{\Lambda_b} dq\, q^2 \frac{1}{(E_n^b)^2 + q^2} = \frac{3}{2\pi^2} \int_0^{\Lambda_b} dq\, q \left[1 + \frac{2}{e^{q/T} - 1} \right]. \tag{9.13}$$

In Eq. (9.10) we have approximated the function $I_2(S^2, n, q, T)$, appearing in the pion propagator, by its value at $n = q = 0$. For sufficiently large cutoff Λ_b, the integral over the thermal distribution function in (9.13) can be expressed by the Riemann zeta function $\zeta(2) = \pi^2/6$. Thus, the final result for (9.13) is $3\Lambda_b^2/4\pi^2 + T^2/2$. Inserting the above result into the gap equation (9.10) we find, with $m = 0$, the following equality:

$$h(S, T) \equiv a^2 - I_1(S^2, T) + \frac{3\Lambda_b^2}{4\pi^2} + \frac{1}{2}T^2 = 0. \tag{9.14}$$

Eq. (9.14) defines implicitly the function $S(T)$, which satisfies the equation

$$\frac{dS}{dT^2} = -\frac{\partial h(S, T)/\partial T^2}{\partial h(S, T)/\partial S} = \left[2\frac{\partial I_1(S^2, T)}{\partial S} \right]^{-1}. \tag{9.15}$$

Here we have neglected the term $\partial I_1(S^2, T)/\partial T^2$, since it is exponentially suppressed by the factor $\exp(-S/T)$. Furthermore, the RHS of (9.15) can be rewritten using the relations [64] $\partial I_1(S^2, 0)/\partial S = 4S I_2(S^2, 0, 0, 0)$ and $-I_2(S^2, 0, 0, 0) = \overline{F}_\pi^2/S^2$, where $\overline{F}_\pi$ is the leading-N_c piece of the pion decay constant. Collecting these equalities we arrive at $dS/dT^2 = -S/(8\overline{F}_\pi^2)$, which finally gives

$$S(T) = S(0) \left[1 - \frac{T^2}{8\overline{F}_\pi^2} \right]. \qquad (9.16)$$

Proportionality (9.9) implies that the above expression coincides (in the large N_c limit, where $\overline{F}_\pi \to F_\pi$) with Eq. (9.12). Hence our method is consistent with a basic requirement of chiral symmetry at the one-meson-loop level.

9.4. Results of numerical calculations

In the exact chiral limit the model has 3 parameters: a, Λ, and Λ_b. Since the objective of this calculation is to explore qualitatively the role of meson loops rather than to come out with accurate fits to many observables, we present the calculations for the arbitrary choice $\Lambda_b/\Lambda = \frac{1}{2}$. We have also done calculations for other values of Λ_b, with similar conclusions as long as it is not too small. The remaining two parameters are fixed by reproducing the physical value of $F_\pi = 93$ MeV and a chosen value for $\langle \bar{q}q \rangle_0$. For the case of $m \neq 0$ we have an extra parameter, m, which is fitted by requiring that the pion has its physical mass. We compare results with meson loops to results with the quark loop only ($\Lambda_b = 0$). Parameters for the two calculations are always adjusted in such a way, that the values of F_π, $\langle \bar{q}q \rangle_0$, and m_π are the same.

The calculation of F_π with meson loops, although straightforward, is rather tedious, so we do not present it here. The method has been presented in detail in Ref. [64,65]. The only difference in our calculation is that the three-momentum cutoff (9.8) rather than the four-momentum cutoff of Ref. [64] is used.

Figure 9.1 shows the dependence of $\langle \bar{q}q \rangle$ on T^2. The solid line represents the case with meson loops. We note that at low temperatures the curve has a finite slope, as requested by Eq. (9.16). The slope is close to the leading-order Gasser-Leutwyler result (dotted curve). As explained earlier, the slopes would overlap in the large-N_c limit. This behaviour is radically different from the case with quark loops only (dashed curve). In this case at low temperatures $\langle \bar{q}q \rangle_T - \langle \bar{q}q \rangle_0 \sim e^{-M/T}$, where M is the mass of the constituent quark. All derivatives of this function vanish at $T = 0$, and $\langle \bar{q}q \rangle$ is flat at the origin. We can also see from the figure that the fall-off of the condensate is faster when the meson loops are included. In fact, for the
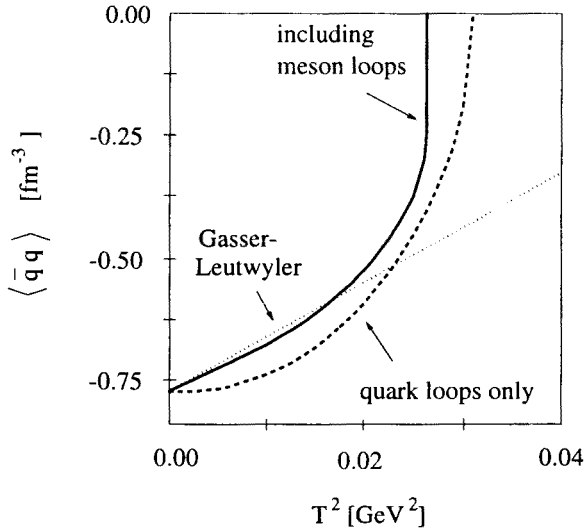
Fig. 9.1. Dependence of the quark condensate on T^2 in the chiral limit $m_\pi = 0$. The curves correspond to the calculation with meson loops (solid line), with quark loops only (dashed line), and the lowest-order chiral expansion (dotted line). The parameters for the solid line and dashed line are adjusted in such a way that $F_\pi = 93$ MeV and $\langle \bar{q}q \rangle_0 = -(184 \text{ MeV})^3$. For the solid line $a = 175$ MeV, $\Lambda = 723$ MeV, and $\Lambda_b = \frac{1}{2}\Lambda$, whereas for the dashed line $a = 201$ MeV, $\Lambda = 682$ MeV, and $\Lambda_b = 0$.

parameters of Fig. 9.1 we have an interesting phenomenon. At $T = 162$ MeV the condensate abruptly jumps to 0. There is a first-order phase transition, with a latent heat necessary to melt the quark condensate. Such a behaviour is not present in the case of calculations without meson loops [6, 10]. We note that with meson loops present the chiral restoration temperature is 162 MeV, *i.e.*, about 10% less than 176 MeV of the quark-loop-only case.

Figure 9.2 shows the same study, but for the physical value of m_π. We note that now $\langle \bar{q}q \rangle$ (solid line) is also flat at the origin, since the pion is no more massless, and at low T we have $\langle \bar{q}q \rangle_T - \langle \bar{q}q \rangle_0 \sim e^{-m_\pi/T}$. Nevertheless, the region of this flatness is small, and at intermediate temperatures the curve remains close to the Gasser-Leutwyler expansion. We note again that meson loops considerably speed up the melting of the condensate compared to the case of quark loops only. However, there is no first-order phase transition such as in Fig. 9.1. Instead, we observe a smooth cross-over typical for the case of $m \neq 0$.

The faster change of the quark condensate in our study is not surprising. It is caused by the presence of light pions which are known to play a dominant role at low-temperatures. See, for example, Ref. [16] where the bulk thermodynamic quantities studied within the NJL model are determined

by the pion quantum numbers. In this case, however, the decrease of the condensate does not agree with the requirements of the chiral perturbation theory, since the scalar-density equation is considered at the quark-loop level only and the slope of $\langle \bar{q}q \rangle$ vs. T^2 vanishes at $T^2 = 0$.
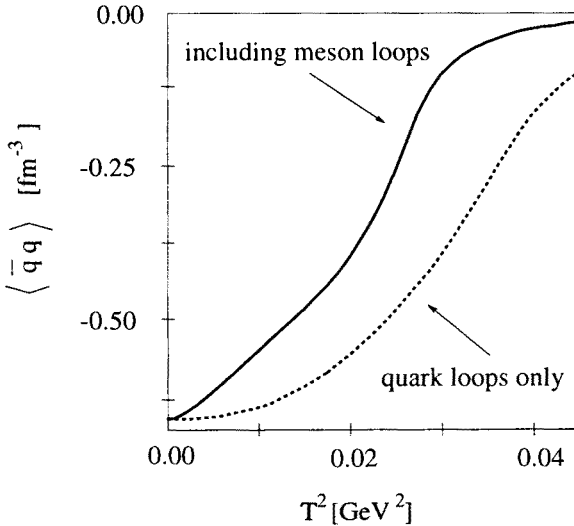
Fig. 9.2. Same as Fig. 9.1. for $m_\pi = 139$ MeV, $F_\pi = 93$ MeV, and $\langle \bar{q}q \rangle_0 = -(174 \text{ MeV})^3$. For the solid line $a = 164$ MeV, $\Lambda = 678$ MeV, $\Lambda_b = \frac{1}{2}\Lambda$, and $m = 15$ MeV, whereas for the dashed line $a = 175$ MeV, $\Lambda = 645$ MeV, $\Lambda_b = 0$, and $m = 15$ MeV.

III NON-EQUILIBRIUM PHENOMENA

10. Real-time formalism

In this Chapter we give a short introduction to the real-time formalism, presenting the most useful concepts and definitions. For our further considerations we do not need to know this method in more detail, nevertheless for a better understanding it is useful to discuss in a separate place the way in which the non-equilibrium Green's functions are introduced. For more information about the real-time formalism we refer the reader to [67].

Since we are interested in the non-equilibrium evolution of a system, we have to calculate the averages of the operators in arbitrary states. Thus, in analogy to (4.9) or (4.10), we define

$$iG(t_1, \boldsymbol{x}_1; t_2, \boldsymbol{x}_2) = \langle T \left[\psi(t_1, \boldsymbol{x}_1) \bar{\psi}(t_2, \boldsymbol{x}_2) \right] \rangle, \qquad (10.1)$$

where the symbol $\langle \ldots \rangle$ denotes an expectation value with respect to the arbitrary initial state. The latter is specified at $t = t_0$ by the density operator $\hat{\rho}$, *i.e.*, we have $\langle \ldots \rangle = \text{tr} \, (\hat{\rho} \ldots)/\text{tr} \, (\hat{\rho})$.

The field operators appearing in (10.1) are in the Heisenberg picture. In the situation when the perturbation expansion is appropriate, the following representation is frequently used

$$O_H(t) = U(t_0, t) \, O_I(t) \, U(t, t_0), \qquad (10.2)$$

where $O_H(t)$ and $O_I(t)$ are the operators in the Heisenberg and interaction pictures, respectively. The quantity $U(t, t_0)$ is the evolution operator. For $t > t_0$ we have

$$U(t, t_0) = \sum_{n=0}^{\infty} \frac{(-i)^n}{n!} T \left[\int_{t_0}^{t} dt_1 \ldots \int_{t_0}^{t} dt_n H_I^1(t_1) \ldots H_I^1(t_n) \right]$$

$$= T \left[\exp \left(-i \int_{t_0}^{t} dt' H_I^1(t') \right) \right] \qquad (10.3)$$

and

$$U(t_0, t) = \tilde{T} \left[\exp \left(-i \int_{t}^{t_0} dt' H_I^1(t') \right) \right], \qquad (10.4)$$

where $H_I^1(t)$ is the interaction Hamiltonian in the interaction picture, and T $(\tilde{T})$ is the chronological-ordering (antichronological-ordering) operator.

Let us now consider the expectation value of the operator $O_H(t)$ in the ground state of an interacting many-body system, denoted later by $|0\rangle$. Using a group property of the evolution operators U as well as the Gell-Mann theorem [41] we find

$$\langle 0 \, | \, O_H(t) \, | \, 0 \rangle = \frac{\langle \Phi \, | \, T \left[\exp \left(-i \int\limits_{-\infty}^{\infty} dt' H_I^1(t') \right) O_I(t) \right] | \, \Phi \rangle}{\langle \Phi \, | \, T \left[\exp \left(-i \int\limits_{-\infty}^{\infty} dt' H_I^1(t') \right) \right] | \, \Phi \rangle}, \qquad (10.5)$$

where $|\Phi\rangle$ is the ground state of the noninteracting system. Eq. (10.5) can be generalized to the case of the Green's functions, namely, we can write

$$iG(t_1, \boldsymbol{x}_1; t_2, \boldsymbol{x}_2) = \Big\langle\, 0 \,\Big|\, T\Big[\psi(t_1, \boldsymbol{x}_1)\bar{\psi}(t_2, \boldsymbol{x}_2)\Big]\,\Big|0\,\Big\rangle$$

$$= \frac{\Big\langle \Phi \,\Big|\, T\Big[\exp\Big(-i\int\limits_{-\infty}^{\infty} dt'H_I^1(t')\Big)\psi_I(t_1, \boldsymbol{x}_1)\bar{\psi}_I(t_2, \boldsymbol{x}_2)\Big]\Big| \Phi \Big\rangle}{\Big\langle \Phi \,\Big|\, T\Big[\exp\Big(-i\int\limits_{-\infty}^{\infty} dt'H_I^1(t')\Big)\Big]\Big| \Phi \Big\rangle}. \quad (10.6)$$

Application of the Wick theorem to (10.6) leads to the usual Feynman rules. In particular, the denominator cancels the disconnected diagrams appearing in the numerator.

The method described above cannot be applied to the average in an arbitrary state. The reason is that such a state, in general, cannot be simply expressed in terms of the ground state of the noninteracting particles. Nevertheless, substituting (10.3) and (10.4) into (10.2) we obtain expression

$$\langle O_H(t) \rangle = \langle U(t_0, t)O_I(t)U(t, t_0) \rangle$$

$$= \Big\langle \tilde{T}\Big[\exp\Big(-i\int\limits_{t}^{t_0} dt'H_I^1(t')\Big)\Big]O_I(t)T\Big[\exp\Big(-i\int\limits_{t_0}^{t} dt'H_I^1(t')\Big)\Big]\Big\rangle. \quad (10.7)$$

which can be put into a form analogous to Eq. (10.5). This can be achieved by introduction of an integral contour $\mathcal{K}$ running along the time axis and the associated operator $T_{\mathcal{K}}$ ordering along this contour, see Fig. 10.1. Using this procedure Eq. (10.7) can be rewritten as follows

$$\langle O_H(t) \rangle = \Big\langle T_{\mathcal{K}}\Big[\exp\Big(-i\int\limits_{\mathcal{K}} dt'H_I^1(t')\Big)O_I(t)\Big]\Big\rangle. \quad (10.8)$$
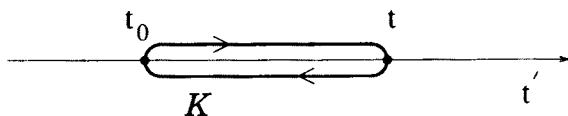

Fig. 10.1. Contour $\mathcal{K}$ used to calculate the operator expectation value $O_H(t)$.

Generalizing the last result, we introduce the Green's function on the contour

$$iG_{\mathcal{K}}(t_1, \boldsymbol{x}_1; t_2, \boldsymbol{x}_2) = \langle T_{\mathcal{K}}\left[\psi(t_1, \boldsymbol{x}_1)\bar{\psi}(t_2, \boldsymbol{x}_2)\right]\rangle, \quad (10.9)$$

which has the following representation

$$iG_\kappa(t_1, \boldsymbol{x}_1; t_2, \boldsymbol{x}_2) = \left\langle T_\kappa \left[\exp\left(-i \int_\kappa dt' H_I^1(t') \right) \psi_I(t_1, \boldsymbol{x}_1) \bar{\psi}_I(t_2, \boldsymbol{x}_2) \right] \right\rangle.$$
(10.10)

Here the contour runs from t_0 to the largest argument of the Green's function and then goes back to t_0. The formal resemblance to (10.6) is recovered since the disconnected diagrams vanish

$$1 = \left\langle T_\kappa \left[\exp\left(-i \int_\kappa dt' H_I^1(t') \right) \right] \right\rangle.$$
(10.11)

Assuming that the initial state allows for the Wick decomposition, $G_\kappa(t_1, \boldsymbol{x}_1; t_2, \boldsymbol{x}_2)$ can be calculated using the standard technique for Feynman diagrams.

Very often it is convenient to divide the contour into the two branches — the upper one (stretching from smaller to larger values of t) and the lower one (stretching from larger to smaller values of t). According to the time ordering T_κ, the time arguments along the upper branch are regarded as earlier than those situated along the lower branch. Depending on the position of its time arguments the contour Green's function fits to one of the following categories:

$$iG_\kappa(t_1^-, \boldsymbol{x}_1; t_2^-, \boldsymbol{x}_2) = iG(t_1, \boldsymbol{x}_1; t_2, \boldsymbol{x}_2),$$
(10.12)

$$iG_\kappa(t_1^-, \boldsymbol{x}_1; t_2^+, \boldsymbol{x}_2) = iG^<(t_1, \boldsymbol{x}_1; t_2, \boldsymbol{x}_2) = -\langle \bar{\psi}(t_2, \boldsymbol{x}_2)\psi(t_1, \boldsymbol{x}_1) \rangle,$$
(10.13)

$$iG_\kappa(t_1^+, \boldsymbol{x}_1; t_2^-, \boldsymbol{x}_2) = iG^>(t_1, \boldsymbol{x}_1; t_2, \boldsymbol{x}_2) = \langle \psi(t_1, \boldsymbol{x}_1)\bar{\psi}(t_2, \boldsymbol{x}_2) \rangle,$$
(10.14)

$$iG_\kappa(t_1^+, \boldsymbol{x}_1; t_2^+, \boldsymbol{x}_2) = i\tilde{G}(t_1, \boldsymbol{x}_1; t_2, \boldsymbol{x}_2).$$
(10.15)

The Green's function $G_\kappa(t_1^-, \boldsymbol{x}_1; t_2^-, \boldsymbol{x}_2)$ is the usual causal (Feynman) function. On the other hand, $G_\kappa(t_1^+, \boldsymbol{x}_1; t_2^+, \boldsymbol{x}_2)$ is anti-causal. In addition, there are two extra functions: $G_\kappa(t_1^+, \boldsymbol{x}_1; t_2^-, \boldsymbol{x}_2)$ and $G_\kappa(t_1^+, \boldsymbol{x}_1; t_2^-, \boldsymbol{x}_2)$. Nevertheless, one can check that only two out of these four functions are independent.

The fact that at least two independent functions are required for description of non-equilibrium situations has a simple physical interpretation: besides the Green's function describing the spectrum of the excitations in a medium, we need another function describing the evolution of the medium
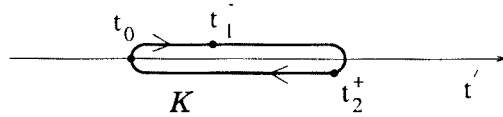
Fig. 10.2 The second time argument of the function $G^<(t_1, \boldsymbol{x}_1; t_2, \boldsymbol{x}_2)$ is later than the first one. Thus, the time ordering along the contour always changes the initial ordering of the field operators (in addition there is a change in sign for fermionic operators).

itself. In the classical limit such evolution is described by the kinetic equation fulfilled by the phase-space distribution functions. In the next Chapter we shall study how the information contained in $G^<(t_1, \boldsymbol{x}_1; t_2, \boldsymbol{x}_2)$ allows us to derive the transport equation for the quark distribution function.

11. Mean-field transport theory

In this Chapter, we shall study how the concept of chiral symmetry can be *explicitly* included into the quantum and classical transport theory based on the NJL Lagrangian. In our investigations, we shall restrict ourselves to the mean-field approximation, since the interesting phenomena (like, *e.g.*, spontaneous symmetry breaking) already take place at this level. Our approach is based on the spinor decomposition of the Wigner function and follows the treatment of [68] and [69]. However, in contrast to [68] we do not neglect the spin degrees of freedom and take into account all the components of the spinor decomposition. On the other hand, we differ from [69], where the spin dynamics is fully discussed, in that we study a system that is governed by a different type of interaction.

A transport theory for the NJL model has been initially formulated by Zhang and Wilets [19], where the closed-time-path formalism (introduced in Chapter 10) combined with the effective-action method has been used to derive the kinetic equations. However, Ref. [19] does not discuss how the symmetry of the underlying theory (*i.e.*, the chiral symmetry of the NJL Lagrangian) should reflect itself in the transport equations. Trying to clarify this point, we derive the general form of the transport equations (in the mean-field approximation) which are chirally invariant. We discuss the properties of these equations and then study their classical limit by performing an expansion in $\hbar$ for all the functions appearing in the spinor decomposition. Throughout our approach, we investigate and check the consistency of our equations under the assumptions of chiral symmetry. In particular, this implies that the axial current should always be conserved. For the spin evolution equation, as will be seen, this turns out to be a non-trivial requirement.

11.1. Wigner function and its spinor decomposition

In general, for a non-equilibrium transport theory, one requires two independent Green's functions to describe the system. However, it turns out that in the mean-field approximation (which neglects the collisions between the particles) only one function is sufficient. We thus choose the Green's function

$$G^<_{\alpha\beta}(x, y) = \langle \bar\psi_\beta(y)\psi_\alpha(x)\rangle \tag{11.1}$$

to be the fundamental quantity in our description (for sake of simplicity we disregard here the imaginary unit appearing in the "canonical" definition (10.13)).

In the following we shall restrict our considerations to the one-flavour model defined in Section 3.1. Moreover, we shall work in the strict chiral limit setting $m = 0$. Only in the end of this Chapter (Section 11.7) the case $m \neq 0$ will be taken into consideration. One can easily notice that the Green's function (11.1) satisfies the same equation as the field $\psi(x)$ does (compare Eq. (3.21))

$$[i\,\partial\!\!\!/ - \sigma(x) - i\gamma_5\pi(x)]G^<(x, y) = 0. \tag{11.2}$$

The mean fields $\sigma(x)$ and $\pi(x)$ are determined by the Green's function $G^<(x, y)$ through the relations

$$\sigma(x) = -2G\,\mathrm{Sp}\,G^<(x, x), \quad \pi(x) = -2G\,\mathrm{Sp}\,i\gamma_5 G^<(x, x), \tag{11.3}$$

where the trace Sp is taken over the spinor indices.

For the description of non-uniform systems, it is convenient to introduce Wigner transforms. This allows one to make an easier physical interpretation of the components of the Green's function and facilitates performing the classical limit. In the case of the Green's function $G^<(x, y)$, its Wigner transform is obtained by introducing the center-of-mass coordinate $X = (x + y)/2$, the relative coordinate $u = x - y$, and by taking the Fourier transform with respect to u. Following the notation of [70], we define

$$W_{\alpha\beta}(X, p) = \frac{1}{\hbar^4}\int d^4u\,\mathrm{e}^{\frac{i}{\hbar}p\cdot u}\,G^<_{\alpha\beta}\left(X + \frac{u}{2}, X - \frac{u}{2}\right). \tag{11.4}$$

In Eq. (11.4) we have explicitly incorporated the Planck constant $\hbar$, since later on we wish to investigate the classical approximation.

The Wigner transforms of the derivative of a two-point function, $\partial f(x, y)/\partial x^\mu$, and of the product of a one-point function with the two-point

one, $f(x)g(x,y)$, are given by the expressions

$$\frac{\partial f(x,y)}{\partial x^\mu} \rightarrow (-ip^\mu + \frac{\hbar}{2}\partial^\mu)f(X,p), \tag{11.5}$$

$$f(x)g(x,y) \rightarrow f(X)g(X,p) - \frac{i\hbar}{2}\partial_\mu f(X)\partial_p^\mu g(X,p), \tag{11.6}$$

with the notation $\partial_\mu = \partial/\partial X^\mu, \partial_p^\mu = \partial/\partial p_\mu$, and where in the second relation (11.6), only the derivatives of first order in ∂_p and ∂_X are kept. This approximation is appropriate only for the systems which are weakly inhomogeneous (see the discussion of this point in [70]).

Using Eq. (11.2) and the properties of the Wigner transform (11.5) and (11.6), we arrive at the following equation for the Wigner function

$$\left[\left(p^\mu + \frac{i\hbar}{2}\partial^\mu\right)\gamma_\mu - \sigma(X) + \frac{i\hbar}{2}\partial_\mu\sigma(X)\partial_p^\mu\right.$$
$$\left. - i\gamma_5\pi(X) - \frac{\hbar}{2}\gamma_5\partial_\mu\pi(X)\partial_p^\mu\right]W(X,p) = 0. \tag{11.7}$$

Eq. (11.7) together with Eqs (11.3) and (11.4) form the system of the coupled equations that we are going to study in detail in this Chapter. We note that there is no collision term in Eq. (11.7). This is a consequence of our mean-field approximation. We observe that under the chiral transformation (3.24), the Wigner function changes according to the prescription

$$W \rightarrow W' = \exp\left(-i\gamma_5\frac{\chi}{2}\right) W \exp\left(-i\gamma_5\frac{\chi}{2}\right). \tag{11.8}$$

Hence, one can check that Eq. (11.7) is invariant under transformations (3.25), (3.26) and (11.8) and thus that the first order in the derivative expansion of the Green's function is symmetry preserving.

The Wigner function $W_{\alpha\beta}(X,p)$ is a 4 by 4 matrix in spinor indices and can be expanded in terms of 16 independent generators of the Clifford algebra. The conventional basis consists of $1, i\gamma_5, \gamma^\mu, \gamma^\mu\gamma_5$, and $\frac{1}{2}\sigma^{\mu\nu}$ which we denote in what follows by Γ_i. In this basis, the Wigner function has the form

$$W = \mathcal{F} + i\gamma_5\mathcal{P} + \gamma^\mu\mathcal{V}_\mu + \gamma^\mu\gamma_5\mathcal{A}_\mu + \frac{1}{2}\sigma^{\mu\nu}\mathcal{S}_{\mu\nu}. \tag{11.9}$$

The properties $\gamma^0 W^\dagger \gamma^0 = W$ and $\gamma^0 \Gamma_i^\dagger \gamma^0 = \Gamma_i$ (the first one results from (11.4), whereas the second one is a simple consequence of the definition of Γ_i) indicate that the coefficients in the spinor decomposition $\mathcal{F}(X,p)$, $\mathcal{P}(X,p)$, $\mathcal{V}_\mu(X,p)$, $\mathcal{A}_\mu(X,p)$ and $\mathcal{S}_{\mu\nu}(X,p)$ are real functions. We note that the spinor decomposition technique has been already used in the formulation of the

transport theory for QED [69,71,72] and for QHD (so-called quantum hadro-dynamics) [68].

The vector and axial currents, see Eqs (3.6) and (3.3), are related to the functions $\mathcal{V}^\mu(X,p)$ and $\mathcal{A}^\mu(X,p)$ by the simple relations

$$V^\mu(X) = 4 \int \frac{d^4p}{(2\pi)^4} \mathcal{V}^\mu(X,p) \qquad (11.10)$$

and

$$A^\mu(X) = -4 \int \frac{d^4p}{(2\pi)^4} \mathcal{A}^\mu(X,p). \qquad (11.11)$$

Therefore $\mathcal{V}^\mu(X,p)$ and $\mathcal{A}^\mu(X,p)$ can be interpreted as the momentum densities of these two currents. For the physical interpretation of the other components we refer the reader to Refs [69,71]. Under the chiral transformation (11.8) the coefficients of the spinor decomposition (11.9) change as follows

$$
\begin{aligned}
\mathcal{F} &\to \mathcal{F}' = \mathcal{F}\cos\chi + \mathcal{P}\sin\chi, \\
\mathcal{P} &\to \mathcal{P}' = -\mathcal{F}\sin\chi + \mathcal{P}\cos\chi, \\
\mathcal{V}_\mu &\to \mathcal{V}'_\mu = \mathcal{V}_\mu, \\
\mathcal{A}_\mu &\to \mathcal{A}'_\mu = \mathcal{A}_\mu, \\
\mathcal{S}_{\mu\nu} &\to \mathcal{S}'_{\mu\nu} = \mathcal{S}_{\mu\nu}\cos\chi + \tilde{\mathcal{S}}_{\mu\nu}\sin\chi, \\
\tilde{\mathcal{S}}_{\mu\nu} &\to \tilde{\mathcal{S}}'_{\mu\nu} = -\mathcal{S}_{\mu\nu}\sin\chi + \tilde{\mathcal{S}}_{\mu\nu}\cos\chi,
\end{aligned}
\qquad (11.12)
$$

where $\tilde{\mathcal{S}}^{\mu\nu}$ is the dual tensor to $\mathcal{S}^{\mu\nu}$, namely

$$\tilde{\mathcal{S}}^{\mu\nu} = \tfrac{1}{2}\varepsilon^{\mu\nu\alpha\beta}\mathcal{S}_{\alpha\beta}. \qquad (11.13)$$

11.2. Kinetic equations

Substituting expression (11.9) into Eq. (11.7) gives the following system of the coupled equations for the coefficients of the decomposition (11.9)

$$K^\mu \mathcal{V}_\mu - \sigma\mathcal{F} + \pi\mathcal{P} = -\frac{i\hbar}{2}\left(\partial_\nu\sigma\partial_p^\nu\mathcal{F} - \partial_\nu\pi\partial_p^\nu\mathcal{P}\right), \qquad (11.14)$$

$$-iK^\mu\mathcal{A}_\mu - \sigma\mathcal{P} - \pi\mathcal{F} = -\frac{i\hbar}{2}\left(\partial_\nu\sigma\partial_p^\nu\mathcal{P} + \partial_\nu\pi\partial_p^\nu\mathcal{F}\right), \qquad (11.15)$$

$$K_\mu\mathcal{F} + iK^\nu\mathcal{S}_{\nu\mu} - \sigma\mathcal{V}_\mu + i\pi\mathcal{A}_\mu = -\frac{i\hbar}{2}\left(\partial_\nu\sigma\partial_p^\nu\mathcal{V}_\mu - i\partial_\nu\pi\partial_p^\nu\mathcal{A}_\mu\right), \qquad (11.16)$$

$$iK^\mu\mathcal{P} - K_\nu\tilde{\mathcal{S}}^{\nu\mu} - \sigma\mathcal{A}^\mu + i\pi\mathcal{V}^\mu = -\frac{i\hbar}{2}\left(\partial_\nu\sigma\partial_p^\nu\mathcal{A}^\mu - i\partial_\nu\pi\partial_p^\nu\mathcal{V}^\mu\right), \qquad (11.17)$$

$$i(K^\mu\mathcal{V}^\nu - K^\nu\mathcal{V}^\mu) - \varepsilon^{\mu\nu\alpha\beta}K_\alpha\mathcal{A}_\beta - \pi\tilde{\mathcal{S}}^{\mu\nu} + \sigma\mathcal{S}^{\mu\nu}$$
$$= \frac{i\hbar}{2}(\partial_\gamma\sigma\partial_p^\gamma\mathcal{S}^{\mu\nu} - \partial_\gamma\pi\partial_p^\gamma\tilde{\mathcal{S}}^{\mu\nu}). \qquad (11.18)$$

In abbreviation we have introduced here the notation $K^\mu = p^\mu + \frac{i\hbar}{2}\partial^\mu$. Eqs (11.14)–(11.18) should be supplemented by the formulae that determine the mean fields. They follow from (11.3) and have the form

$$\sigma(X) = -2G \int \frac{d^4p}{(2\pi)^4} \text{ Sp } W(X,p) = -8G \int \frac{d^4p}{(2\pi)^4} \mathcal{F}(X,p) \qquad (11.19)$$

and

$$\pi(X) = -2G \int \frac{d^4p}{(2\pi)^4} \text{ Sp } i\gamma_5 W(X,p) = 8G \int \frac{d^4p}{(2\pi)^4} \mathcal{P}(X,p). \qquad (11.20)$$

Using the transformation properties (3.25), (3.26) and (11.12) we can check that this system of equations is chirally invariant. Strictly speaking, each of Eqs (11.14), (11.15) and (11.18) is separately a chirally invariant equation. On the other hand, Eqs (11.16) and (11.17), after a chiral transformation, form linear combinations of each other. These combinations imply, however, that each of their components must vanish separately. In consequence, we can treat *the system of the two* equations (11.16) and (11.17) as a chirally invariant expression. In the analogous way, one can check that the system of Eqs (11.19) and (11.20) is chirally invariant.

For further analysis, it is convenient to discuss separately the real and imaginary parts of Eqs (11.14)–(11.18). The real parts give

$$p^\mu \mathcal{V}_\mu - \sigma\mathcal{F} + \pi\mathcal{P} = 0, \qquad (11.21)$$

$$\frac{\hbar}{2}\partial_\mu\mathcal{A}^\mu - \sigma\mathcal{P} - \pi\mathcal{F} = 0, \qquad (11.22)$$

$$p_\mu\mathcal{F} - \frac{\hbar}{2}\partial^\nu\mathcal{S}_{\nu\mu} - \sigma\mathcal{V}_\mu = -\frac{\hbar}{2}\partial_\nu\pi\partial_p^\nu\mathcal{A}_\mu, \quad (11.23)$$

$$-\frac{\hbar}{2}\partial^\mu\mathcal{P} - p_\nu\tilde{\mathcal{S}}^{\nu\mu} - \sigma\mathcal{A}^\mu = -\frac{\hbar}{2}\partial_\nu\pi\partial_p^\nu\mathcal{V}^\mu, \quad (11.24)$$

$$-\frac{\hbar}{2}\left(\partial^\mu\mathcal{V}^\nu - \partial^\nu\mathcal{V}^\mu\right) - \varepsilon^{\mu\nu\alpha\beta}p_\alpha\mathcal{A}_\beta + \sigma\mathcal{S}^{\mu\nu} - \pi\tilde{\mathcal{S}}^{\mu\nu} = 0. \qquad (11.25)$$

One can notice that integrating of Eq. (11.22) over the momentum gives

$$\hbar \int \frac{d^4p}{(2\pi)^4}\partial_\mu\mathcal{A}^\mu(X,p) = 0, \qquad (11.26)$$

where the definitions (11.19) and (11.20) have been used. This equation is nothing other than the statement that the axial current should be conserved (3.3). We thus see that after making the gradient expansion, this conservation law is still included in the transport equations. The imaginary parts of

Eqs (11.14)–(11.18) yield

$$\frac{\hbar}{2}\partial^\mu\mathcal{V}_\mu = -\frac{\hbar}{2}\left(\partial_\nu\sigma\partial_p^\nu\mathcal{F} - \partial_\nu\pi\partial_p^\nu\mathcal{P}\right), \quad (11.27)$$

$$p^\mu\mathcal{A}_\mu = \frac{\hbar}{2}\left(\partial_\nu\sigma\partial_p^\nu\mathcal{P} + \partial_\nu\pi\partial_p^\nu\mathcal{F}\right), \quad (11.28)$$

$$\frac{\hbar}{2}\partial_\mu\mathcal{F} + p^\nu\mathcal{S}_{\nu\mu} + \pi\mathcal{A}_\mu = -\frac{\hbar}{2}\partial_\nu\sigma\partial_p^\nu\mathcal{V}_\mu, \quad (11.29)$$

$$p^\mu\mathcal{P} - \frac{\hbar}{2}\partial_\nu\tilde{\mathcal{S}}^{\nu\mu} + \pi\mathcal{V}^\mu = -\frac{\hbar}{2}\partial_\nu\sigma\partial_p^\nu\mathcal{A}^\mu, \quad (11.30)$$

$$(p^\mu\mathcal{V}^\nu - p^\nu\mathcal{V}^\mu) - \frac{\hbar}{2}\varepsilon^{\mu\nu\alpha\beta}\partial_\alpha\mathcal{A}_\beta = \frac{\hbar}{2}\left(\partial_\gamma\sigma\partial_p^\gamma\mathcal{S}^{\mu\nu} - \partial_\gamma\pi\partial_p^\gamma\tilde{\mathcal{S}}^{\mu\nu}\right). \quad (11.31)$$

Although we have neglected the higher order gradients, Eqs (11.21)–(11.31) are still quantum kinetic equations. In order to obtain the classical equations one makes an expansion of $\mathcal{F}$ in powers of $\hbar$

$$\mathcal{F} = \mathcal{F}_{(0)} + \hbar\mathcal{F}_{(1)} + \hbar^2\mathcal{F}_{(2)} + \dots, \quad (11.32)$$

and similarly of $\mathcal{P}, \mathcal{V}^\mu, \mathcal{A}^\mu, \mathcal{S}^{\mu\nu}, \pi$ and σ. Expansions of the form (11.32) are inserted into Eqs (11.21)–(11.31) and the expressions at the appropriate powers of $\hbar$ are compared. The detailed description of this procedure will be the subject of the next Sections.

11.3. Constraint equations in the leading order of $\hbar$

Substituting expansions of the type (11.32) into Eqs (11.21)–(11.25), we find to leading (zeroth) order of $\hbar$

$$p^\mu\mathcal{V}_\mu^{(0)} - \sigma_{(0)}\mathcal{F}_{(0)} + \pi_{(0)}\mathcal{P}_{(0)} = 0, \quad (11.33)$$

$$\sigma_{(0)}\mathcal{P}_{(0)} + \pi_{(0)}\mathcal{F}_{(0)} = 0, \quad (11.34)$$

$$p^\mu\mathcal{F}_{(0)} - \sigma_{(0)}\mathcal{V}_{(0)}^\mu = 0, \quad (11.35)$$

$$\tilde{\mathcal{S}}_{(0)}^{\mu\nu}p_\nu - \sigma_{(0)}\mathcal{A}_{(0)}^\mu = 0, \quad (11.36)$$

$$-\varepsilon^{\mu\nu\alpha\beta}p_\alpha\mathcal{A}_\beta^{(0)} + \sigma_{(0)}\mathcal{S}_{(0)}^{\mu\nu} - \pi_{(0)}\tilde{\mathcal{S}}_{(0)}^{\mu\nu} = 0. \quad (11.37)$$

Correspondingly, the zeroth order of Eqs (11.27)–(11.31) has the form

$$p^\mu\mathcal{A}_\mu^{(0)} = 0, \quad (11.38)$$

$$p^\nu\mathcal{S}_{\nu\mu}^{(0)} + \pi^{(0)}\mathcal{A}_\mu^{(0)} = 0, \quad (11.39)$$

$$p^\mu\mathcal{P}^{(0)} + \pi^{(0)}\mathcal{V}_{(0)}^\mu = 0, \quad (11.40)$$

$$p^\mu\mathcal{V}_{(0)}^\nu - p^\nu\mathcal{V}_{(0)}^\mu = 0. \quad (11.41)$$

These are only four equations, since Eq. (11.27) is already of first order in $\hbar$. From Eqs (11.34) and (11.35) one finds

$$\mathcal{P}_{(0)} = -\pi_{(0)} \frac{\mathcal{F}_{(0)}}{\sigma_{(0)}} \tag{11.42}$$

and

$$\mathcal{V}_{(0)}^{\mu} = p^{\mu} \frac{\mathcal{F}_{(0)}}{\sigma_{(0)}}. \tag{11.43}$$

Then Eqs (11.40) and (11.41) are automatically fulfilled. Moreover, Eqs (11.33)–(11.35) lead to the mass-shell constraint for the function $\mathcal{F}_{(0)}(X, p)$, namely

$$[p^2 - M^2(X)]\mathcal{F}_{(0)}(X, p) = 0, \quad M^2(X) = \sigma_{(0)}^2(X) + \pi_{(0)}^2(X). \tag{11.44}$$

From Eq. (11.37), we find the following expression for the spin tensor

$$\mathcal{S}_{(0)}^{\mu\nu} = -\frac{\pi_{(0)}}{M^2}\left[p^{\mu}\mathcal{A}_{(0)}^{\nu} - p^{\nu}\mathcal{A}_{(0)}^{\mu}\right] + \frac{\sigma_{(0)}}{M^2}\varepsilon^{\mu\nu\alpha\beta}p_{\alpha}\mathcal{A}_{\beta}^{(0)}, \tag{11.45}$$

and the dual spin tensor

$$\tilde{\mathcal{S}}_{(0)}^{\mu\nu} = -\frac{\sigma_{(0)}}{M^2}\left[p^{\mu}\mathcal{A}_{(0)}^{\nu} - p^{\nu}\mathcal{A}_{(0)}^{\mu}\right] - \frac{\pi_{(0)}}{M^2}\varepsilon^{\mu\nu\alpha\beta}p_{\alpha}\mathcal{A}_{\beta}^{(0)}. \tag{11.46}$$

Substituting now Eq. (11.46) into Eq. (11.36), and using (11.38) one obtains a mass-shell constraint for $\mathcal{A}_{(0)}^{\mu}(X, p)$ also, $i.e.,$

$$[p^2 - M^2(X)]\mathcal{A}_{(0)}^{\nu}(X, p) = 0. \tag{11.47}$$

Finally, using (11.45), (11.38) and (11.47) we find that (11.39) is satisfied. In summary, Eqs (11.33)–(11.41) lead to the expressions for $\mathcal{P}_{(0)}$ and $\mathcal{V}_{(0)}^{\mu}$ in terms of $\mathcal{F}_{(0)}$, and for $\mathcal{S}_{(0)}^{\mu\nu}$ and $\tilde{\mathcal{S}}_{(0)}^{\mu\nu}$ in terms of $\mathcal{A}_{(0)}^{\mu}$. Furthermore, they lead to the two mass-shell constraints.

The mean fields appearing in Eqs (11.33)–(11.37), (11.39) and (11.40) are required to be calculated in a self-consistent way from Eqs (11.19) and (11.20). Doing so, we find

$$\sigma_{(0)}(X) = -8G \int \frac{d^4p}{(2\pi)^4}\mathcal{F}_{(0)}(X, p), \tag{11.48}$$

$$\pi_{(0)}(X) = 8G \int \frac{d^4p}{(2\pi)^4}\mathcal{P}_{(0)}(X, p). \tag{11.49}$$

Due to the relation (11.34), one finds that these two equations are not independent and can be reduced to a single equation which determines the *invariant* mass $M(X)$. To see this relation more clearly, let us define the distribution function $F(X, p)$ via the expression

$$F(X, p) = \frac{\mathcal{F}_{(0)}(X, p)}{\sigma_{(0)}(X)} = -\frac{\mathcal{P}_{(0)}(X, p)}{\pi_{(0)}(X)} \tag{11.50}$$

and the angle $\Phi(X)$ via the relations

$$\pi_{(0)} = M(X) \sin \Phi(X), \quad \sigma_{(0)} = M(X) \cos \Phi(X). \tag{11.51}$$

$F(X, p)$ is a chirally invariant quantity, and knowledge of it determines the value of $M(X)$. In addition, it allows us to calculate the vector current density $\mathcal{V}^{\mu}_{(0)}$. However, Eqs (11.48) and (11.49) do not determine separately the fields $\pi_{(0)}$ and $\sigma_{(0)}$, *i.e.*, the angle $\Phi(X)$. This fact is in agreement with the requirements of the chiral symmetry of the problem: under the chiral transformations $\Phi(X) \to \Phi'(X) = \Phi(X) + \chi$ and, consequently, the absolute value of $\Phi(X)$ has no physical significance.

With this result, we conclude the discussion of the expressions obtained to zeroth order in $\hbar$. The derived equations all display the chirally invariant form. Let us turn now to the discussion of the equations which follow from Eqs (11.27)–(11.31), considered to first order in $\hbar$.

11.4. Kinetic equation for the quark distribution functions

Employing Eqs (11.42) and (11.43) in Eq. (11.27), one immediately finds

$$p^{\mu} \partial_{\mu} F(X, p) + M(X) \partial_{\mu} M(X) \partial_p^{\mu} F(X, p) = 0, \tag{11.52}$$

where we have used the definition (11.50). This is again a chirally invariant equation. Due to the mass-shell condition (11.44), we can express $F(X, p)$ as the sum of the quark and antiquark distribution functions $f^+(X, \boldsymbol{p})$ and $f^-(X, \boldsymbol{p})$ defined by

$$F(X, p) = 2\pi \left\{ \frac{\delta(p^0 - E_p(X))}{2E_p(X)} f^+(X, \boldsymbol{p}) + \frac{\delta(p^0 + E_p(X))}{2E_p(X)} \left[f^-(X, -\boldsymbol{p}) - 1 \right] \right\}. \tag{11.53}$$

Here $E_p(X) = \sqrt{\boldsymbol{p}^2 + M^2(X)}$, and $\boldsymbol{p}$ is a three-momentum. Substituting expression (11.53) into Eq. (11.52), and integrating over p^0 gives

$$p^{\mu} \partial_{\mu} f^{\pm}(X, \boldsymbol{p}) + M(X) \partial_{\mu} M(X) \partial_p^{\mu} f^{\pm}(X, \boldsymbol{p}) = 0. \tag{11.54}$$

Since the last procedure involves non-trivial cancellations let us discuss it in more detail. Eq. (11.52) can be shortly written as $\hat{L}F(X, p) = 0$, where $\hat{L}$ is a linear differential operator, *i.e.*, $\hat{L} = p^\mu \partial_\mu + M\partial_\mu M \partial_p^\mu$. After some algebra, we find that

$$\hat{L}E_p(X) = \frac{(p^0 M \partial_0 M)}{E_p(X)}$$

and

$$\hat{L}\delta(p^0 \mp E_p(X)) = M\partial_0 M\delta'(p^0 \mp E_p(X))\left[1 \mp \frac{p^0}{E_p(X)}\right],$$

where the prime denotes the derivative with respect to p^0. Since $\hat{L}$ is a linear operator, one also gets

$$\hat{L}\left\{\left[\delta(p^0 \mp \frac{E_p(X)}{E_p(X)})\right]f^\pm(X, \pm\boldsymbol{p})\right\} = \hat{L}\left[\frac{\delta(p^0 \mp E_p(X))}{E_p(X)}\right]f^\pm(X, \pm\boldsymbol{p})$$

$$+ \left[\frac{\delta(p^0 \mp E_p(X))}{E_p(X)}\right]\hat{L}f^\pm(X, \pm\boldsymbol{p}).$$

Of course, if $\hat{L}$ acts on $f^\pm(X, \pm\boldsymbol{p})$ its energy component ∂_p^0 produces zero. Now using our previous results we can check that

$$\int_{\Delta_\pm} dp^0 \hat{L}\left[\delta(p^0 \mp E_p(X))/E_p(X)\right] = 0,$$

where $\Delta_\pm$ is an interval containing either $E_p(X)$ or $-E_p(X)$. Consequently, integrating the whole formula (11.52) over $\Delta_\pm$, one gets the desired equation (11.54). We note that in the case of antiquarks still the replacement $\boldsymbol{p} \to -\boldsymbol{p}$ should be made.

Eq. (11.54) displays a typical form for fermion mean-field theories. In our case, however, a characteristic feature of this equation is the appearance of the chirally invariant mass $M(X)$. We emphasize that the four-momentum p^μ occurring in (11.54) is to be taken on the mass shell, *i.e.*, in this case $p^0 = E_p(X)$. At the same time the distribution functions $f^\pm$ are functions of the space-time coordinate X and the three-momentum $\boldsymbol{p}$, with the derivative with respect to the energy defined to be zero.

Using Eqs (11.48), (11.50) and (11.53) we find that the NJL gap equation takes the form

$$\sigma_{(0)}(X) = \sigma_{(0)}(X)\, 4G \int \frac{d^3p}{(2\pi)^3}\frac{1}{E_p(X)}\left[1 - f^+(X, \boldsymbol{p}) - f^-(X, \boldsymbol{p})\right],$$

(11.55)

which determines the mass $M(X)$ appearing in $E_p(X)$ in terms of the distribution functions $f^\pm(X, \boldsymbol{p})$. One can easily notice that using Eq. (11.49) instead of (11.48) we would obtain the same equation as (11.55), with the appearance of $\pi_{(0)}$ instead of $\sigma_{(0)}$. *We note that Eq. (11.55) is the generalization of formulae (5.16) and (5.17) to the case of non-equilibrium quark distribution functions.*

Using now Eqs (11.10) and (11.53), we find the following expression for the baryon current

$$V^\mu(X) = 2 \int \frac{d^3p}{(2\pi)^3} \frac{p^\mu}{E_p(X)} \left[f^+(X, \boldsymbol{p}) - f^-(X, \boldsymbol{p}) + 1 \right], \qquad (11.56)$$

where p^μ is again on the mass shell, *i.e.*, $p^0 = E_p(X)$. The constant appearing at the end of the square bracket can be neglected, since it does not contribute to $\boldsymbol{V}(X)$, and for $V^0(X)$ it introduces a constant (although infinite) charge.

We note that Eqs (11.54) and (11.55) form a closed system of equations: the distribution functions $f^\pm(X, \boldsymbol{p})$ determine the invariant mass $M(X)$ through Eq. (11.55), whereas the space dependence of $M(X)$ determines in (11.54) the time evolution of $f^\pm(X, \boldsymbol{p})$. In the case $\pi_{(0)} = 0$ this system of equations was first derived by Zhang and Wilets [19], whose calculations were based on the closed-time-path formalism. Our approach represents an alternative derivation and generalizes their results to the case $\pi_{(0)} \neq 0$. The numerical solutions of Eqs (11.54) and (11.55), describing the expansion of quark matter possibly created in the ultra-relativistic heavy-ion collisions, were found in [21]. Another class of solutions of this system of equations will be discussed by us in the next Chapter.

11.5. Spin evolution

In the classical limit the spin dynamics is described by the behaviour of the function $\mathcal{A}^\mu_{(0)}(X, p)$ [69, 71]. In order to derive the kinetic equation for $\mathcal{A}^\mu_{(0)}(X, p)$, we use Eq. (11.30) and substitute into it the expression for $\mathcal{V}^\mu$ obtained from Eq. (11.23). Such a procedure gives, to the first order in $\hbar$, the following equation

$$p^\mu \partial_\nu \mathcal{A}^\nu_{(0)} - \sigma_{(0)} \partial_\nu \tilde{\mathcal{S}}^{\nu\mu}_{(0)} - \pi_{(0)} \partial_\nu \mathcal{S}^{\nu\mu}_{(0)} + M \partial_\nu M \partial^\nu_p \mathcal{A}^\mu_{(0)} = 0. \qquad (11.57)$$

Substituting the expression for the spin tensor (11.45) and the dual spin tensor (11.46) into Eq. (11.57) leads to the equation determining the space-

time evolution of $\mathcal{A}_{(0)}^{\mu}(X, p)$, namely

$$p^{\nu}\partial_{\nu}\mathcal{A}_{(0)}^{\mu} + M\partial_{\nu}M\partial_{p}^{\nu}\mathcal{A}_{(0)}^{\mu} + \frac{\partial_{\nu}M}{M}\left[p^{\mu}\mathcal{A}_{(0)}^{\nu} - p^{\nu}\mathcal{A}_{(0)}^{\mu}\right] - \varepsilon^{\mu\nu\alpha\beta}\partial_{\nu}\Phi p_{\alpha}\mathcal{A}_{\beta}^{(0)} = 0.$$
(11.58)

We note that Eq. (11.58) is again a chirally invariant equation, since both the mass $M(X)$ and the gradient of the angle $\Phi(X)$ are chirally invariant quantities. Due to the condition (11.38), only three out of four equations in (11.58) are independent. In fact, one can check that multiplication of (11.58) by p^{μ} gives zero.

The mass $M(X)$ appearing in (11.58) has to be calculated from the system of equations (11.54) and (11.55). Hence, it can be treated in (11.58) as an externally prescribed function. On the other hand, the gradient $\partial_{\mu}\Phi(X)$ is not known, and until we specify how to calculate it, Eq. (11.58) cannot be used to determine the time evolution of $\mathcal{A}_{(0)}^{\mu}(X, p)$. Moreover, one has to check whether the solutions of (11.58) satisfy the requirement of axial current conservation (3.3). The last two points will be discussed in more detail in the next Section, where we examine the consistency of our all equations up to the first order in $\hbar$.

In analogy to the QED calculations [69] we introduce the spin up and spin down phase-space densities

$$F_{\pm s}(X, p) = F(X, p) \pm S_{\mu}(X, p)\frac{\mathcal{A}_{(0)}^{\mu}(X, p)}{M(X)},$$
(11.59)

where $S_{\mu}(X, p)$ is defined by

$$S_{\mu}(X, p) = \frac{\mathcal{A}_{\mu}^{(0)}(X, p)}{\left[-\mathcal{A}_{\nu}^{(0)}(X, p)\mathcal{A}_{(0)}^{\nu}(X, p)\right]^{1/2}}.$$
(11.60)

Due to the condition (11.38), the four-vector $\mathcal{A}_{(0)}^{\mu}(X, p)$ is space-like, $\mathcal{A}_{(0)}^{\mu}(X, p)\mathcal{A}_{\mu}^{(0)}(X, p) < 0$, therefore $S_{\mu}(X, p)S^{\mu}(X, p) = -1$. The quantity $S^{\mu}(X, p)$ describes the mean spin orientation of the classical particles placed at the space-time point X and having the four-momentum p. On the other hand, the magnitude of $\mathcal{A}_{(0)}^{\mu}(X, p)$, through Eq. (11.59), determines how many spin up and spin down particles are present in the system. Using Eq. (11.58), we find

$$p^{\nu}\partial_{\nu}S^{\mu} + M\partial_{\nu}M\partial_{p}^{\nu}S^{\mu} + \frac{\partial_{\nu}M}{M}p^{\mu}S^{\nu} - \varepsilon^{\mu\nu\alpha\beta}\partial_{\nu}\Phi p_{\alpha}S_{\beta} = 0,$$
(11.61)

and consequently

$$p^\nu \partial_\nu F_{\pm s}(X, p) + M\partial_\nu M \partial_p^\nu F_{\pm s}(X, p) = 0. \tag{11.62}$$

Hence, similarly as in transport equations for QED [69], we find that the spin components decouple. Since both functions $F(X, p)$ and $\mathcal{A}_{(0)}^\mu(X, p)$ are the mass-shell, we can write the analogous decomposition as in (11.53), namely

$$F_{\pm s}(X, p) = 2\pi \left\{ \frac{\delta(p^0 - E_p(X))}{2E_p(X)} f_{\pm s}^+(X, \boldsymbol{p}) \right.$$
$$\left. + \frac{\delta(p^0 + E_p(X))}{2E_p(X)} \left[f_{\mp s}^-(X, -\boldsymbol{p}) - 1 \right] \right\}. \tag{11.63}$$

Substituting Eq. (11.63) into Eq. (11.62), and integrating over p^0 gives

$$p^\mu \partial_\mu f_{\pm s}^\pm(X, \boldsymbol{p}) + M\partial_\mu M \partial_p^\mu f_{\pm s}^\pm(X, \boldsymbol{p}) = 0. \tag{11.64}$$

By a direct comparison of (11.53) and (11.63), we find

$$f^\pm(X, \boldsymbol{p}) = \tfrac{1}{2} \left[f_{+s}^\pm(X, \boldsymbol{p}) + f_{-s}^\pm(X, \boldsymbol{p}) \right].$$

Therefore the functions $f^\pm(X, \boldsymbol{p})$ simply represent the spin-averaged densities. This has been given in agreement with the normalization of (11.55) and (11.56).

11.6. Consistency of the classical transport equations

The kinetic equations for the quark densities (11.52) and for the spin (11.58) follow from Eqs (11.27) and (11.30) considered to the first order in $\hbar$. We have yet to examine (i) whether equations (11.28), (11.29) and (11.31) are consistent with these to the same order and (ii) whether the additional information for the angle $\Phi(X)$ appearing in (11.58) can be obtained. We note that this kind of checking has been done in the case of QED in [69].

First, in order to illustrate that there is no contradiction between (11.27) and (11.29) we substitute the quantities $\mathcal{A}_\mu$ and $\mathcal{S}_{\nu\mu}$ obtained from Eqs (11.24) and (11.25), respectively into Eq. (11.29). In this way, we find the following equation

$$\hbar \left\{ \partial_\mu \mathcal{F}_{(0)} - \frac{p^\nu}{\sigma_{(0)}} \left[\partial_\mu \left(p_\nu \frac{\mathcal{F}_{(0)}}{\sigma_{(0)}} \right) - \partial_\nu \left(p_\mu \frac{\mathcal{F}_{(0)}}{\sigma_{(0)}} \right) \right] - \frac{\pi_{(0)}}{\sigma_{(0)}} \partial_\mu \mathcal{P}_{(0)} \right.$$
$$\left. + \frac{1}{\sigma_{(0)}} \left[\pi_{(0)} \partial_\nu \pi_{(0)} \partial_p^\nu \mathcal{V}_\mu^{(0)} + \sigma_{(0)} \partial_\nu \sigma_{(0)} \partial_p^\nu \mathcal{V}_\mu^{(0)} \right] \right\} = 0. \tag{11.65}$$

Since we are interested in retaining terms to the first order in $\hbar$ we can use the relations (11.34), (11.35), (11.44), and the kinetic equation (11.52) to find that (11.65), and consequently (11.29), is fulfilled.

In an analogous fashion, using the kinetic equation for spin (11.58), the constraints (11.38) and (11.47), and the definition (11.51), we can show that Eq. (11.31) is fulfilled again to the first order in $\hbar$. To do this, we multiply both sides of (11.31) by $\varepsilon_{\alpha\beta\mu\nu}$. Using the formula for $\mathcal{V}^{\nu}$ from (11.23), we find that the multiplication of the left-hand-side of (11.31) gives the expression

$$-\frac{\hbar}{\sigma_{(0)}}\left\{\varepsilon_{\alpha\beta\mu\nu}p^{\mu}\left[\partial_{\gamma}\mathcal{S}_{(0)}^{\gamma\nu} - \partial_{\gamma}\pi_{(0)}\partial_{p}^{\gamma}\mathcal{A}_{(0)}^{\nu}\right] - \sigma_{(0)}\left(\partial_{\alpha}\mathcal{A}_{\beta}^{(0)} - \partial_{\beta}\mathcal{A}_{\alpha}^{(0)}\right)\right\}.$$

(11.66)

On the other hand, the multiplication of the RHS of (11.31) yields

$$\hbar\left[\partial_{\gamma}\sigma_{(0)}\partial_{p}^{\gamma}\tilde{\mathcal{S}}_{\alpha\beta}^{(0)} + \partial_{\gamma}\pi_{(0)}\partial_{p}^{\gamma}\mathcal{S}_{\alpha\beta}^{(0)}\right].$$

(11.67)

Using now the expressions for $\mathcal{S}_{\mu\nu}^{(0)}$ and $\tilde{\mathcal{S}}_{\mu\nu}^{(0)}$, after a rather lengthy calculation in which Eqs (11.38), (11.47), (11.51) and (11.58) are used, we find that the two expressions above are equal to each other. Consequently, Eq. (11.31) is fulfilled up to the first order in $\hbar$ as well.

In this way, we have shown that Eqs (11.27), (11.29)–(11.31) are satisfied in the first order. To prove this fact, we have used Eqs (11.21)–(11.25), treating them as if they were satisfied up to the first order. Is this procedure admissible? The answer to this question is yes. Only $\mathcal{F}$ and $\mathcal{A}^{\mu}$ are independent functions (with $\mathcal{A}^{\mu}$ restricted by the axial current conservation (11.26)). Eqs (11.22), (11.23) and (11.25) are just the definitions of $\mathcal{P}$, $\mathcal{V}^{\mu}$ and $\mathcal{S}^{\mu\nu}$, and therefore are in our approach always satisfied. On the other hand Eq. (11.21) gives in the first order

$$(p^2 - M^2)\mathcal{F}_{(1)} = 2\left[\sigma_{(0)}\sigma_{(1)} + \pi_{(0)}\pi_{(1)}\right]\mathcal{F}_{(0)} + \partial_{\nu}\pi_{(0)}\mathcal{A}_{(0)}^{\nu}$$

(11.68)

and

$$(p^2 - M^2)\mathcal{P}_{(1)} = 2\left[\sigma_{(0)}\sigma_{(1)} + \pi_{(0)}\pi_{(1)}\right]\mathcal{P}_{(0)} + \partial_{\nu}\sigma_{(0)}\mathcal{A}_{(0)}^{\nu},$$

(11.69)

whereas using Eq. (11.24) one finds

$$(p^2 - M^2)\mathcal{A}_{(1)}^{\mu} = 2\left[\sigma_{(0)}\sigma_{(1)} + \pi_{(0)}\pi_{(1)}\right]\mathcal{A}_{(0)}^{\mu} - M^2 F\partial^{\mu}\Phi.$$

(11.70)

One can notice that Eq. (11.70) as it stands is a chirally invariant expression. On the other hand Eqs (11.68) and (11.69) form a system of chirally invariant equations in the same way as equations (11.16) and (11.17), or equations

(11.19) and (11.20). One can also check, that using formula (11.22) as the definition of $\mathcal{P}$ and Eq. (11.68), we can derive Eq. (11.69). Therefore, only one of equations (11.68) and (11.69) is really independent. We observe that all the expressions (11.68)–(11.70) are just the generalized mass-shell constraints for $\mathcal{F}_{(1)}$, $\mathcal{P}_{(1)}$ and $\mathcal{A}^\mu_{(1)}$, and they do not influence the relations in the zeroth order.

The last equation that we are still required to check is Eq. (11.28). Substituting the quantity $\mathcal{P}$, calculated from (11.22) into (11.28), gives

$$\frac{M^2(X)}{2}\partial_\mu\Phi(X)\partial^\mu_p F(X,p) = p^\mu\mathcal{A}^{(1)}_\mu(X,p). \tag{11.71}$$

We see that Eq. (11.71) defines the parallel part of $\mathcal{A}^\mu$ in the first order. Multiplying (11.70) by p^μ and using Eqs (11.71) and (11.44) we obtain zero. Hence Eqs (11.71) and (11.70) are consistent.

After deriving all possible equations up to the first order in $\hbar$ and checking their consistency, we are still faced with two problems. Firstly, the system of our equations in the leading order is not closed, since we do not have an equation for $\Phi(X)$. Secondly, it is still not clear whether our kinetic equation for spin satisfies the requirement of the axial current conservation.

One *a priori* possible situation is that the condition of the axial current conservation eliminates the freedom connected with the choice of $\partial_\mu\Phi(X)$. However, by studying some simple situations, one can convince oneself that this is not the case. For example, assuming that $M = $ const and that initially the spin distribution is homogeneous $\mathcal{A}^\mu_{(0)}(t = 0, \boldsymbol{x}, p) = B^\mu(p)$ we find $p^0\partial_0\mathcal{A}^0_{(0)} = \varepsilon^{0ijk}\,\partial_i\Phi\,p_j\,B_k(p)$. In this situation, the axial current conservation at $t = 0$ requires that $\partial_i\Phi\int d^4p\,\varepsilon^{0ijk}\,(p_j/p^0)\,B_k(p) = 0$. We can see that this equation is not sufficient to determine the gradient of Φ and consequently the derivative $\partial_0\mathcal{A}^0_{(0)}$ remains not well defined. Consequently, in order to obtain the closed system of equations in the classical limit we have to make some assumption on the form of $\partial_\mu\Phi(X)$. The simplest chirally invariant choice is

$$\partial_\mu\Phi(X) = 0. \tag{11.72}$$

In the case (11.72), our kinetic equation (11.58) allows us to determine the time evolution of the function $\mathcal{A}^\mu_{(0)}(X,p)$ from its knowledge at some initial time. One can notice, however, that this equation allows for solutions which do not satisfy the requirement of the axial current conservation. One of these solutions, for the case $M = $ const, has the form $\mathcal{A}^\mu_{(0)}(X,p) = s^\mu(p)s_\nu(p)X^\nu\delta^{(4)}(p - \tilde{p})$, where $s^\mu(p)$ is a vector satisfying the conditions $s^\mu(p)p_\mu = 0$ and $s^\mu(p)s_\mu(p) = -1$, and $\tilde{p}$ is some given value of the four-momentum, with $\tilde{p}^\mu\tilde{p}_\mu = M^2$. On the other hand, there also exist

solutions of Eq. (11.58) which satisfy the requirement of the axial current conservation. These are, *e.g.*, the static homogeneous solutions (for the case $M = $ const) or the solutions which are odd functions of momentum.

In consequence, we observe that Eq. (11.58) neither guarantees nor contradicts Eq. (3.3). Therefore the axial current conservation should be used as an external condition which selects the physical solutions of (11.58).

11.7. Explicit breaking of chiral symmetry

In the case $m \neq 0$, the chiral invariance of the Lagrangian (3.1) is explicitly broken by the expression $-m\bar{\psi}\psi$. In this situation, the additional term in the Dirac equation leads to a simple modification of our kinetic equations (11.14)–(11.18); we have to replace the mean field σ by the sum $\sigma + m$. Of course, in practice, this change affects only the real parts of our equations, *i.e.*, the formulae (11.21)–(11.25), since the imaginary parts (11.27)–(11.31) depend only on the gradients of σ. On the other hand, we observe that Eqs (11.48) and (11.49) remain unchanged because they are just definitions of the mean fields.

The important fact in the non-symmetric case is that the relations between the functions $\mathcal{F}_{(0)}, \mathcal{P}_{(0)}$ and $\mathcal{V}_{(0)}^\mu$ look different. In particular, instead of Eqs (11.42) and (11.43), we now find

$$\mathcal{P}_{(0)} = -\pi_{(0)}\frac{\mathcal{F}_{(0)}}{\sigma_{(0)} + m}, \quad \mathcal{V}_{(0)}^\mu = p^\mu \frac{\mathcal{F}_{(0)}}{\sigma_{(0)} + m}. \tag{11.73}$$

Using the first of the relations (11.73) in Eqs (11.48) and (11.49), we obtain

$$\sigma_{(0)}(X) + 8G \int \frac{d^4p}{(2\pi)^4}\mathcal{F}_{(0)}(X,p) = 0, \tag{11.74}$$

and

$$\pi_{(0)}(X) \left[\sigma_{(0)}(X) + m + 8G \int \frac{d^4p}{(2\pi)^4}\mathcal{F}_{(0)}(X,p)\right] = 0. \tag{11.75}$$

A straightforward consequence of these two equations is the condition

$$\pi_{(0)}(X) = 0, \tag{11.76}$$

which implies also that $\mathcal{P}_{(0)}(X,p) = 0$ and $\Phi(X) = 0$. Therefore, we observe that if the system is not chirally invariant, equations (11.48) and (11.49) allow for the determination of the angle $\Phi(X)$.

For $m \neq 0$, the mass-shell constraints (11.44) and (11.47), as well as the kinetic equations (11.52) and (11.58) preserve their form, only in this case we should use the definitions

$$F(X, p) = \frac{\mathcal{F}_{(0)}}{\sigma_{(0)} + m}, \quad M(X) = \sigma_{(0)} + m. \tag{11.77}$$

The gap equation (11.55) has now the form

$$M(X) = m + 4GM \int \frac{d^3p}{(2\pi)^3} \frac{1}{\sqrt{M^2(X) + p^2}} \left[1 - f^+(X, \boldsymbol{p}) - f^-(X, \boldsymbol{p})\right]. \tag{11.78}$$

Let us now discuss the behaviour of the axial current in the case when $m \neq 0$. In this situation, we no longer have an axial current conservation law, and using Eq. (11.22), we can write

$$\hbar \left\{ \tfrac{1}{2} \partial_\mu \mathcal{A}^\mu_{(0)} - (\sigma_{(0)} + m)\mathcal{P}_{(1)} - \pi_{(1)}\mathcal{F}_{(0)} \right\} = 0. \tag{11.79}$$

The integration of (11.79) over momentum gives

$$\partial_\mu A^\mu_{(0)}(X) = -\frac{m}{G}\pi_{(1)}(X). \tag{11.80}$$

In contrast to the $m = 0$, case we observe that such an integration does not lead to any constraint for $\mathcal{A}^\mu_{(0)}$ itself. Therefore, without any restrictions on $\partial_\mu \mathcal{A}^\mu_{(0)}$ we can treat Eq. (11.79) as a defining equation for $\mathcal{P}_{(1)}$. One can still check that Eq. (11.79) leads to the mass-shell constraint for $\mathcal{P}_{(1)}$ which agrees with (11.69). The latter formula, for the case $m \neq 0$, should be rewritten in the form $(p^2 - M^2)\mathcal{P}_{(1)} = \partial_\nu M\mathcal{A}^\nu_{(0)}$. We note that Eq. (11.80) describes the partial conservation of the axial current (PCAC) in our case.

12. Large time-scale fluctuations of the quark condensate

In this Chapter we deal with the transport equations, again reducing our interest only to quark dynamics in the mean (Vlasov) field. We shall consider the systems which are not uniform but close to equilibrium. This allows us to linearize the kinetic equations and to use a combination of analytical and numerical methods to look for solutions.

Our main aim is to study the properties of a hadronic system in which the energy density is very large but which still exhibits a chirally broken phase. One could think of a fireball formed in high-energy heavy-ion collisions but at energies below the threshold for production of a chirally restored phase. The temperature range of interest for us lies between 100 and 150 MeV, and

we assume that the critical temperature is 190 MeV. The baryon density is zero in our case, therefore, our considerations are appropriate for the description of the central rapidity region. We cannot study the systems at temperatures close to T_c, because one of the ingredients of our approach is that the mean field contains a large constant component in addition to the fluctuating part. The former vanishes (becomes negligible) at T_c and this fact makes our approach inappropriate for very high temperatures.

Because the energy density of such a fireball is large, we hope that the description of its space-time evolution in terms of quarks is meaningful. As we shall see later, our equations will not lead to the separation of colour, although the NJL model does not include confinement. In principle, one has to take into account the dynamics of mesons as well. However, in practice it is not completely clear how this can be done in the situation out of equilibrium and in the fully satisfactory way, *i.e.*, protecting all the conservation laws and symmetries.

It is important to notice that already a quantum fluctuation of the condensate, *i.e.*, the sigma meson, exists. However, due to its large mass the typical time scale over which the sigma meson wave function changes is a fraction of fermi: $\Delta t < 1/m_\sigma \approx 0.2$ fm. In the approach presented here we study the large time-scale (classical) fluctuations of the condensate and neglect such oscillating short time-scale changes, although if the latter are taken into account the interesting phenomena can occur from couplings of the fluctuations on both scales. Nevertheless, the inclusion of these short time-scale fluctuations is equivalent to taking into account the mesonic degrees of freedom and, as it was discussed above, represents a separate, as yet unsolved problem.

The non-uniformity of our system will lead to fluctuations of the mean field around its average value that is determined by the thermal background. Since in the NJL model a change in the mean field is proportional to a change in the condensate, the latter will also fluctuate. As a consequence, through the use of our transport equations for the quark-antiquark plasma we are able to predict the space-time development of such fluctuations.

12.1. Linearized kinetic equations

The starting point for our investigations are Eqs (11.54) and (11.78). Their straightforward generalization to the case of arbitrary number of flavours (N_f) and colours (N_c) has the form

$$p^\mu \partial_\mu f(X, \boldsymbol{p}) + M(X) \partial_\mu M(X) \partial_p^\mu f(X, \boldsymbol{p}) = 0 \qquad (12.1)$$

and

$$1 = \frac{m}{M(X)} + 4N_c N_f G \int \frac{d^3 p}{(2\pi)^3} \frac{1}{p^0} \left[1 - f(X, \boldsymbol{p})\right]. \qquad (12.2)$$

Here $p^\mu = (p^0, \boldsymbol{p})$ is the four-momentum of a quark, $X^\mu = (t, \boldsymbol{r})$ is its space-time position, m is the current quark mass, and G is the coupling constant. The function $f(X, \boldsymbol{p})$ is the sum of the quark and antiquark distribution functions, *i.e.*, $f(X, \boldsymbol{p}) = f^+(X, \boldsymbol{p}) + f^-(X, \mathbf{p})$. Each of the latter two functions satisfies equation (11.54) so we can add and subtract such two equations. Assuming that $f^+(X, \boldsymbol{p}) = f^-(X, \boldsymbol{p})$ the equation for the difference of two distributions is trivially fulfilled and we are left only with Eq. (12.1). In the case $N_f = 2$ the constituent quark mass $M(X)$ is related to the quark condensate by the relation

$$M(X) = m - 4G\langle \overline{q}(X)q(X)\rangle, \tag{12.3}$$

which is a generalization of formula (5.28) for non-equilibrium situations.

In our approach quarks are always on the mass shell, *i.e.*, $p^0 = E_p(X) = \sqrt{\boldsymbol{p}^2 + M^2(X)}$, but their mass is a function of space-time position. Therefore, the distribution function depends only on space-time variables and three-momentum $\boldsymbol{p}$. Consequently, the derivative with respect to energy, p^0, in (12.1) vanishes. However, we have included it in our expression (12.1) to show the relativistic invariance of the kinetic equation explicitly. The gap equation (12.2) is also relativistically invariant, but the integral appearing there is divergent [12]. For the sake of simplicity and also in order to make connection to other calculations done in the framework of the NJL model, we shall regularize (12.2) using a 3-dimensional cutoff Λ. This procedure, of course, introduces an explicit breaking of the Lorentz invariance. In the following, whenever the integration is restricted to the region $|\boldsymbol{p}| < \Lambda$ we shall indicate this explicitly in the expressions.

It is interesting to observe that the equality of the quark and the antiquark distribution functions (for each colour separately) has some nice consequences for us; we can think that on the average colour is compensated by anticolour at each point and, therefore, the discussed states of the plasma are colourless. In other words, although we describe the evolution of our system in terms of the motion of quarks our equations will not lead to the separation of colour. (We note that our assumption concerning the equality of the quark and the antiquark distribution functions is reasonable only for the systems with net baryon number density equal to zero.)

In the following we are going to consider the situation in which the distribution function can be written as a sum of the isotropic background distribution and a small perturbation, namely,

$$f(t, \boldsymbol{r}, \boldsymbol{p}) = f_0(p^2) + \delta f(t, \boldsymbol{r}, \boldsymbol{p}). \tag{12.4}$$

---

[12] The quark distribution function vanishes fast for $\boldsymbol{p} \to \infty$, however the integrand in Eq. (12.2), containing the difference $1 - f(X, p)$, does not.

Correspondingly, the mean field can be written as

$$M(t, r) = M_c + \delta M(t, r), \qquad (12.5)$$

where M_c is the constant part and $\delta M(t, r)$ is the temporally and spatially varying fluctuation. We shall assume that the background distribution is a thermal one

$$f_0(p^2) = \frac{2}{e^{\sqrt{p^2 + M_c^2}/T} + 1}. \qquad (12.6)$$

Here T is the temperature and the factor 2 comes from summing up the quark and the antiquark distribution functions as was discussed above (the chemical potential $\mu = 0$ in our case). According to Eq. (12.2) the fluctuating part of the condensate can be written as $\delta \langle \bar{q}(X) q(X) \rangle = -\delta M(X)/4G$, therefore, from now on we shall discuss simply the disturbances of the mean field.

Substituting expressions (12.4) and (12.5) into Eqs (12.1) and (12.2) and keeping only the zeroth and first order terms in the deviations $\delta f(t, r, p)$ and $\delta M(t, r)$ gives us the following three equations:

$$1 = \frac{m}{M_c} + 4N_c N_f G \int^{\Lambda} \frac{d^3 p}{(2\pi)^3} \frac{1}{E_p} \left[1 - f_0(p^2)\right], \qquad (12.7)$$

$$\frac{\partial}{\partial t} \delta f(t, r, p) + v \cdot \frac{\partial}{\partial r} \delta f(t, r, p) - \frac{M_c}{E_p} \frac{\partial}{\partial r} \delta M(t, r) \cdot \frac{\partial}{\partial p} f_0(p^2) = 0, \qquad (12.8)$$

$$\delta M(t, r) \left[\frac{m}{M_c} + 4N_c N_f G \int^{\Lambda} \frac{d^3 p}{(2\pi)^3} \frac{M_c^2}{E_p^3} \left(1 - f_0(p^2)\right) \right]$$

$$= -4N_c N_f G \int^{\Lambda} \frac{d^3 p}{(2\pi)^3} \frac{M_c}{E_p} \delta f(t, r, p). \qquad (12.9)$$

Here E_p and v are the leading order expressions for the energy of a quark, $E_p = \sqrt{p^2 + M_c^2}$, and its velocity $v = p/E_p$.

Equation (12.7) is the zeroth order gap equation connecting the constant part of the mean field M_c with the background distribution $f_0(p^2)$ and has a form known from the NJL calculations at finite temperature (see, e.g., Eq. (5.16)). Solving (12.7) we find M_c as a function of the temperature T, see Fig. 12.1. Assuming that $m = 0$ and fitting other parameters as in Ref. [16], i.e., $N_c = 3, N_f = 2, G = 5.01$ GeV $^{-2}$, and $\Lambda = 650$ MeV, we find that at zero temperature $M_c = 313$ MeV and the corresponding value of the quark condensate is $(-250$ MeV$)^3$. We note that this set of parameters gives the same temperature dependence of the mean field as the parameters of the one-flavour model used in Section 5.1.
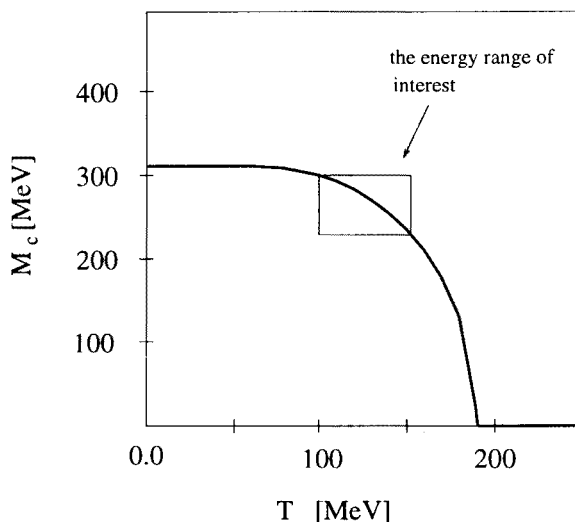
Fig. 12.1. Temperature dependence of the background mean field M_c. The values of the parameters were taken in such a way as to get the agreement with the temperature dependence shown in Fig. 5.3. The temperature range of interest (together with the corresponding range of M_c) is framed by the box.

12.2. Conservation laws

Because we neglect the processes of $q\bar{q}$ annihilation the total number of quarks and antiquarks should be conserved. We can write this conservation law formally as

$$\partial_\mu N^\mu(X) = 0, \tag{12.10}$$

where the number current is defined as

$$N^\mu(X) = 2N_c N_f \int \frac{d^3p}{(2\pi)^3} \frac{p^\mu}{p^0} f(X, \boldsymbol{p}). \tag{12.11}$$

In fact, starting from (12.11) one can derive (12.10) using the kinetic equation (12.1) and integrating by parts. Similarly, we can show that the entropy of the system is conserved, namely,

$$\partial_\mu S^\mu(X) = 0, \tag{12.12}$$

where

$$S^\mu(X) = -2N_c N_f \int \frac{d^3p}{(2\pi)^3} \frac{p^\mu}{p^0} \Big[f(X, \boldsymbol{p}) \ln f(X, \boldsymbol{p})$$
$$+ [1 - f(X, \boldsymbol{p})] \ln [1 - f(X, \boldsymbol{p})] \Big] \tag{12.13}$$

is the entropy flux. The latter is conserved because we consider a collisionless plasma.

Let us now define the energy-momentum tensor of quarks in the standard way by

$$T^{\mu\nu}_{\text{quarks}}(X) = 2N_cN_f \int \frac{d^3p}{(2\pi)^3} \frac{p^\mu p^\nu}{p^0} f(X, \boldsymbol{p}). \qquad (12.14)$$

Using again the kinetic equation (12.1) and integrating by parts one obtains

$$\partial_\mu T^{\mu\nu}_{\text{quarks}}(X) = 2N_cN_f M(X)\partial^\nu M(X) \int \frac{d^3p}{(2\pi)^3} \frac{1}{p^0} f(X, \boldsymbol{p}). \qquad (12.15)$$

The result (12.15) shows that the total energy and the total momentum of quarks alone are not conserved; this is due to the fact that (12.14) includes only the kinetic energy of particles. The question arises: What tensor, describing the potential energy, should be added to (12.14) in order to obtain a conserved quantity? In the thermodynamic approach of [15, 16] it was found that the expression

$$\Omega_{\text{vac}}(X) = \frac{[M(X) - m]^2}{4G} - 2N_cN_f \int^\Lambda \frac{d^3p}{(2\pi)^3} p^0 \qquad (p^0 = E_p(X)) \quad (12.16)$$

represents the energy density of the vacuum (with the corresponding vacuum pressure given by $-\Omega_{\text{vac}}(X)$). Because the vacuum is isotropic we write its energy-momentum tensor as

$$T^{\mu\nu}_{\text{vac}}(X) = g^{\mu\nu}\Omega_{\text{vac}}(X). \qquad (12.17)$$

where $g^{\mu\nu}$ is the metric tensor. Using now the gap equation (12.2) we can show that

$$\partial_\mu T^{\mu\nu}_{\text{vac}}(X) = -2N_cN_f M(X)\partial^\nu M(X) \int^\Lambda \frac{d^3p}{(2\pi)^3} \frac{1}{p^0} f(X, \boldsymbol{p}). \qquad (12.18)$$

We see that for $\Lambda \to \infty$ the summed energy of the quarks and of the vacuum is conserved. This is an interesting result showing that one has to include the energy of the zero modes of quarks (the second term on the RHS of Eq. (12.16)) to have the conservation law. Since Λ is finite in our approach, it means that the energy is not exactly conserved. However, as long as we look at the leading terms of the quantities in our expansion defined by Eqs (12.4) and (12.5) we find that this violation is very small and, therefore, can be disregarded.

One can check that it is possible to obtain a strict conservation of energy if the gap equation (12.2) is regularized in a slightly different way: The

integral on the RHS of (12.2) should be written as a sum of two terms. The first one, independent of $f(X, \boldsymbol{p})$, has to be regularized with the cutoff, whereas the second term containing $f(X, \boldsymbol{p})$ is converging and should not be additionally regularized. Such a scheme yields the exact conservation laws but at very high temperatures it can lead to negative and, therefore, non-acceptable solutions for the mean field — this is the situation discussed in Section 5.1 below Eq. (5.14).

12.3. Energy-momentum representations

We now come back to the discussion of Eqs (12.8) and (12.9). Since these equations are linear, it is useful to expand the functions $\delta M(t, \boldsymbol{r})$ and $\delta f(t, \boldsymbol{r}, \boldsymbol{p})$ as Fourier integrals

$$\delta f(t, \boldsymbol{r}, \boldsymbol{p}) = \int \frac{d^3 k}{(2\pi)^3} \delta f(t, \boldsymbol{k}, \boldsymbol{p}) \, e^{i\boldsymbol{k}\cdot\boldsymbol{r}}, \qquad (12.19)$$

$$\delta M(t, \boldsymbol{r}) = \int \frac{d^3 k}{(2\pi)^3} \delta M(t, \boldsymbol{k}) \, e^{i\boldsymbol{k}\cdot\boldsymbol{r}}, \qquad (12.20)$$

and substitute them into (12.8) and (12.9). In this way we find two coupled equations for each Fourier component separately

$$\left[\frac{\partial}{\partial t} + i\boldsymbol{k}\cdot\boldsymbol{v} \right] \delta f(t, \boldsymbol{k}, \boldsymbol{p}) - \frac{iM_c}{E_p} \delta M(t, \boldsymbol{k})\boldsymbol{k}\cdot\frac{\partial f_0}{\partial \boldsymbol{p}} = 0, \qquad (12.21)$$

$$\delta M(t, \boldsymbol{k}) \left[\frac{m}{M_c} + 4N_c N_f G \int^\Lambda \frac{d^3 p}{(2\pi)^3} \frac{M_c^2}{E_p^3} (1 - f_0) \right]$$

$$= -4N_c N_f G \int^\Lambda \frac{d^3 p}{(2\pi)^3} \frac{M_c}{E_p} \delta f(t, \boldsymbol{k}, \boldsymbol{p}). \qquad (12.22)$$

In the situation under consideration the system is perturbed at $t = 0$ and the perturbations propagate forward in time, i.e., $\delta M(t, \boldsymbol{k})$ and $\delta f(t, \boldsymbol{k}, \boldsymbol{p})$ are only different from zero for $t > 0$. Consequently, to solve (12.21) and (12.22), we use a one-sided Fourier transform in time [13]. For the fluctuating part of the mean field it is defined as

$$\delta M(\omega, \boldsymbol{k}) = \int_0^\infty e^{i\omega t} \, \delta M(t, \boldsymbol{k}) \, dt. \qquad (12.23)$$

---

[13] In what follows we adopt the Landau method [73, 74] for studying the relaxation of the initial perturbations in electron-ion plasmas.

Assuming $|\delta M(t, \boldsymbol{k})| < \mathcal{M} \exp(\sigma t)$, where $\mathcal{M}$ and σ are some positive numbers, we find that Eq. (12.23) is well defined for frequencies ω having an imaginary part $\omega_I > \sigma$. Thus, the inverse transformation is given by

$$\delta M(t, \boldsymbol{k}) = \int\limits_{-\infty+i\sigma}^{\infty+i\sigma} \frac{d\omega}{2\pi} \, \mathrm{e}^{-i\omega t} \, \delta M(\omega, \boldsymbol{k}), \qquad (12.24)$$

where the integration contour is taken to be a straight line parallel to the real axis. We note that the assumption discussed above means that all singularities of $\delta M(\omega, \boldsymbol{k})$ lie below the contour. The one-sided Fourier transform of $\delta f(t, \mathbf{k}, \boldsymbol{p})$ is defined in the analogous way.

Multiplying (12.21) by $\exp(i\omega t)$ and integrating over time from zero to infinity gives

$$\delta f(\omega, \boldsymbol{k}, \boldsymbol{p}) = \frac{1}{i(\boldsymbol{k} \cdot \boldsymbol{v} - \omega)} \left[g(\boldsymbol{k}, \boldsymbol{p}) + \frac{iM_\mathrm{c}}{E_p} \delta M(\omega, \boldsymbol{k}) \, \boldsymbol{k} \cdot \frac{\partial f_0}{\partial \boldsymbol{p}} \right], \qquad (12.25)$$

where $g(\boldsymbol{k}, \boldsymbol{p})$ represents the initial condition for the distribution function $\delta f(t, \boldsymbol{r}, \boldsymbol{p})$, namely,

$$\delta f(t = 0, \boldsymbol{r}, \boldsymbol{p}) = g(\boldsymbol{r}, \boldsymbol{p}) = \int \frac{d^3 k}{(2\pi)^3} g(\boldsymbol{k}, \boldsymbol{p}) \, \mathrm{e}^{i\boldsymbol{k} \cdot \boldsymbol{r}} . \qquad (12.26)$$

Making the one-sided Fourier transformation of Eq. (12.22) and substituting into its RHS Eq. (12.25) we find the following expressions

$$\delta M(\omega, \boldsymbol{k}) \, \gamma(\omega, \boldsymbol{k}) = \mathsf{G}(\omega, \boldsymbol{k}), \qquad (12.27)$$

where

$$\gamma(\omega, \boldsymbol{k}) = \frac{m}{M_\mathrm{c}} + 4N_\mathrm{c}N_f \, G \int\limits^{\Lambda} \frac{d^3 p}{(2\pi)^3} \left[\frac{M_\mathrm{c}^2}{E_p^3}(1 - f_0) + \frac{M_\mathrm{c}^2}{E_p^2} \frac{1}{\boldsymbol{k} \cdot \boldsymbol{v} - \omega} \boldsymbol{k} \cdot \frac{\partial f_0}{\partial \boldsymbol{p}} \right] \qquad (12.28)$$

and

$$\mathsf{G}(\omega, \boldsymbol{k}) = 4iN_\mathrm{c}N_f \, G \int\limits^{\Lambda} \frac{d^3 p}{(2\pi)^3} \frac{M_\mathrm{c}}{E_p} \frac{g(\boldsymbol{k}, \boldsymbol{p})}{\boldsymbol{k} \cdot \boldsymbol{v} - \omega}. \qquad (12.29)$$

Equation (12.27) is very much similar to that found in the case of investigations of the oscillations of the electron-ion plasma [75]. Relying on this analogy, we shall call $\gamma(\omega, \boldsymbol{k})$ the *permittivity* of the quark-antiquark plasma. Substituting Eq. (12.27) into (12.24) we obtain

$$\delta M(t, \boldsymbol{k}) = \int\limits_{-\infty+i\sigma}^{\infty+i\sigma} \frac{d\omega}{2\pi} \, \mathrm{e}^{-i\omega t} \frac{\mathsf{G}(\omega, \boldsymbol{k})}{\gamma(\omega, \boldsymbol{k})}. \qquad (12.30)$$

The analysis of this equation will be the subject of the next two Sections.

12.4. Dispersion relation and analytic properties of the functions γ and G

We already know that the integration in (12.30) must be performed above all singularities of the function $\mathsf{G}(\omega, \boldsymbol{k})/\gamma(\omega, \boldsymbol{k})$. Eq. (12.28) defines $\gamma(\omega, \boldsymbol{k})$ as the function of the complex frequency, $\omega = \omega_R + i\omega_I$, which is analytic everywhere except for the interval on the real axis where $-v^{\mathrm{max}}k \leq \omega_R \leq v^{\mathrm{max}}k$. Here $v^{\mathrm{max}} = \Lambda/\sqrt{\Lambda^2 + M_c^2}$ is the limiting maximal velocity of quarks, which because of the presence of the cutoff is slightly smaller than 1. The structure of the singularities of $\mathsf{G}(\omega, \boldsymbol{k})$ is analogous to that of $\gamma(\omega, \boldsymbol{k})$; they all lie on the real axis in the interval defined above. The additional singularities which can appear in the integrand of (12.30) come from the zeros of the denominator, *i.e.*, they are solutions to the equation

$$\gamma(\omega, \boldsymbol{k}) = 0. \tag{12.31}$$

Equation (12.31) is nothing else than the dispersion relation defining modes in the plasma, which have momentum $\boldsymbol{k}$ and energy $\omega(k)$ such that $\gamma[\omega(k), k] = 0$.

Let us now try to find a solution to Eq. (12.31). We first perform the angle integration in (12.28) and find the following representation of the function $\gamma(\omega, k)$:

$$\gamma(\omega, k) = \frac{m}{M_c} + \frac{2N_cN_fGM_c^2}{\pi^2} \int\limits_0^\Lambda dp \frac{p}{E_p} \left[\frac{p}{E_p^2}(1 - f_0) - \frac{\partial f_0}{\partial p} \Phi\left(\frac{E_p\omega}{pk}\right) \right], \tag{12.32}$$

where

$$\Phi(z) = \frac{1}{2}z \ln \frac{z+1}{z-1} - 1. \tag{12.33}$$

One can notice that $\Phi(z)$ has a cut for real values of z contained in the interval $-1 \leq z_R \leq 1$. This is in agreement with an earlier remark that $\gamma(\omega, k)$ has a cut for $-v^{\mathrm{max}}k \leq \omega_R \leq v^{\mathrm{max}}k$.

For the arguments slightly shifted from the real axis we find

$$\Phi(z = z_R \pm i\epsilon) = \frac{1}{2}z_R \left[\ln \frac{|z_R + 1|}{|z_R - 1|} \mp i\pi\theta(1 - |z_R|) \right] - 1, \tag{12.34}$$

where $\theta(x)$ is the step function. One of the consequences of Eqs (12.32) and (12.34) is that the dispersion relation (12.31) can have a solution for real frequencies ($\omega = \omega_R$) only if $|\omega_R| > kv^{\mathrm{max}}$. Otherwise, $\gamma(\omega, k)$ has a non-vanishing imaginary part. A closer examination of the function (12.33) shows, however, that for $|\omega_R| > kv^{\mathrm{max}}$ the real part of $\Phi(E_p\omega_R/pk)$ is always positive and so is the real part of $\gamma(\omega, k)$. To see the last point one can

notice that the derivative of the thermal background distribution is always negative. Consequently, we conclude that the dispersion relation (12.31) has no solution for real frequencies.

For purely imaginary arguments $\Phi(z)$ has the form

$$\Phi(z = i z_I) = |z_I| \left(\frac{\pi}{2} - \arctan|z_I| \right) - 1, \qquad (12.35)$$

hence it is a negative real function. In this case (12.32) is a difference of two real positive functions and one can numerically check if there exists a solution to Eq. (12.31). In the temperature range of interest, $i.e.$, for 100 MeV $\leq T \leq$ 150 MeV, we have found that $\gamma(\omega, k)$ is always larger than zero. This fact again means that our dispersion relation has no solution.

To complete our investigation we have studied numerically the imaginary part of $\gamma(\omega, k)$ for $\omega_R, \omega_I > 0$ again in the temperature range 100 MeV $\leq T \leq$ 150 MeV. We have checked that Im $\gamma(\omega, k)$ is always negative in the discussed region and vanishes at infinity, $i.e.$, for $|\omega| \to \infty$. Employing the symmetries Im$\gamma(\omega_R - i\omega_I, k) = -Im\gamma(\omega_R + i\omega_I, k)$ and Im$\gamma(-\omega_R + i\omega_I, k) = -Im\gamma(\omega_R + i\omega_I, k)$ we find that Im$\gamma(\omega, k)$ is different from zero also in other quadrants. This result, together with the two previous ones, indicates that there is no solution to Eq. (12.31) for any finite ω.

Because the only singularities of the integrand in (12.30) are those coming from the cut discussed earlier (placed on the real axis) our parameter σ can be taken to be an arbitrarily small positive number. For $t < 0$ we can close the contour of integration in the upper half-plane. Because the integrand in (12.30) has no singularities in this region, we find in this case that $\delta M(t, \mathbf{k}) = 0$, what is in agreement with the requirements of causality. For $t > 0$ we can close the contour of the integration in the lower half-plane and, later, we contract it to go just around the cut. As the result of this procedure we obtain the expression

$$\delta M(t, \mathbf{k}) = \int_{-k v^{\max}}^{k v^{\max}} \frac{d\omega}{2\pi} \, e^{-i\omega t} \left[\frac{\mathsf{G}(\omega + i\epsilon, \mathbf{k})}{\gamma(\omega + i\epsilon, \mathbf{k})} - \frac{\mathsf{G}(\omega - i\epsilon, \mathbf{k})}{\gamma(\omega - i\epsilon, \mathbf{k})} \right]. \qquad (12.36)$$

For further use, it will be convenient to represent $\gamma(\omega_R \pm i\epsilon, k)$ explicitly as the sum if its real and imaginary parts, $i.e.$,

$$\gamma(\omega_R \pm i\epsilon, k) = \alpha \left(\frac{\omega_R}{k} \right) \pm i\beta \left(\frac{\omega_R}{k} \right), \qquad (12.37)$$

where

$$\alpha(\Omega) = \frac{m}{M_c} + \frac{2 N_c N_f G M_c^2}{\pi^2} \left[\int_0^\Lambda \frac{dp \, p}{E_p} \left[\frac{p}{E_p^2} (1 - f_0) + \frac{\partial f_0}{\partial p} \right] \right.$$

$$-\frac{\Omega}{2}\int\limits_{0}^{\Lambda}dp\frac{\partial f_0}{\partial p}\ln\frac{|\Omega + p/E_p|}{|\Omega - p/E_p|}\Bigg]$$ (12.38)

and

$$\beta(\Omega) = \frac{N_c N_f G M_c^2}{\pi}\Omega\left[f_0(\Lambda) - f_0\left(\frac{M_c\Omega}{\sqrt{1-\Omega^2}}\right)\right]\theta\left(v^{\max} - |\Omega|\right).$$ (12.39)

The reader may be surprised by our result, since we have a contribution from the cut but, on the other hand, we do not find a solution to the dispersion relation (12.31). In the standard case [73, 75] the situation is quite opposite: the permittivity is an entire function of the frequency and one does find solutions to (12.31). The point is that for a non-relativistic Maxwellian plasma one can analytically continue $\gamma(\omega, k)$ from the upper half-plane into the lower half-plane. In this way, one obtains a function $\gamma'(\omega, k)$ such that *(i)* for $\omega_I > 0$ it coincides with $\gamma(\omega, k)$, *(ii)* for $\omega_I = 0$ it has no cut, *(iii)* for $\omega_I < 0$ it is different from $\gamma(\omega, k)$, *(iv)* it is an entire function of ω, and finally *(v)* there are solutions to the dispersion relation $\gamma'(\omega, k) = 0$. Because these solutions are for complex energies in the lower half-plane it means that the modes are damped — this is the famous Landau damping [73–75] caused by a transfer of the energy from the wave to the particles of the medium.

In our case, although the mathematics is slightly different we can expect similar physics. *Our contribution from the cut is a superposition of waves which can exhibit destructive coherence phenomena, i.e., they can be damped as in the standard case.* The main mathematical difference between our approach here and the typical non-relativistic one is that we do not perform the analytic continuation of $\gamma(\omega, k)$ from the upper half-plane into the lower one because, in our case, this does not appear to be a straightforward procedure.

12.5. Results

As the initial conditions for our equations, we shall consider two extreme cases which lead to spectacularly quite different behaviour of the plasma. The first case corresponds to the perturbation which is at $t = 0$ independent of the momentum $\boldsymbol{p}$, whereas the second case describes the situation when the initial perturbation is strongly peaked at some value of $\boldsymbol{p}$. The second case can be regarded as a more interesting one, because any initial perturbation (including the first one) can be treated as a superposition of such peaked elementary perturbations. Moreover, as we shall see later, the solutions are also superpositions of elementary solutions corresponding to such initial conditions. Let us, however, start our considerations with the discussion of the first case.

12.5.1. Initial perturbation independent of momentum

Writing the initial perturbation of the quark distribution function in the form

$$g(\boldsymbol{k}, \boldsymbol{p}) = g_1(\boldsymbol{k}), \qquad (12.40)$$

and using the above expression in (12.29) one can find that

$$\mathsf{G}(\omega_R \pm i\epsilon, \boldsymbol{k}) = g_1(\boldsymbol{k}) \frac{M_c}{k} \left[\pm A\left(\frac{\omega_R}{k}\right) + iB\left(\frac{\omega_R}{k}\right) \right], \qquad (12.41)$$

where

$$A(\Omega) = \frac{N_c N_f G}{2\pi} \left[\frac{M_c^2 \Omega^2}{1 - \Omega^2} - \Lambda^2 \right] \theta(v^{\max} - |\Omega|) \qquad (12.42)$$

and

$$B(\Omega) = -\frac{N_c N_f G}{\pi^2} \int\limits_0^\Lambda dp\, p \, \ln \frac{|\Omega + p/E_p|}{|\Omega - p/E_p|}. \qquad (12.43)$$

Equations (12.36), (12.37)–(12.39), and (12.41)–(12.43) allow us to write the final expression for the fluctuating part of the mean field as

$$\delta M(t, \boldsymbol{k}) = g_1(\boldsymbol{k}) \, M_c \, F_1(kt), \qquad (12.44)$$

where

$$F_1(kt) = \int\limits_{-v^{\max}}^{v^{\max}} \frac{d\Omega}{\pi} \frac{\alpha A + \beta B}{\alpha^2 + \beta^2} \cos(\Omega kt). \qquad (12.45)$$

One can obtain the space-time dependent function $\delta M(t, \boldsymbol{r})$ by calculation of the Fourier transform (12.20). The time evolution of the fluctuations is completely determined by the function $F_1(kt)$.

In Fig. 12.2 we show the function $F_1(kt)$ calculated numerically for two different values of the temperature: $T = 100$ MeV and $T = 150$ MeV, respectively. The parameters were fitted as in [16], see also the discussion following Eqs (12.7)–(12.9). For small time arguments $F_1(kt)$ is negative as it should be — if we add particles to the system, $g_1(\boldsymbol{k}) > 0$, the mean field decreases. For $t = 0$ the change of the mean field can be independently calculated either from Eq. (12.44) or directly from Eq. (12.9). The condition that two methods give the same result was used by us as a check of our numerical code.

For both values of the temperature we observe that $F_1(kt)$ oscillates in time but with the amplitude strongly decreasing. In our opinion, we observe here a phenomenon having features in common with the Landau
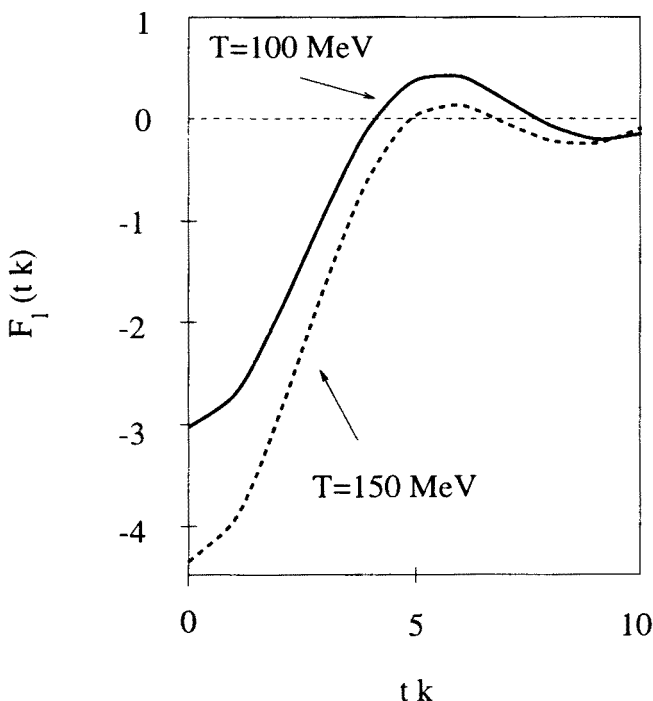
Fig. 12.2. Function $F_1(kt)$ calculated for two values of the temperature: $T = 100$ MeV and $T = 150$ MeV. The values of other parameters are: $m = 0$, $N_c = 3$, $N_f = 2$, $G = 5.01$ GeV^{-2}, and $\Lambda = 650$ MeV.

damping in ordinary plasmas, *i.e.*, the energy of the wave is transferred to the medium without entropy production, see Eq. (12.12). There exist, however, differences between the damping observed here and the standard Landau damping. First of all, one can check that the suppression of the oscillations is much weaker than exponential. Moreover, the damping seems to be independent of the temperature. In fact, our calculations indicate that it is a relativistic effect connected with the existence of the finite maximal velocity, *i.e.*, the velocity of light. The latter determines the size of the integration interval in (12.45) — in practice we have always $v^{\max} \approx 1$. For the considered values of the temperatures one can check that the function $(\alpha A + \beta B)/(\alpha^2 + \beta^2)$ is very regular and, therefore, we expect that for $kt = 2\pi$ the integral becomes negligible. This result is due to the fact that $\cos(2\pi\Omega)$ takes on equally positive and negative values in the interval between -1 and 1. By inspection of Fig. 12.2, one can convince oneself that the initial perturbation of the mean field becomes strongly suppressed for $kt > 2\pi$.

It is perhaps also interesting to observe that our suppression of oscillations has some features in common with the Friedel oscillations analyzed in Chapter 8. The latter are caused by the existence of the sharp Fermi surface, in our case there exists a sharp maximal velocity $v^{\max} \approx 1$.

12.5.2. Initial perturbation strongly peaked in momentum

Let us now turn to the discussion of the opposite case, where the initial perturbation is strongly peaked in momentum. Employing (12.29) and (12.36) and exchanging order of integration we obtain the formula

$$\delta M(t, \boldsymbol{k}) = 4 N_c N_f G \int^{\Lambda} \frac{d^3 p}{(2\pi)^3} \frac{1}{E_p} \delta M(t, \boldsymbol{k}; \boldsymbol{p}), \qquad (12.46)$$

where we used the definitions

$$\delta M(t, \boldsymbol{k}; \boldsymbol{p}) = \int\limits_{-kv^{\max}}^{kv^{\max}} \frac{d\omega}{2\pi} \mathrm{e}^{-i\omega t} \left[\frac{\mathsf{G}(\omega + i\epsilon, \boldsymbol{k}; \boldsymbol{p})}{\gamma(\omega + i\epsilon, \boldsymbol{k})} - \frac{\mathsf{G}(\omega - i\epsilon, \boldsymbol{k}; \boldsymbol{p})}{\gamma(\omega - i\epsilon, \boldsymbol{k})} \right] \quad (12.47)$$

and

$$\mathsf{G}(\omega + i\epsilon, \boldsymbol{k}; \boldsymbol{p}) = g(\boldsymbol{k}, \boldsymbol{p}) \frac{i M_c}{\boldsymbol{k} \cdot \boldsymbol{v} - \omega \mp i\epsilon}. \qquad (12.48)$$

Equations (12.46)–(12.48) have a clear physical meaning, they say that the fluctuation of the mean field (12.46) can be treated as a superposition of the modes (12.47) which correspond to elementary initial conditions (12.48). Such elementary initial conditions are realized by adding to the system, at $t = 0$, particles with well-defined momentum $\boldsymbol{p}$.

Using Eqs (12.47), (12.37)–(12.39), and (12.48) we find that

$$\delta M(t, \boldsymbol{k}; \boldsymbol{p}) = g(\boldsymbol{k}, \boldsymbol{p}) M_c \left[F_{2c} \left(\frac{\boldsymbol{v} \cdot \boldsymbol{k}}{k}, kt \right) - i F_{2s} \left(\frac{\boldsymbol{v} \cdot \boldsymbol{k}}{k}, kt \right) \right], \quad (12.49)$$

where

$$
\begin{aligned}
F_{2c}(x, y) = & -\cos(xy) \frac{\alpha(x)}{\alpha^2(x) + \beta^2(x)} \\
& + \mathcal{P} \int\limits_{-v^{\max}}^{v^{\max}} \frac{d\Omega}{\pi} \cos(\Omega y) \frac{\beta(\Omega)}{\alpha^2(\Omega) + \beta^2(\Omega)} \frac{1}{x - \Omega},
\end{aligned} \quad (12.50)
$$

and

$$
\begin{aligned}
F_{2s}(x, y) = & -\sin(xy) \frac{\alpha(x)}{\alpha^2(x) + \beta^2(x)} \\
& + \mathcal{P} \int\limits_{-v^{\max}}^{v^{\max}} \frac{d\Omega}{\pi} \sin(\Omega y) \frac{\beta(\Omega)}{\alpha^2(\Omega) + \beta^2(\Omega)} \frac{1}{x - \Omega}.
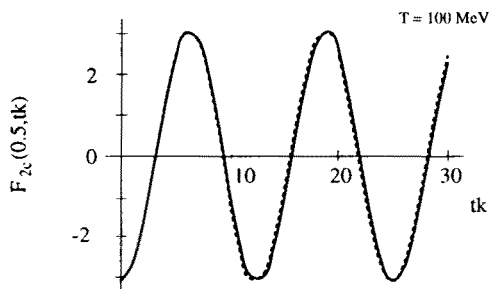\end{aligned} \quad (12.51)
$$

Fig. 12.3. The function $F_{2c}(0.5, kt)$ plotted for $T = 100$ MeV. The dashed line shows the complete result obtained from Eq. (12.50), whereas the solid line is the approximation for $F_{2c}(0.5, kt)$ obtained by keeping only the pole contribution (the first term on the RHS of (12.50)). Other parameters as in Fig. 12.2.
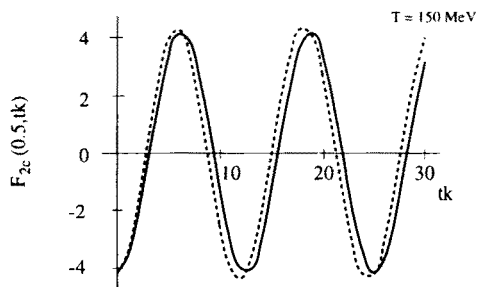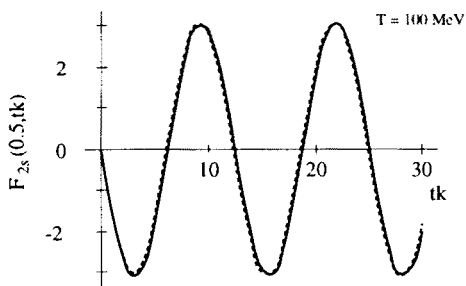

Fig. 12.4 The same as Fig. 12.3 but for $T = 150$ MeV.

Fig. 12.5. The function $F_{2s}(0.5, kt)$ plotted for $T = 100$ MeV. The dashed line shows the complete result obtained from Eq. (12.51), whereas the solid line is the approximation for $F_{2s}(0.5, kt)$ obtained by keeping only the pole contribution (the first term on the RHS of (12.51)).

In Figs 12.3 and 12.4 we show the function $F_{2c}(\boldsymbol{v}\cdot\boldsymbol{k}/k, kt)$ for two different values of the temperature, *i.e.*, for $T = 100$ MeV and $T = 150$ MeV. All the parameters are fitted in the same way as in the previous cases. We fixed the projection of the velocity $\boldsymbol{v}$ on the wave vector $\boldsymbol{k}$ to be $\boldsymbol{v}\cdot\boldsymbol{k}/k = 0.5$. The dashed curve represents in both cases the complete result obtained from (12.50), whereas the solid line shows only the pole contribution (only the first term on the RHS of Eq. (12.50)). Similarly, in Figs 12.5 and 12.6 we show the function $F_{2s}(\boldsymbol{v}\cdot\boldsymbol{k}/k, kt)$.
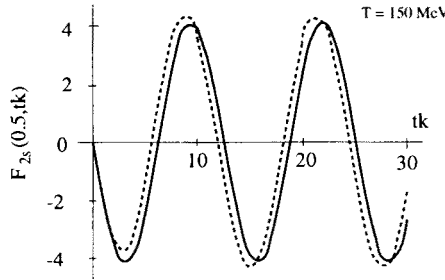

Fig. 12.6. The same as Fig. 12.5 but for $T = 150$ MeV.

One can see in Figs 12.3–12.6 that the functions $F_{2c}(\boldsymbol{v}\cdot\boldsymbol{k}/k, kt)$ and $F_{2s}(\boldsymbol{v}\cdot\boldsymbol{k}/k, kt)$ oscillate in time without any damping. It means that our elementary fluctuations (12.49) will be undamped as well. This phenomenon is caused by the singularity of the initial quark distribution function.

We want to point out that one finds similar waves in the theory of ordinary plasmas in the form of so-called Van Kampen modes [76]. Landau's calculation [73] emphasized the case where the initial perturbations were entire functions of the momentum. The Van Kampen modes are excited by the perturbation being a δ function in momentum. Of course, such a perturbation is not an entire function in the complex ω space. It gives rise to singularities on the real axis and leads to undamped oscillations.

In Figs 12.3–12.6 one can also see that the functions $F_{2c}(\boldsymbol{v}\cdot\boldsymbol{k}/k, kt)$ and $F_{2s}(\boldsymbol{v}\cdot\boldsymbol{k}/k, kt)$ can be quite well approximated just by the first terms on the RHS of Eqs (12.50) and (12.51). Using this fact we can find the following approximate form for the fluctuating part of the mean field:

$$
\begin{aligned}
\delta M(t, \boldsymbol{r}) \approx -4N_c N_f G \int^\Lambda \frac{d^3 p}{(2\pi)^3} \frac{M_c}{E_p} \int \frac{d^3 k}{(2\pi)^3} \frac{\alpha(\boldsymbol{v}\cdot\boldsymbol{k}/k)}{\alpha^2(\boldsymbol{v}\cdot\boldsymbol{k}/k) + \beta^2(\boldsymbol{v}\cdot\boldsymbol{k}/k)} \\
\times \Big[\frac{g(\boldsymbol{k}\cdot\boldsymbol{p}) + g(-\boldsymbol{k}\cdot\boldsymbol{p})}{2} \cos(\boldsymbol{v}\cdot\boldsymbol{k}t - \boldsymbol{k}\cdot\boldsymbol{r}) \\
+ \frac{g(\boldsymbol{k}\cdot\boldsymbol{p}) - g(-\boldsymbol{k}\cdot\boldsymbol{p})}{2i} \sin(\boldsymbol{v}\cdot\boldsymbol{k}t - \boldsymbol{k}\cdot\boldsymbol{r}) \Big].
\end{aligned}
\tag{12.52}
$$

Equation (12.52) shows that an arbitrary fluctuation can be written as a sum of undamped waves. Nevertheless, such a superposition itself is very likely to be damped because of the destructive coherence phenomena among the elementary excitations; this is the reason why the fluctuations are damped in our first case.

13. Critical scattering at the chiral phase transition

The calculations based on the NJL model indicate the presence of singularities in the elastic and hadronization cross sections [23]. This is a manifestation of criticality at a second order phase transition which favors the production of low-energy pions. In this Chapter we study the time evolution of the transition from partons to mesons and investigate to which degree the low-p_T enhancement observed in ultra-relativistic heavy-ion collisions may reflect criticality.

13.1. Critical opalescence

Critical scattering (called also a critical opalescence) is a rather general phenomenon observed in the vicinity of a second order phase transition [78]: The cross section $d^3\sigma/d\boldsymbol{q}$ for the scattering of light, X-rays or neutrons on a medium is given by the expression

$$\frac{d^3\sigma}{d\boldsymbol{q}} \propto \int d^3r \int d^3r' \, e^{i\boldsymbol{q}(\boldsymbol{r}-\boldsymbol{r}')} \langle n(\boldsymbol{r})n(\boldsymbol{r}')\rangle_T, \qquad (13.1)$$

where $\boldsymbol{q}$ is the momentum transfer and $\langle n(\boldsymbol{r})n(\boldsymbol{r}')\rangle_T$ is the density-density correlation function for the particles in the medium at the temperature T. In the neighborhood of a phase transition a long-range ordering develops and the cross section for small values of $\boldsymbol{q}$ has the form

$$\frac{d^3\sigma}{d\boldsymbol{q}} \propto \frac{1}{k^2(T) + \boldsymbol{q}^2}, \qquad (13.2)$$

where

$$k^2(T) \propto \left|1 - \frac{T}{T_c}\right|^\gamma \qquad (13.3)$$

is the inverse correlation length with γ being the critical exponent. Criticality manifests itself by the fact that the system becomes opaque to an external observer.

An experiment, where an *external* test particle is scattered on the system in its critical state, cannot be performed for a quark-gluon plasma which

only lives for 10^{-23} s. Nevertheless, also particles which are created *inside* the plasma can experience critical scattering. One has to find, however, a suitable observable, which makes the internal critical scattering visible to an outside observer. In the following we shall argue that critical scattering leads to a faster production of low momentum pions and thus to an intermediate non-thermal distribution. The pions which escape to the detector, before the thermal equilibration of the hadron gas sets in, can be observed as an enhancement at low momenta of the pion distribution.

A low-p_T enhancement in pion and kaon spectra is indeed observed in ultra-relativistic heavy-ion collisions. At small values of the transverse mass, $m_T = \sqrt{m^2 + p_T^2}$, the observed distributions of pions and kaons, dN/dm_T, considerably exceed the thermal distribution [28–30]. Various effects have been proposed to explain this phenomenon: *e.g.*, existence of the transverse flow [79, 80], creation of small plasma droplets [81], decays of resonances [82], formation of the pion system out of chemical equilibrium [83, 84], or the medium modification of the pion dispersion relation [85]. To which degree the critical phenomena contribute to the observed phenomenon, is the subject of this Chapter.

13.2. Kinetic description of the hadronization of the quark plasma

The phase transition from a quark-gluon plasma to a hadron gas has two aspects: chiral restoration and deconfinement. The NJL model is a useful framework to study the chiral aspect. For a vanishing mass of the current quarks, a phase transition of the second order is predicted at a critical temperature T_c above which the constituent quarks have zero mass while below T_c the pions are the Goldstone particles with $m_\pi = 0$.

In explicit calculations [23], using the NJL model for a description of the quark-meson plasma (no gluons), it has been shown that singularities occur in the cross sections at small center-of-mass energies $\sqrt{s}$ of the colliding particles, when the phase transition is approached. In particular, the integrated elastic quark-antiquark cross-section $\sigma_{q\bar{q}\to q\bar{q}}(s, T)$ diverges like s^{-1} for $T \to T_c$. A singularity is also found for the hadronization cross-section $q\bar{q} \to \pi\pi$. In both cases the singularity arises because the quark condensate $\langle\bar{q}q\rangle_T$, which is the order parameter of the chiral phase transition, goes to zero at the critical temperature.

Although these results have been obtained for a particular model they may be of more general relevance, provided the parton-hadron phase transition is second order. We use the results for the energy dependence of the cross sections in order to model the time evolution from quark to hadron matter: The cross sections are incorporated into the kinetic equations proposed for the description of the transition of a spatially homogeneous quark plasma

(described by the single particle quark distribution function $f_q(p, t)$, $p = |\boldsymbol{p}|$) into a pion gas (with a corresponding distribution function $f_\pi(p, t)$).

In order to keep the model as transparent as possible we work in the relaxation time approximation. However, in contrast to the usual approaches, the relaxation times $\tau(p, t)$ depend on momenta via the energy dependence of the cross sections. The singularities in the cross sections due to criticality of the medium translate themselves into singularities of the inverse relaxation times $1/\tau(p, t)$ in the momentum p.

The above ideas are translated into the following set of kinetic equations

$$\frac{df_q(p, t)}{dt} = -\frac{f_q(p, t) - f_{q,\text{th}}(p, t)}{\tau_\text{th}(p, t)} - \frac{f_q(p, t)}{\tau_\text{had}(p, t)} + \frac{f_\pi(p, t)}{\tau_\text{dec}(p, t)}, \quad (13.4)$$

$$\frac{df_\pi(p, t)}{dt} = -\frac{f_\pi(p, t) - f_{\pi,th}(p, t)}{\tau_\text{th}(p, t)} + \frac{f_q(p, t)}{\tau_\text{had}(p, t)}$$

$$- \frac{f_\pi(p, t)}{\tau_\text{dec}(p, t)} - \frac{f_\pi(p, t)}{\tau_\text{em}(p)}, \quad (13.5)$$

$$\frac{df_\text{em}(p, t)}{dt} = \frac{f_\pi(p, t)}{\tau_\text{em}(p)}. \quad (13.6)$$

Eq. (13.4) determines the time evolution of the quark distribution function $f_q(p, t)$ (it describes both quarks and antiquarks, *i.e.*, $f_q(p, t) = f_\text{quarks}(p, t) + f_\text{antiquarks}(p, t)$). The first term on the RHS of Eq. (13.4) is the collision term written in the relaxation time approximation; it is responsible for the thermalization of quarks since the distribution function $f_q(p, t)$ is always attracted to the thermal one $f_{q,\text{th}}(p, t)$. The second (third) term describes the loss (gain) of quarks due to the hadronization (deconfinement) process where we limit ourselves to the reaction $q\bar{q} \to \pi\pi$ $(q\bar{q} \leftarrow \pi\pi)$.

In Eq. (13.5), for the time evolution of the distribution functions of pions, the first three terms on the RHS describe the thermalization of pions, appearance of pions due to hadronization of quarks, and the two-pion reaction into quark-antiquark pairs, respectively. The last (fourth) term accounts for the emission of pions from the plasma into the detector. For $t \to \infty$ the distribution function $f_\text{em}(p, t)$ describes the observed spectrum of pions.

Eqs (13.4)–(13.6) can be solved for any initial conditions (*i.e.*, assuming some particular form of the distribution functions at the initial time $t = 0$) provided the thermal distribution functions $f_{q,\text{th}}(p, t)$ and $f_{\pi,th}(p, t)$ are known at all times. Since the first terms on the RHS of Eq. (13.4) and (13.5) represent the collision terms (in the relaxation time approximation) they must obey the symmetry leading to the energy conservation. This gives the following constraint for $f_{q,\text{th}}(p, t)$ and $f_{\pi,th}(p, t)$ at each time t

$$\int \frac{d^3p}{(2\pi)^3} \sqrt{p^2 + m_i^2} \; \frac{f_i(p,t) - f_{i,\mathrm{th}}(p,t)}{\tau_{\mathrm{th}}(p,t)} \; = 0 \qquad (13.7)$$

(here $i = q$ or π). Eq. (13.7) determines the temperature $T_i(t)$ appearing in the thermal distributions. For simplicity we assume the low-density high-temperature form of these functions, namely a Boltzmann distribution

$$f_{i,th}(p,t) = g_i \exp\left[-\frac{\sqrt{p^2 + m_i^2}}{T_i(t)} \right], \qquad (13.8)$$

where g_i are the degeneracy factors: $g_q = 24$ (quarks and antiquarks having two different spin projections, 3 colours and 2 flavours) and $g_\pi = 3$ (three different values of the isospin). One can notice that the distributions (13.8) correspond to the case when the chemical potential μ_i is zero, consequently we allow in our approach for number changing processes like: $q\bar{q} \to 2(q\bar{q})$ or $\pi\pi \to 2(\pi\pi)$.

13.3. Relaxation times and cross sections

The analysis of the exact collision term in the Boltzmann kinetic equation (analogous to that in [86]) leads to an expression for the average time for hadronization of two quarks into two pions

$$\frac{1}{\tau_{had}(p,t)} = \frac{1}{2\sqrt{p^2 + m_q^2}} \int \frac{d^3p_1}{(2\pi)^3\sqrt{p_1^2 + m_q^2}} f_q(p_1,t) F_{qq}(s)\sigma_{q\bar{q}\to\pi\pi}(s),$$

$$(13.9)$$

where $\sigma_{q\bar{q}\to\pi\pi}(s)$ denotes the total cross section for this process. The relativistic flux factor of incoming quarks is $F_{qq}(s) = \frac{1}{2}\sqrt{s(s - 4m_q^2)}$, with $\sqrt{s}$ being the center-of-mass energy of the quarks with momenta p and p_1, respectively. The expression giving the deconfinement relaxation time, $\tau_{\mathrm{dec}}(p,t)$, has the form similar to Eq. (13.9). In the analogous way one also defines the relaxation time for thermalization $\tau_{\mathrm{th}}(p,t)$ which is mainly due to elastic processes ($qq \to qq$, $q\pi \to q\pi$) with the respective cross sections.

In the chiral limit and at the temperature of the phase transition, only for which the singularities in the cross sections are observed, the masses of quarks and pions have to be set to zero. We shall also assume that all cross sections: $\sigma_{q\bar{q}\to\pi\pi}(s), \sigma_{qq\to qq}(s), \sigma_{\pi\pi\to\pi\pi}(s)$ and $\sigma_{q\pi\to q\pi}(s)$ are given by the generic expression

$$\sigma(s) = \sigma_0 \left[1 + \frac{s_0}{s} \right], \tag{13.10}$$

where σ_0 represents a constant contribution to the cross sections, and the appearance of the singular term s_0/s accounts for the critical phenomena. The hadronization and deconfinement cross sections, $\sigma_{q\bar{q} \to \pi\pi}(s)$ and $\sigma_{\pi\pi \to q\bar{q}}(s)$, are related to each other by the principle of detailed balance

$$g_q^2 \sigma_{q\bar{q} \to \pi\pi}(s) = g_\pi^2 \sigma_{\pi\pi \to q\bar{q}}(s). \tag{13.11}$$

This relation guarantees that in the absence of emission ($\tau_{\mathrm{em}} \to \infty$), the kinetic equations lead to the chemical equilibrium $n_q/n_\pi = g_q/g_\pi$.

The possibility of the emission of preequilibrium pions, *i.e.*, the emission of pions at each stage of the hadronization process is crucial for our description. In the model defined by the kinetic equations (13.4)–(13.6) this emission is only treated in a very global and rather crude way. The emission time τ_{em} is a free parameter of the theory, which allows us to decouple a certain fraction of pions from the interacting, non-equilibrium system. We have no good model for the momentum dependence of τ_{em}. Therefore we test two assumptions:

$$\frac{1}{\tau_{\mathrm{em}}^{(a)}} = \frac{\mathcal{R}}{\tau_{\mathrm{th}}(p = T_{\mathrm{c}}, t = 0)} \tag{13.12}$$

and

$$\frac{1}{\tau_{\mathrm{em}}^{(b)}} = \frac{p}{T_{\mathrm{c}}} \frac{\mathcal{R}}{\tau_{\mathrm{th}}(p = T_{\mathrm{c}}, t = 0)}. \tag{13.13}$$

In the first case the emission time is independent of momentum, whereas in the second case the inverse emission time depends linearly on p (the emission of low energetic pions is suppressed). The magnitude of $\mathcal{R}$ indicates how much faster the emission is, in comparison to the rate of the thermalization processes inside the system.

13.4. Results of numerical calculations

In order to reduce the number of free parameters in our calculation we have set all the cross sections: $\sigma_{q\bar{q} \to \pi\pi}(s), \sigma_{qq \to qq}(s), \sigma_{q\pi \to q\pi}(s)$ and $\sigma_{\pi\pi \to \pi\pi}(s)$ to be equal (within a factor of 3 such a result is supported by calculations within the NJL model) and use the form (13.10) which is appropriate for $T = T_c$. Then, we are left with three parameters: σ_0, s_0 and $\mathcal{R}$. One can notice that σ_0 sets the overall time-scale and is unimportant if we are interested in the final ($t \to \infty$) pion distributions.

We start solving our kinetic equations by assuming that the initial quark distribution is a thermal one and that there are no pions in the system. After integrating Eqs (13.4)–(13.6) till the time when all quarks are hadronized and all pions are emitted, one obtains the distribution function $f_{em}(p, t \to \infty)$ of the observed pions for a set of parameters s_0 and $\mathcal{R}$.
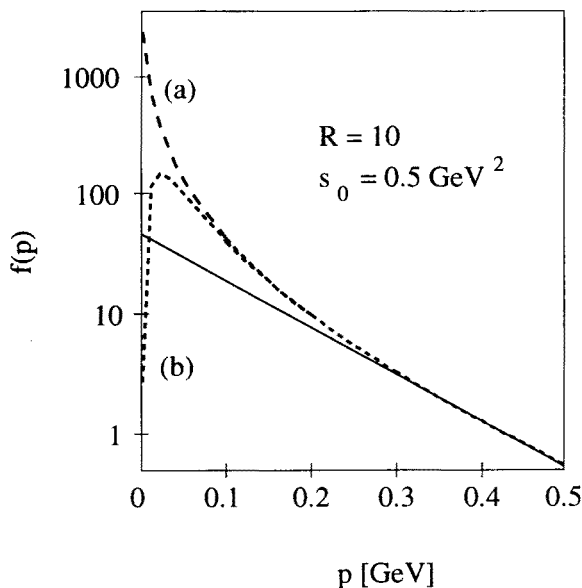

Fig. 13.1. The distribution functions of the emitted pions (dashed lines) together with the thermal distribution (solid line) fitted to them in the high momentum region. The cases (a) and (b) correspond to the emission times calculated according to Eqs (13.12) and (13.13), respectively.

In Fig. 13.1 we show our results for the initial temperature of quarks $T_q(t = 0) = T_c = 140$ MeV, and for $s_0 = 0.5$ GeV^2 and $\mathcal{R} = 10$. The two dashed lines represent the distribution functions of the emitted (observed) pions. The upper one (a) corresponds to the emission independent of momentum (according to Eq. (13.12)), and the lower one (b) corresponds to p-dependent emission (according to Eq. (13.13)). One can notice that the resulting pion distributions are non-equilibrium ones. We can also see that they coincide for large values of momenta. The solid line represents the thermal distribution fitted to these two curves in the high momentum region. One can see that for small momenta, 25 MeV $< p <$ 200 MeV, both pion distributions exceed the thermal one. In the case (a) the pion distribution is very much peaked in the limit $p \to 0$. This behaviour reflects directly the criticality of the hadronization cross section. On the other hand, in the case (b) the pion distribution function drops to zero for $p \to 0$ since the effect

of critical hadronization is, in this situation, partially destroyed by the slow emission of low energetic pions.

In consequence, our model calculation indicates that the criticality in the hadronization cross sections leads to the excess in the production of low energetic pions. The effect becomes particularly strong if the produced pions, independently of their momenta, can manage to decouple fast from the interacting system. The question whether the discussed scenario is really the realistic one and responsible for the observed low-p_T enhancement can only be checked by more detailed calculations. They should include, in particular, the dynamics of the space-time evolution of the system and of the freeze-out process. As we showed in our simple approach it is, in general, very important to take into account the possibility that the cross sections exhibit non-trivial energy dependence. This can lead to interesting phenomena connected with the existence of the phase transition and even serve as a diagnose of its occurrence.

IV SUMMARY

1 In general the vacuum correlation functions in the meson channels are screened and, due to Lorentz invariance, the screening mass of a stable meson equals its dynamic mass. For unstable mesons the screening mass equals the mass of the branch point, since the asymptotic form of the correlation function picks out the lowest lying singularity. As demonstrated by our work, these results are reproduced by the NJL model: the pion screening mass is equal to its dynamic mass, whereas the sigma screening mass is $2M_0$, where M_0 is the constituent quark mass in vacuum.

At finite temperature and zero density, the correlation functions are again exponentially damped. Moreover the screening and dynamic masses differ — this fact indicates that at finite temperature it is impossible to obtain the exact information about time-like excitations by studying space-like correlation functions. The overall temperature dependence of the screening masses in the NJL model agrees with the corresponding lattice results.

We carefully explored the analytic structure of the correlation functions. In the complex momentum plane they have two cuts (scalar channel) or two cuts and a pole (pseudoscalar channel). At sufficiently high temperature the pion pole disappears and we have to deal, in both channels, with two cuts. The contributions from these cuts show large cancellations which lead to the exponential decay of the correlation functions.

2 We have demonstrated that the correlation functions at $T = 0$ and finite density differ qualitatively from those in vacuum and those at $T > 0$: they exhibit long ranged oscillations, of the Friedel type, rather than exponential damping. We found that the appearance of the oscillations is connected with the existence of a cut of finite range in the complex momentum plane. This cut is responsible for the leading contribution to the correlation function at large distances. The length of the cut, which is proportional to the Fermi momentum of the constituent quarks, is reflected in the oscillation period at large distances $\delta r = \pi/p_F$. Consequently this form of the correlation function is quite general and is expected in all normal Fermi liquids. In particular, the existence of the oscillations is independent of whether the basic fermionic degrees of freedom are quarks or nucleons. Therefore, we feel the oscillatory behaviour of the correlation function at finite density will not change qualitatively by confinement.

The fact that the correlation function exhibits Friedel-type oscillations indicates again that in medium it is impossible to obtain the information about time-like excitations by studying space-like correlations. Their long distance behaviour is dominated by low lying particle-hole excitations, and consequently not connected with the dynamic mass.

3 Our NJL studies concerning static meson correlation functions were supplemented by the calculation within the perturbative QCD. Keeping only the lowest order term we obtained compact analytic results. This work extends some of the earlier results, which were concentrated only on the asymptotics of the correlation functions.

4 Temperature dependence of the quark condensate was studied in the NJL model with meson loops. Substantial differences were found compared to the standard results obtained in the Hartree–Fock approximation. In particular, we found finite slope of the condensate vs. T^2 for $T \to 0$ in the chiral limit, faster melting of the condensate, and a lower chiral restoration temperature. The importance of pions is connected with the smallness of their mass, much smaller than the masses of other hadrons. In the particular case of the NJL model, the pion mass is much smaller than the mass of the non-confined constituent quarks. The behaviour of $\langle \bar{q}q \rangle$ is affected by the coupling of the quarks with pions. This happens in such a way that the presence of pions leads to the destruction of the condensate. Therefore, including meson loops we speed up the decrease of the condensate with increasing temperature. We demonstrated consistency of our results with the chiral perturbation theory. Our calculation represents the first self-consistent treatment of the NJL model with meson loops at finite temperature.

5 The chiral symmetry concepts have been explicitly included in the construction of the transport equations for quark matter. Our starting point was the chirally invariant Lagrangian of the NJL model and we derived the transport equations via a spinor decomposition of the Wigner function and a gradient expansion. Our calculation was restricted to the mean-field approximation. We have taken into account the spin dynamics and discussed the possibility of having a non-zero pseudoscalar condensate. In this aspect, our results are a generalization of some earlier results.

The classical quark distribution functions satisfy the kinetic equations of the standard form with the effective chirally invariant mass $M^2(X) = \pi^2_{(0)}(X) + \sigma^2_{(0)}(X)$, where $\pi_{(0)}(X)$ and $\sigma_{(0)}(X)$ are leading terms in the classical expansion of the pseudoscalar and scalar condensates. Furthermore, the angle $\Phi(X)$, defined through the relation $\pi_{(0)}(X)/\sigma_{(0)}(X) = \tan\Phi(X)$, must be a constant. However, its value remains undefined, which reflects the chiral symmetry of the problem.

The classical equation for the spin evolution, which has been derived for the first time by us, is also invariant under chiral transformations. However, its solutions are constrained by the additional condition of the axial current conservation, which is not simple to incorporate.

The inclusion of the quark mass term into the Lagrangian explicitly breaks the chiral invariance. Consequently, we find that $\Phi(X)$ as well as $\pi_{(0)}(X)$ must be zero. Nevertheless, the general form of the kinetic equations does not change and we can still use them with the substitution $M(X) = \sigma_{(0)}(X) + m$, where m is the current quark mass. Moreover, in this case the requirement of the axial current conservation reduces to a form familiar from PCAC.

6 The chirally invariant kinetic theory for quark matter was used to study large time-scale fluctuations of the quark condensate. Our results showed that the general features of the propagation of the excitations in the system were very similar to those characterizing the wave propagation in a non-relativistic Maxwellian plasma. The elementary fluctuations of the condensate (Van Kampen modes) are not damped; they correspond to initial perturbations of the quark distribution function, which are strongly peaked for some given value of momentum. On the other hand, the superpositions of such elementary fluctuations are in practice always damped due to a phenomenon of destructive coherence (Landau damping). The overall results of this study showed the stability of the in-medium gap equation with respect to small perturbations of the quark distribution functions.

7 The system of kinetic equations describing hadronization of the quark-antiquark plasma was analyzed. It was found the the singularities in the elastic and hadronization cross sections, as described by the NJL model in connection with the critical behaviour at a second order phase transition, favor production of low-energetic mesons. We found that this effect can give a contribution to the observed low-p_T enhancement of pions observed in the ultra-relativistic heavy-ion collisions.

REFERENCES

General texts on QCD

[1] F. J. Ynduráin, *Quantum Chromodynamics*, Springer-Verlag, New York 1983.
[2] G. Sterman *et al.*, *Handbook of Perturbative QCD*, *Rev. Mod. Phys.* **157** (1995).
[3] K. Kanaya, *Finite Temperature QCD on the Lattice*, talk given at International Symposium on Lattice Field Theory, Melbourne, Australia, 11-15 July 1995, eprint hep-lat/9510040.

Formulation of the NJL model

[4] Y. Nambu, G. Jona-Lasinio, *Phys. Rev.* **122**, 345 (1961); **124**, 246 (1961).

Phase Transitions in QCD

[5] H. Meyer-Ortmanns, *Rev. Mod. Phys.* **68**, 473 (1996).

NJL model at finite temperature or density

[6] T. Hatsuda, T. Kunihiro, *Phys. Rev. Lett.* **55**, 158 1985).
[7] V. Bernard, U.-G. Meissner, I. Zahed, *Phys. Rev.* **D36**, 819 (1987).
[8] W. Florkowski, W. Broniowski, *Phys. Lett.* **B386**, 62 (1996).
[9] T. Hatsuda, T. Kunihiro, *Phys. Lett.* **B185**, 304 (1987).
[10] V. Bernard, U.-G. Meissner, I. Zahed, *Phys. Rev. Lett.* **59**, 966 (1987).
[11] V. Bernard, U.-G. Meissner, *Nucl. Phys.* **A489**, 647 (1988).
[12] V. Bernard, U.-G. Meissner, *Phys. Rev.* **D38**, 1551 (1988).
[13] T. Kunihiro, *Nucl. Phys.* **B351**, 593 (1991).
[14] M. Asakawa, M. Yazaki, *Nucl. Phys.* **A504**, 668 (1989).
[15] J. Hüfner, S.P. Klevansky, P. Zhuang, H. Voss, *Ann. Phys.* (N.Y.) **234**, 225 (1994).
[16] P. Zhuang, J. Hüfner, S.P. Klevansky, *Nucl. Phys.* **A576**, 525 (1994).
[17] T. Kunihiro, *Phys. Lett.* **271**, 395 (1991).
[18] W. Florkowski, B.L. Friman, *Acta Phys. Pol.* **B25**, 49 (1994).

Transport theory for the NJL model

[19] W.-M. Zhang, L. Wilets, *Phys. Rev.* **C45**, 1900 (1992).
[20] W. Florkowski, J. Hüfner, S.P. Klevansky, L. Neise, Ann. Phys. (N.Y.) **245** (1996) 445
[21] A. Abada, J. Aichelin, *Phys. Rev. Lett.* **74**, 3130 (1995).
[22] W. Florkowski, *Phys. Rev.* **C50**, 3069 (1994).
[23] P. Zhuang, J. Hüfner, S.P. Klevansky, L. Neise, *Phys. Rev.* **D51**, 3728 (1995); J. Hüfner, S.P. Klevansky, E. Quack, P. Zhuang, *Phys. Lett.* **B337**, 30 (1994); P. Rehberg, S.P. Klevansky, J. Hüfner, *Nucl. Phys.* **A608**, 356 (1996).
[24] J. Dolejší, W. Florkowski, J. Hüfner, *Phys. Lett.* **B349**, 18 (1995).

Reviews of the NJL model

[25] U. Vogel, W. Weise, *Prog. Part. Nucl. Phys.* **27**, 195 (1991); S.P. Klevansky, *Rev. Mod. Phys.* **64**, 649 (1992); M.K. Volkov, *Phys. Part. Nucl.* **24**, 35 (1993); T. Hatsuda, T. Kunihiro, *Phys. Rep.* **247**, 221 (1994).

Properties of the ρ meson in medium

[26] Gy. Wolf, W. Cassing, U. Mosel, *Nucl. Phys.* **A552**, 549 (1993); HADES collaboration, Proc. Int. Workshop XXI on Gross Properties of Nuclei and Nuclear Excitations, Hirschegg (1993) p. 144; M. Herrmann, *Eigenschaften des ρ-Mesons in dichter Kernmaterie*, PhD thesis, TH Darmstadt Report 92-10, GSI Darmstadt; M. Herrmann, B.L. Friman, W. Nörenberg, *Nucl. Phys.* **A560**, 411 (1993).

Quark-gluon plasma

[27] *Quark-Gluon Plasma*, World Scientific, Singapore, 1990 ed. R.C. Hwa; *Quark-Gluon Plasma 2*, World Scientific, Singapore, 1995, ed. R.C. Hwa.

[28] QUARK MATTER '90. Proceedings, 8th International Conference on Ultra-Relativistic Nucleus-Nucleus Collisions, MENTON, FRANCE, MAY 7-11, 1990, eds. J.P. Blaizot, C. Gerschel, B. Pire, A. Romana *Nucl. Phys.* **A525**, 1c-741c (1991).

[29] QUARK MATTER '91. Proceedings, 9th International Conference on Ultra-Relativistic Nucleus-Nucleus Collisions, GATLINBURG, USA, November 11-15, 1991, eds. T.C. Awes, F.E. Obenshain, F. Plasil, M.R. Strayer, C.Y. Wong, *Nucl. Phys.* **A544**, 1c-669c (1992).

[30] QUARK MATTER '93. Proceedings, 10th International Conference on Ultra-Relativistic Nucleus-Nucleus Collisions, BORLAENGE, SWEDEN, June 20-24, 1993, eds. E. Stenlund, H.A. Gustafsson, A. Oskarsson, I. Otterlund, *Nucl. Phys.* **A566**, 1c-681c (1994).

[31] C.P. Singh, *Phys. Rep.* **236**, 147 (1993).

Transport theory for a quark-gluon plasma

[32] U. Heinz, *Phys. Rev. Lett.* **51**, 351 (1983); *Ann. Phys.* (N.Y) **161**, 48 (1985).

[33] H.-Th. Elze, M. Gyulassy, D. Vasak, *Nucl. Phys.* **B276**, 706 (1986); *Phys. Lett.* **B177**, 402 (1986).

[34] A. Bialas, W. Czyż, A. Dyrek, W. Florkowski, *Nucl. Phys.* **B296**, 611 (1988).

Monte-Carlo simulations of hadronic collisions

[35] B. Andersson, G. Gustafson, G. Ingelman, T. Sjostrand, *Phys. Rep.* **97**, 33 (1983).

[36] K. Werner, *Nucl. Phys.* **A544**, 593c (1992).

[37] K. Geiger, B. Müller, *Nucl. Phys.* **A544**, 467c (1992).

Gross-Neveu model

[38] D.J. Gross, A. Neveu, *Phys. Rev.* **D10**, 3235 (1974).

't Hooft instantons

[39] G. 't Hooft, *Phys. Rev. Lett.* **37**, 8 (1976); *Phys. Rev.* **D14**, 3432 (1976).

Disoriented chiral condensates

[40] J.D. Bjorken, *Int. J. Mod. Phys.* **A7**, 4189 (1992); K. Rajagopal, F. Wilczek, *Nucl. Phys.* **B379**, 395 (1993); K. Rajagopal, F. Wilczek, *Nucl. Phys.* **B404**, 577 (1993); J.-P. Blaizot, A. Krzywicki, *Phys. Rev.* **D50**, 442 (1994).

Imaginary-time formalism

[41] A. Fetter, J. Walecka *Quantum Theory of Many Particle Systems*, McGraw Hill, New-York 1971.

[42] J. Kapusta, *Finite Temperature Field Theory*, Cambridge University Press, 1989.

[43] G.D. Mahan, *Many-Particle Physics*, Plenum, New York 1981.

[44] G. Baym, N.D. Mermin, *J. Math. Phys.* **2**, 232 (1961).

[45] M.B. Kislinger, P.D. Morley, *Phys. Rev.* **D13**, 2771 (1976).

Lattice calculations

[46] C. DeTar, J. Kogut, *Phys. Rev. Lett.* **59**, 399 (1987); *Phys. Rev.* **D36**, 2828 (1987).

[47] S. Gottlieb, W. Liu, R.L. Renken, R.L. Sugar, D. Touissant, *Phys. Rev. Lett.* **59**, 1881 (1987).

[48] A. Gocksch, P. Rossi, M. Heller, *Phys. Lett.* **B205**, 334 (1988).

[49] K. Born, S. Gupta, A. Irbäck, F. Karsch, E. Laermann, B. Peterson, H. Satz, *Phys. Rev. Lett.* **67**, 302 (1991).

[50] V. L. Eletskii, B. L. Ioffe, *Sov. J. Nucl. Phys.* **48**, 384 (1988).

[51] E.V. Shuryak, *Rev. Mod. Phys.* **65**, 1 (1993).

[52] W. Florkowski, B. Friman, *Z. Phys.* **A347**, 271 (1994).

Mathematical tables

[53] M. Abramowitz, I. Stegun, *Handbook of Mathematical Functions*, Dover Publications, New York 1972.

[54] S. Gradshteyn, I. M. Ryzhik *Table of Integrals, Series, and Products*, Academic Press, 1980.

Hadron structure in the NJL model

[55] M. Lutz, W. Weise, *Nucl. Phys.* **A518**, 156 (1990).

[56] Th. Meissner, K. Goeke, *Nucl. Phys.* **A524**, 719 (1991); A.Z. Górski, F. Grümmer, K. Goeke, *Phys. Lett.* **B278**, 24 (1992); E.N. Nikolov, W. Broniowski, K. Goeke, *Nucl. Phys.* **A579**, 398 (1994).

Friedel oscillations

[57] W. Florkowski, B. Friman, *Nucl. Phys.* **A611**, 409 (1996).
[58] J. Diaz Alonso, A. Perez, H. Sivak, *Nucl. Phys.* **A505**, 695 (1989).
[59] E. Gallego, J. Diaz Alonso, A. Perez, *Nucl. Phys.* **A578**, 542 (1994).
[60] J. Diaz Alonso, E. Gallego, A. Perez, *Phys. Rev. Lett.* **73**, 2536 (1994).

Low-density theorem

[61] E.G. Drukarev, E.M. Levin, *Nucl. Phys.* **A511**, 679 (1990); *Prog. Part. Nucl. Phys.* **27**, 77 (1991).
[62] T.D. Cohen, R.J. Furnstahl, D.K. Griegel, *Phys. Rev.* **C45**, 1881 (1992).

Effective-action method

[63] C. Itzykson, J.-B. Zuber, *Quantum Field Theory*, McGraw-Hill, New York 1980.
[64] E.N. Nikolov, W. Broniowski, C.V. Christov, G. Ripka, K. Goeke, *Nucl. Phys.* **A608**, 411 (1996).
[65] E. Nikolov, Ph.D. thesis, Ruhr-Univ. Bochum 1995.

Chiral perturbation theory

[66] J. Gasser, H. Leutwyler, *Phys. Lett.* **184B**, 83 (1987); *Phys. Lett.* **188B**, 477 (1987); *Nucl. Phys.* **B307** 763 (1988).

Real-time formalism

[67] P. Danielewicz, *Ann. Phys.* **152**, 239 (1984).

Transport theory — spinor decomposition

[68] H.-T. Elze *et al.*, *Mod. Phys. Lett.* **A2**, 451 (1987).
[69] D. Vasak, M. Gyulassy, H.-T. Elze, *Ann. Phys.* (N.Y.) **173**, 462 (1987).
[70] St. Mrówczyński, U. Heinz, *Ann. Phys.* (N.Y.) **173**, 462 (1987).
[71] I. Bialynicki-Birula, P. Górnicki, J. Rafelski, *Phys. Rev.* **D44**, 1825 (1991).
[72] P. Zhuang, U. Heinz, *Ann. Phys.* (N.Y.) **245**, 311 (1996); *Phys. Rev.* **D53**, 2096 (1996).

Electron-ion plasma, plasma oscillations

[73] *Collected Papers of L. D. Landau*, Pergamon, Oxford, England, 1965, p. 445.
[74] D. Sogan, *Am. J. Phys.* **62**, 450 (1994).
[75] E.M. Lifschitz, L.P. Pitaevskii, *Physical Kinetics*, Pergamon, Oxford, England, 1981.
[76] N.G. Van Kampen, *Physica* **21**, 949 (1955).

[77] T.H. Stix, *Waves in Plasmas*, American Institute of Physics, New York 1992.

Critical phenomena

[78] H.E. Stanley, *Introduction to Phase Transitions and Critical Phenomena*, Oxford University Press, New York 1971.

Soft pion production

[79] T.W. Atwater, P.S. Freier, J.I. Kapusta, *Phys. Lett.* **B199**, 30 (1987).
[80] K. Lee, U. Heinz, E. Schnedermann, *Z. Phys.* **C48**, 525 (1990).
[81] L. Van Hove, CERN preprint, TH-5236/88 (1988).
[82] G.E. Brown, J. Stachel, G.M. Welke, *Phys. Lett.* **B253**, 19 (1991).
[83] M. Kataja, P.V. Ruuskanen, *Phys. Lett.* **B243**, 181 (1990).
[84] S. Gavin, P.V. Ruuskanen, *Phys. Lett.* **B262**, 326 (1991).
[85] E. Shuryak, *Phys. Rev.* **D42**, 1764 (1990).

Relaxation-time approximation

[86] K. Huang, *Statistical Physics*, Wiley, New York 1987, Sect. 5.4.